Development of a Real-time Cortical Rhythmic Activity Imaging Technology and Its Applications

Han-Jeong Hwang

The Graduate School

Yonsei University

Department of Biomedical Engineering

Development of a Real-time Cortical Rhythmic Activity Imaging Technology and Its Applications

A Dissertation
Submitted to the Department of Biomedical Engineering
and the Graduate School of Yonsei University
in partial fulfillment of the
requirements for the degree of
Doctor of Philosophy

Han-Jeong Hwang

December 2011

This certifies that the dissertation of Han-Jeong Hwang is approved.

Thesis Supervisor: Sang-Woo Lee

Thesis Committee Member: Chang-Hwan Im

Thesis Committee Member: Jongbum Seo

Thesis Committee Member: Dae Sung Yoon

Thesis Committee Member: Kiwoon Kwon

The Graduate School

Yonsei University

December 2011

Acknowledgements

학위 기간 동안 가족과 주변 많은 사람들의 애정어린 관심과 도움으로 학위 논문을 무사히 마무리 짓게 되었습니다. 이 글을 빌어 제가 작은 학문적 결실을 맺을 수 있도록 도와주신 분들에게 미약하지만 감사의 마음을 전하고자 합니다.

먼저, 지금까지 부족한 제가 작지만 소중한 학문적 성과를 이룰 수 있도록 항상 열정적으로 지도해주신 임창환 교수님께 감사를 드립니다. 연구 방향에 대해 항상 함께 고민해주시고, 앞으로 한걸음 나아 갈수 있도록 조언을 해주시지 않으셨다면 그 동안의 연구 성과를 이루지 못했을 것 입니다. 표현이 서툴러 평소에 감사한 마음을 많이 표현하지 못했지만, 이 글을 빌어 다시 한번 감사의 마음을 전하고 싶습니다. 또한, 항상 열정적으로 연구를 수행하시며 부족한 저의 학위 논문이 좀 더 완성도 있게 지도해주신 이상우 교수님께 감사 드립니다. 그리고 부심으로서 바쁘신 와중에도 저의 논문 지도와 격려를 아끼지 않고 해주신 권기운 교수님, 서종범 교수님, 윤대성 교수님께도 감사의 말을 전하고 싶습니다. 대학원에서 수학하는 동안 수업을 통해 많은 학문적 가르침을 주신 김경환 교수님, 공동 연구를 수행한 유승현 교수님께도 감사 드립니다. 학부 재학 시절 연구실에 공부할 자리를 선뜻 내어주시어, 제가 공부를 열심히 할 수

있는 초석을 마련해주신 최태영 교수님께도 진심어린 감사를 드리고 싶습니다.

대학원 생활을 하며 가족보다도 많은 시간을 함께 하고 서로 힘이 되어준 연구실 식구들에게도 감사의 말을 전하고 싶습니다. 철없던 20 살 때 처음 만나 지금까지 여러 방면으로 나를 도와주고 내가 의공학이라는 학문을 접하게 해준 정영진 박사에게 감사의 말을 전하고 싶습니다. 그리고 연구실 입학 동기이자 얼마전 한 가정의 가장이 된 희제형, 듬직하게 연구실을 잘 이끌어 주고 있는 방장 도원이, 항상 꼼꼼하고 부지런한 재현이, 같은 연구를 수행하며 나를 도와 많은 실험을 수행하다 뇌파 실험의 달인이 된 정환이, 변리사 준비하는 지혜, 막둥이 미선이, BCI 팀의 일원이 된 창희, 한이에게도 진심으로 고맙고 감사하다는 말을 전하고 싶습니다. 그리고 1 년간 연구실 생활을 같이 한 착한 범준이, 트레이너 태준이, 여자친구 생긴 인수, 햇반 수호, 싱글벙글 재우에게도 고맙다는 말을 전하고 싶습니다.

새로운 캠퍼스에서 대학원 생활을 시작할 때 많은 정보를 제공해주며 적응을 도와준 효기씨, 비슷한 분야의 연구를 수행하며 고민 거리를 함께 공유한 종호, 선애, 상백이형, 정우, 종승이형, 윤 진, 성진이, 종구, 은경이, 공동 연구를 수행한 재활학과 이남기, 이동률, 강성국, 신윤겸 선생님께도 고맙다는 말을 전하고 싶습니다. 대학원 생활에 활력소가 되어준 농구 동아리 멤버인 태균이형, 인철이형, 성필이형, 성재형, 균정이형, 희성이형,

연식이형, 량희형, 대곤이형, 현석이형, 예일이형, 명헌이형, 상오형, 휘헌이, 현철이, 범준이, 재원이, 운모, 태윤이, 동수, 민용이 에게도 감사하다는 말을 전하고 싶습니다. 인생 멘토인 병훈이형, 소방관이 된 철중이형, 네이버 지인식이 된 관호형에게도 고마운 마음을 전하고 싶습니다.

지금은 태권도 국가대표가 된 종현이와 육아교육과에 진학한 보라의 과외 선생님으로 인연을 맺어 학부 시절 공부하는데 큰 도움을 주신 종현이와 보라 부모님, 사회복지사가 꿈인 다슬이, 씩씩한 청년이 된 동우와 자취하는 저에게 따뜻한 밥을 자주 해주신 다슬이와 동우 어머님과 아버님께도 감사의 말을 전하고 싶습니다.

마지막으로, 나라는 사람을 지금 여기에 존재하게 해준 세상에서 가장 존경하고 사랑하는 어머니에게 감사하다는 말을 하고 싶습니다. 어떠한 미사여구로도 표현할 수 없는 어머니의 사랑과 희생이 있었기에 지금의 제가 존재하고 이렇게 무사히 박사 학위를 마칠 수가 있었습니다. 그리고 이제는 삶의 동행자로 훌쩍 커버린 든든하고 멋진 동생 길정이와 같은 대학원생으로서 고민을 공유하고 항상 옆에서 힘이 되어준 사랑하는 현영이에게 감사의 마음을 전하고 싶습니다. 이 글을 통해 미처 언급하지 못했지만 제가 박사 학위를 받을 수 있도록 저를 도와 주신 주변의 모든 분들에게 감사합니다.

2011 년 12 월 황한정

Table of Contents

Table of Contents i
List of Figures iv
List of Tables x
Abstract xi

Chapter 1: Introduction ..... - 1 -

Chapter 2: Electroencephalography (EEG) ..... - 8 -
2.1. Source of EEG ..... - 8 -
2.2. Measuring Method ..... - 11 -
2.3. Rhythmic EEG Activity ..... - 13 -

Chapter 3: An EEG-based Real-time Cortical Rhythmic Activity Monitoring System ..... - 16 -
3.1. Methods ..... - 16 -
3.1.1. Concept of a Real-time Cortical Rhythmic Activity Monitoring System- 16 -
3.1.2. Forward Calculation and Inverse Estimation ..... - 18 -
3.1.3. Processing and Visualization ..... - 23 -
3.2. Possibility of the Real-time Cortical Rhythmic Activity Monitoring System: a Preliminary Simulation Study ..... - 25 -
3.2.1. Simulation Setups and Materials ..... - 25 -
3.2.2. Results of the Simulation Study ..... - 26 -
3.3. A First Pilot System: Experimental Results ..... - 31 -

3.4. Discussions and Summary ..... - 34 -

Chapter 4: Neurofeedback-based Motor Imagery Training for Brain-Computer Interface (BCI) ..... - 36 -

4.1. Research Background ..... - 36 -

4.2.1. Participants and Environment of Experiments ..... - 39 -

4.2.2. Motor Imagery Training ..... - 41 -

4.2.3. EEG Data Acquisition ..... - 42 -

4.2.4. EEG Data Analysis ..... - 46 -

4.3. Results ..... - 48 -

4.3.1. Changes in Brain Activity after Motor Imagery Training ..... - 48 -

4.3.2. Classification Accuracy before and after the Motor Imagery Training ..... - 51 -

4.4. Discussions and Summary ..... - 53 -

Chapter 5: An EEG-based Real-time Cortical Functional Connectivity Imaging System ..... - 57 -

5.1. Research Background ..... - 57 -

5.2. Methods ..... - 61 -

5.2.1. Methods for Real-time Connectivity Imaging ..... - 61 -

5.2.2. EEG Recording Environments ..... - 65 -

5.2.3. Implementation of a Real-time Cortical Connectivity Imaging System ..... - 65 -

5.3. Results ..... - 69 -

5.3.1. Gamma-band Cortical Connectivity Monitoring (Exp. 1) ..... - 70 -

5.3.2. Alpha/Beta-band Cortical Connectivity Monitoring (Exp. 2) ..... - 75 -

5.3.3. Theta-band Cortical Connectivity Monitoring (Exp. 3) ..... - 77 -

5.4. Discussions and Summary ..... - 80 -

Chapter 6: Brain Fingerprinting: Classification of Mental States Based on Spatiospectral Patterns of Brain Electrical Activity ..... - 84 -

6.1. Research Background ..... - 84 -

6.2. Methods ..... - 87 -

6.2.1. Participants and Experimental Conditions ..... - 87 -

6.2.2. Mental Tasks ..... - 88 -

6.2.3. EEG Data Acquisition ..... - 90 -

6.2.4. EEG Data Analysis ..... - 92 -

6.2.4.1. Regions of Interest (ROIs) ..... - 92 -

6.2.4.2. Feature Extraction ..... - 93 -

6.2.4.3. Classification of Mental States ..... - 95 -

6.3. Results ..... - 98 -

6.4. Discussions and Summary ..... - 102 -

Chapter 7: Conclusion ..... - 106 -

References ..... - 109 -

Appendix A: Two-dimensional Spatiospectral Pattern Maps ..... - 126 -

Abstract in Korean ..... - 132 -

List of Figures

Figure 2.1. Schematic structure of a cortical neuron.

Figure 2.2. Pyramidal neurons' arrangement along the cortical surface.

Figure 2.3. A typical electrode cap used in EEG recording systems.

Figure 2.4. The (extended) international 10-20 system for electrode positioning: (a) left view and (b) top view for the international 10-20 system, (c) top view for the extended international 10-20 system. The letters A, F, T, C, P, and O stand for Ear lobe, Frontal, Temporal, Central, Parietal, and Occipital, respectively.

Figure 3.1. Schematic diagram to elucidate the concept of the real-time cortical activation monitoring system.

Figure 3.2. Generation of cortical source space and boundary element model: (a) original tessellated cortical surface; (b) inflated cortical surface; (c) down-sampled cortical surface model; (d) boundary element model with 99 electrodes. The colors in (a) and (b) represent the distribution of sulci and gyri.

Figure 3.3. Cortical alpha (8-13 Hz) activity changes of dementia patients during a resting EEG recording: (a) dementia patient #1; (b) dementia patient #2.

Figure 3.4. Cortical alpha (8-13 Hz) activity changes of normal subjects during a resting EEG recording: (a) control subject #1; (b) control subject #2.

Figure 3.5. Cortical alpha (8-13 Hz) activity changes of subject YJ: The left figure shows a photograph of the experiment; the center and right figures show the alpha activity changes when the subject opened and closed his eyes, respectively. Cortical activity maps are viewed from top. 'L' and 'R' represent 'left' and 'right', respectively. Values in the source images were normalized to a predetermined threshold which was obtained from some preliminary experiments.

Figure 3.6. Cortical alpha (8-12 Hz) activity changes of subject JJ: The left figure shows a photograph of the experiment; the center and right figures show the mu activity changes when the subject raised his left and right hand, respectively. Cortical activity maps are viewed from top. 'L' and 'R' represent 'left' and 'right', respectively. Values in the source images were normalized to a predetermined threshold which was obtained from some preliminary experiments.

Figure 4.1. Screenshots of real-time mu rhythm activity (8-12 Hz) monitoring. The participant (EK) was instructed to continuously attempt to generate cortical activations around the sensorimotor cortex by imagining his left or right hand movement (see Supplementary movie, http://www.sciencedirect.com/science/article/pii/S0165027009000454). A cortical activation map at rest state (left) and when the participant was performing motor imagery (right).

Figure 4.2. The experimental paradigm used for EEG recording: after presenting a blank screen for 3 s, a circle with a black-and-white checkerboard pattern appeared randomly on either the left or right side of the screen for the next 0.25 s, indicating which hand movement the participant was to imagine. After a 1 s preparation time (blank screen), the letter 'X' appeared at the center of the screen and lasted for 0.25 s. At that time, the participant was to being performing either left or right hand motor imagery. The time period used for the data analysis (3.0 s) is depicted in the figure.

Figure 4.3. Changes in EMG power recorded at both of the participants' forearms before and during performing the motor imagery task. No statistically significant difference between the two EMG data sets (two-tailed paired t-test, $p < 0.05$) was found for all five participants of the trained group, indicating that the participants did not move their hands when they were attempting to perform the motor imagery task. A, B, C, D, and E indicate the EMG power changes of each participant, EK, GS, DK, KS and JN, respectively. In the figure, 'before' and 'during' represent 'before the motor imagery' and 'during the motor imagery', respectively.

Figure 4.4. Time-frequency pattern maps at the two electrode locations. The black colored blocks represent the time-frequency combinations that showed statistically significant difference ($p < 0.05$) between left and right motor imagery tasks. The time-frequency pattern maps did not show any distinguishable features before the training session, while the number of the 'black' blocks increased and the blocks were clustered around the mu rhythm (around 10 and 20 Hz) after the training session. 'Before' and 'after' represent

the time-frequency patterns calculated before the training session and those calculated after the training session, respectively.

Figure 5.1. (a) Process of generating cortical source space: a high-resolution cortical surface was smoothed and down-sampled for the real-time source imaging. (b) Locations of 12 regions of interest (ROIs): *colors* represent the ROI number (see the *color bar* on the *right side*).

Figure 5.2. A snapshot of a test experiment (*left*), and a screenshot of the real-time cortical functional connectivity monitoring software (*right*): dual LCD monitors were connected to a single computer system and were separated with a partition. The monitoring software can visualize both the on-going EEG signals and the current connectivity patterns.

Figure 5.3. Variations in the number of connection in the first experiment (Exp. 1) investigating the dynamics of gamma-band cortical connectivity: (a) Screenshots regularly sampled from the supplementary movie file (4 frames per second). *Numbers* in each picture represent the sequence of the pictures. Visual stimulus appeared in third *picture* and disappeared after *sixth picture*; (b) variation in the number of connections with respect to time: arrows represent stimulus onset. The threshold was set to 0.96. These examples are parts of one participant's data (subject JK).

Figure 5.4. Variations in the number of connections in the second experiment (Exp. 2) investigating the dynamics of alpha/beta-band cortical connectivity: Screenshots regularly sampled from a movie file (2 frames per second).

Numbers in each picture represent the sequence of the pictures. The subject moved his *left fingers* in *fourth picture*.

Figure 5.5. Variations in the number of connections in the third experiment (Exp. 3) investigating the dynamics of theta -band cortical connectivity: Screenshots regularly sampled from a movie file (1.5-s interval). *Numbers* in each picture represent the sequence of the pictures. A 6-digit word was presented in *third picture* and the retention interval started in *sixth picture*.

Figure 6.1. Experimental paradigm used in this study. There was a variable delay from 3 s to 8 s before instructing a subject to perform one of the mental tasks. The preparation periods were set to be 2 s for Task A, Task C, and Task D and 4 s for Task B. The preparation period for Task B was longer than the others because the subjects had to memorize a pair of two-digit numbers presented on a screen in order to perform the task. After a warning signal was presented for 125 ms (a beeping pure tone sound), the subject was asked to perform the instructed mental task for 10 s. During the data acquisition period, a cross fixation was presented at the center of the screen, except the Task A for which four Chinese characters were presented instead of the cross fixation.

Figure 6.2. Locations of 18 regions of interest (ROIs): (a) the left hemisphere; (b) the right hemisphere. The color bar on the right side represents the ROI number in which odd numbers are for the left hemisphere and even numbers are for the right hemisphere.

Figure 6.3. Schematic illustration of the proposed mental task classification method: (a) A two-dimensional source power pattern map for a specific mental task was constructed by calculating spectral source power at each ROI and frequency. The 2D source power pattern map (denoted as “Task Map”) was converted into a 2D spatiospectral pattern map consisting of event-related (de)synchronization (ERD/S) values (ERS: red color; ERD: blue color), based on the 2D source power pattern map constructed for the resting state (denoted as “Baseline Map”). This procedure was applied to all trials of four mental tasks, Tasks A-D, and template ERD/S maps for each mental task were obtained. (b) When a new 2D spatiospectral pattern map was fed into the proposed classification algorithm, this pattern map was compared with the template pattern maps constructed from the process described in (a). The input pattern map was then assigned to the class with the highest fitness value.

Figure 6.4. Two-dimensional spatiospectral pattern maps for all mental tasks performed by subject IU. Event-related synchronization (ERS) is plotted in red while event-related desynchronization (ERD) is plotted in blue. Consistent intra-class similarity was commonly observed for each task.

Figure 6.5. Two-dimensional spatiospectral pattern maps for all mental tasks performed by subject DK. Event-related synchronization (ERS) is plotted in red while event-related desynchronization (ERD) is plotted in blue. Consistent intra-class similarity was commonly observed for each task.

Figure 6.6. Comparison of classification accuracies between cortical level and sensor level analyses.

List of Tables

Table 4.1. The total number of time-frequency combinations showing a significant difference between left and right hand motor imagery.

Table 4.2. Changes in classification accuracy before and after motor imagery training (or first and second EEG recordings in control group). We first selected the two time-frequency combinations that had the smallest *p*-values as the features for classifying left and right hand motor imagery. A Euclidean distance algorithm was then used to estimate the classification accuracy.

Table 5.1. The ratio of the average numbers of connectivity connections observed during a 2 s period after presenting the facial images to those observed during a 2 s period before presenting the images.

Abstract

Development of a Real-time Cortical Rhythmic Activity Imaging Technology and Its Applications

Han-Jeong Hwang

Dept. of Biomedical Engineering

The Graduate School

Yonsei University

The principal aim of this dissertation is to develop a real-time cortical rhythmic activity imaging technology and to apply this technology to a variety of potentially practical applications, such as real-time brain activity monitoring, diagnosis of brain diseases, advanced neurofeedback, brain-computer interface (BCI), and classification of human thoughts.

To this end, the author first implemented an EEG-based, real-time, cortical rhythmic activity monitoring system to investigate whether or not a real-time cortical rhythmic activity imaging is feasible. In the monitoring system, a frequency domain inverse operator is preliminarily constructed, considering the subject's anatomical information and sensor configurations, and then the spectral current power at each cortical vertex is calculated for the Fourier transforms of successive sections of continuous data, when a particular frequency band is given. A preliminary offline simulation study using four sets of artifact-free, eye-closed, resting EEG data acquired from two dementia patients and two normal subjects demonstrates that spatiotemporal changes of cortical rhythmic activity can be monitored at the cortical level with a maximal delay time of about 200 ms, when 18 channel EEG data are analyzed under a Pentium4 3.4 GHz environment. The first pilot system is applied to two human experiments– (1) cortical alpha rhythm changes induced by opening and closing eyes and (2) cortical mu rhythm changes originated from the arm movements– and demonstrated the feasibility of the developed system.

The developed real-time cortical rhythmic activity monitoring system was utilized as a motor imagery training system for EEG-based brain-computer interface (EEG). Ten healthy participants took part in this study, half of whom were trained by the suggested training system and the others did not use any training. All participants succeeded in performing motor imagery after a series of trials to activate their motor cortex without any physical movements of their limbs. To confirm the effect of the

suggested system, EEG signals were recorded for the trained group around sensorimotor cortex while they were imaging either left or right hand movements according to the experimental design, before and after the motor imagery training. For the control group, EEG signals were also measured twice without any training sessions. The participants' intentions were then classified using a time-frequency analysis technique, and the results of the trained group showed significant differences in the sensorimotor rhythms between the signals recorded before and after training. Classification accuracy was also enhanced considerably in all participants after motor imagery training, compared to the accuracy before training. On the other hand, the analysis results for the control EEG data set did not show consistent increment in both the number of meaningful time-frequency combinations and the classification accuracy, demonstrating that the suggested system can be used as a tool for training motor imagery tasks in BCI applications.

With just slight modifications of the real-time cortical rhythmic activity monitoring system, the author developed an EEG-based, real-time, cortical functional connectivity imaging system capable of monitoring and tracing dynamic changes in cortical functional connectivity between different regions of interest (ROIs) on the brain cortical surface. To verify the implemented system, the author performed three test experiments in which the author monitored temporal changes in cortical functional connectivity patterns in various frequency bands during structural face processing, finger movements, and working memory task. The author also traced the

changes in the number of connections between all possible pairs of ROIs whose correlations exceeded a predetermined threshold. The quantitative analysis results were consistent with those of previous off-line studies, thereby demonstrating the possibility of imaging cortical functional connectivity in real-time.

The cortical source imaging was used to decode various mental states more accurately than sensor-level analyses. Eight participants took part in this study; their EEG data were recorded while they performed four different cognitive imagery tasks. The spectral power at each preliminarily determined cortical ROIs was estimated, and then a 2D spatiospectral pattern map was constructed for each task, of which each element was filled with 1, 0, and -1 reflecting the degree of event-related synchronization (ERS) and event-related desynchronization (ERD). Consistent ERS/ERD patterns were observed more frequently between trials in the same class than those in different classes, indicating that these spatiospectral pattern maps could be used to classify different mental states. Classification of a specific mental state was performed through the similarity evaluation between a current 2D pattern map and the template pattern maps, by taking the inner-product of two pattern matrices. The classification accuracy was evaluated using the leave-one-out cross-validation (LOOCV) and that for sensor-level analysis using the raw EEG signals was also calculated for comparison. An average accuracy of 76.31% ($\pm$12.84%) was attained for the cortical-level analysis; whereas an average accuracy of 68.13% ($\pm$9.67%) was

attained for the sensor-level analysis, demonstrating cortical-level analysis can interpret various human thoughts more correctly than sensor-level analysis.

In summary, the author developed a real-time cortical rhythmic activity imaging technology and demonstrated the usefulness of the developed technology by successfully realizing a variety of practical applications.

Key Words: cortical source imaging, real-time neuroimaging, cortical rhythmic activity, electroencephalography (EEG), inverse problem, brain-computer interface (BCI), motor imagery, neurofeedback, functional connectivity, diagnosis of psychiatric disease, mental task classification, mind reading

Chapter 1: Introduction

Cortical rhythmic activity, which is often called spontaneous brain activity or oscillatory brain activity, is generated intrinsically rather than as phase-locked responses to external stimuli [1]. In electroencephalography (EEG) and magnetoencephalography (MEG), the first recorded signal was the alpha rhythm, which is a kind of cortical oscillation peaking at about 10 Hz.

Recently, an increasing number of neuroscientists are becoming interested in cortical rhythmic activity since various *in vivo* studies in both humans and animals have revealed that cortical rhythmic activity at various frequencies might be closely related to information encoding in the brain [2-7]. For instance, cortical rhythmic activity might reflect specific body movements and behavioral states. The alpha rhythmic peaking at around 10 Hz becomes strongest when the subject has his eyes closed and is suppressed when the subject is exposed to visual stimuli [6]. The mu rhythm, with both 10 Hz and 20 Hz components, is dampened by limb movements or tactile stimulations [7]. It has also been revealed by numerous studies [2, 3, 5] that gamma-band activity (30–100 Hz) can be modulated by various behavioral states such as attention, working memory and associative brain diseases such as schizophrenia [4] and Alzheimer's disease [8].

EEG and MEG are excellent tools to investigate human cortical rhythmic activity noninvasively thanks to their superior temporal resolutions to other noninvasive brain mapping techniques such as functional magnetic resonance imaging (fMRI), positron emission tomography (PET), near infrared spectroscopy (NIRS) and so on. Many studies have been performed to evaluate the coherence between signals acquired at different scalp EEG electrodes or MEG sensors, and investigated spatial signal power patterns appearing in the scalp potential maps or magnetic field maps on the sensor plane [1-9]. However, the EEG or MEG topographies cannot be directly attributed to the underlying cortical regions since sensors may contain information from multiple brain sources, some of which might overlap, and the topographic maps might be smeared out due to the inhomogeneous conductivity distributions in the human head. A deep tangential source might generate two distinct peaks on the topographic map, which are hard to distinguish from two radial sources around the peak locations. Moreover, a very small cortical activation in some cortical areas could yield widespread filed distribution in the topographic maps, preventing one from identifying the correct location of the actual cortical source and investigating the coherence between different sensors. If a subject's head is tilted especially in a helmet-type MEG, so that one hemisphere is closer to the sensors than the other is, one could observe stronger activity at sensors closer to the subject's head even when the strengths are equal at the cortical level. Therefore, to overcome these limitations, source imaging rhythmic activity at the cortical level is necessary.

Over the last decade, several methods for source imaging of cortical rhythmic activity have been proposed, such as sequential dipole modeling [10], dynamic imaging of coherent sources (DICS) [11], frequency-domain minimum current estimation (FD-MCE) [12], synthetic aperture magnetometry (SAM)[13] and spectral spatiotemporal imaging [14]. Despite the recent progress in the imaging techniques, source imaging of cortical rhythmic activity has rarely been applied to the real-time brain activation monitoring system. Congedo *et al* [10, 15] attempted to apply inverse solutions to the EEG neurofeedback system for the first time. They applied low-resolution electromagnetic tomography (LORETA) software (http://www.unizh.ch/keyinst) to the EEG data which were bandpass-filtered for a specific frequency band. Their system enhanced the efficiency of conventional neurofeedback systems which relied only upon the EEG or MEG topographic maps, by tracking spectral power changes at a region of interest (ROI) in a standard human brain. Their approach is meaningful enough in that they first implemented a real-time cortical rhythmic activity monitoring system. Basically, however, the conventional approach that used LORETA-key software resulted in too widespread low-resolution images and did not visualize 3D cortical activation changes in real-time. Moreover, they did not concern themselves about the delay time seriously because their application could be implemented without a very high temporal resolution.

In this dissertation, the first goal was to realize a real-time cortical rhythmic activity monitoring system that visualizes instantaneous cortical activation images,

and is generally applicable to a variety of potential applications such as brain computer interface (BCI), neurofeedback, real-time diagnosis of brain diseases, and so on, with just slight modifications in the operating software. Before implementing a pilot system, offline analysis software which simulates the real-time cortical activation monitoring system was implemented and applied to four sets of artifact-free, eye-closed, resting EEG data acquired from two dementia patients and two normal male subjects, in order to investigate if the real-time cortical activity monitoring system is possible. After confirming the possibility of the system, the author implemented a first online pilot system which was integrated with a commercial EEG recording device and applied it to two well-known experiments– (1) cortical alpha rhythm changes induced by opening and closing eyes and (2) cortical mu rhythm changes originated from the arm movements– which demonstrate the validity of the real-time cortical activity monitoring system. The detailed processes of real-time cortical rhythmic source imaging, experimental procedures, and results will be presented in Chapter 3 of this dissertation.

After the verification of the real-time cortical rhythmic activity monitoring system, this real-time source imaging system was used as a motor imagery training system for brain-computer interface (BCI). Motor imagery, defined as mental simulation of a kinesthetic movement [16, 17], is one of the widely used effectors in EEG-based BCI systems. However, many individuals have difficulty in getting used to the feel of motor imagery because most people do not easily recognize how they

can have a concrete feeling of motor imagery. Therefore, the author proposed a neurofeedback-based motor imagery training system based on the developed real-time cortical rhythmic source imaging system, with the expectation that the motor imagery training system can help individuals to easily get the concrete feeling on the motor imagery. In the experiment, half of 10 human volunteers, who had no prior experience of BCI experiments, were asked imagine either left or right hand movement while they were watching their cortical activation maps through the real-time monitoring system. During the experiment, the participants were asked to continuously try to increase their mu rhythm activations (8–12 Hz) around the sensorimotor cortex areas. The author then investigated changes in the EEG signals recorded before and after motor imagery training to demonstrate the effect of the motor imagery training system. The other five control participants did not had any motor imagery training and the changes in the EEG signals recorded before and after a 30-min break were investigated. The detailed processes of motor imagery training, experimental procedures, and results will be found in Chapter 4 of this dissertation.

The author also developed a real-time cortical functional connectivity imaging system capable of monitoring and tracing temporal changes in source-level connectivity between different regions of interest (ROIs) on the cortical surface, after the simple modification of the real-time cortical rhythmic activity motoring system. To implement this system, scalp EEG signals were converted into frequency domain data-sets in real-time and mapped onto cortical source space by applying frequency

domain inverse estimation. Then, the cortical signals were spatially grouped for each ROI and analyzed in order to find the correlations among the ROIs. To demonstrate the feasibility of the implemented system, the author performed three test experiments in which the author monitored the changes in cortical functional connectivity patterns while participants were performing different tasks. The experimental procedures and results for each test experiment will be fully presented in Chapter 5 of this dissertation.

Lastly, the cortical source imaging method was applied to decoding various mental states in order to more accurately interpret individuals' intentions. Eight participants took part in this mind reading study, and performed four different mental tasks. EEG signals recorded for each mental task were firstly transformed into the frequency domain using the fast Fourier transform (FFT), and the spectral power at each cortical region of interest (ROI) is calculated using preliminarily constructed inverse operator. Then, the author constructed two-dimensional spatiospectral pattern maps, consisting of quantized event-related synchronization (ERS) and event-related desynchronization (ERD) values evaluated at every combination of ROI and frequency bin. A similarity between the spatiospectral pattern maps was evaluated by computing the inner-product of two pattern matrices and was then used to classify the current mental states; the resultant classification accuracy was also compared to that of the same analysis method using raw EEG signals. The detailed mental state

classification method and experimental results will be found in Chapter 6 of this dissertation.

Chapter 2: Electroencephalography (EEG)

This chapter briefly introduces basic knowledge on electroencephalography (EEG) that will help readers to understand this dissertation. Section 2.1 describes how neurons generate brain signals capable of being measured on the surface of the scalp. Section 2.2 introduces how EEG activity is recorded on the surface of the scalp. Finally, Section 2.3 introduces five brain waves divided based on frequency and explains their characteristics associated with mental states and brain functions.

2.1. Source of EEG

Neurons in the human cerebral cortex are electrically excitable cells that process and transmit information by means of electrical signals and thus enable the electrical recordings of their activity.

Figure 2.1 depicts the structure of a cortical neuron. A cortical neuron largely consists of three main parts: the dendrites, the soma, and the axon. The dendrites of the neuron are cellular extensions with many branches and receive the electrical signals from upstream neurons via synapses. The soma containing the nucleus of the neuron is the central part of the neuron at which the electrical signals from the

dendrites are joined and passed on. The axon is a long and slender projection that carries the electrical signals away from soma.

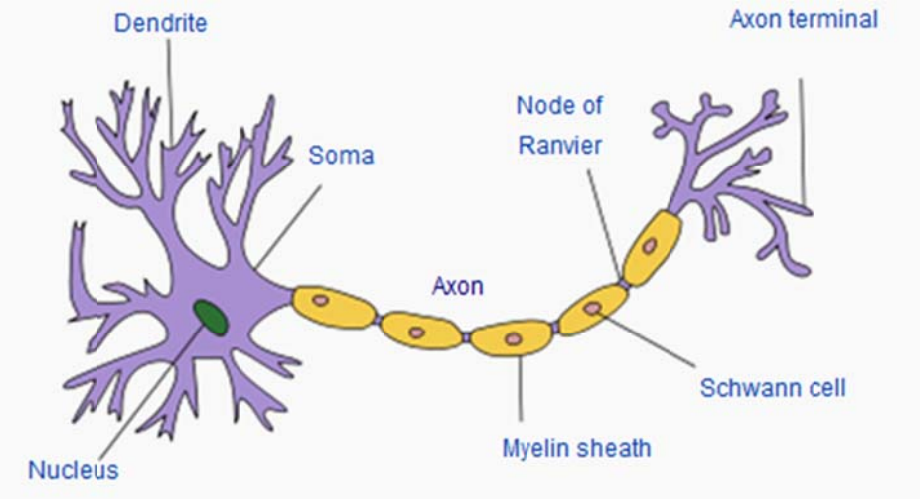

Figure 2.1. Schematic structure of a cortical neuron (source: www.wikipidea.org).

Figure 2.2 shows the arrangement of the cortical neurons generally called pyramidal neurons. As described in the Figure 2.2, the apical dendrites of the pyramidal neurons are parallel to each other, and perpendicular to the cortical surface. The electrical potentials generated by single pyramidal neurons are too small to be detected extracellularly on the scalp. However, if thousands or millions of neurons are activated synchronously, the sum of the synchronous activity can be measurable on

the scalp using electrodes. The recorded electrical signals on the scalp are generally called ‘electroencephalography (EEG)’.

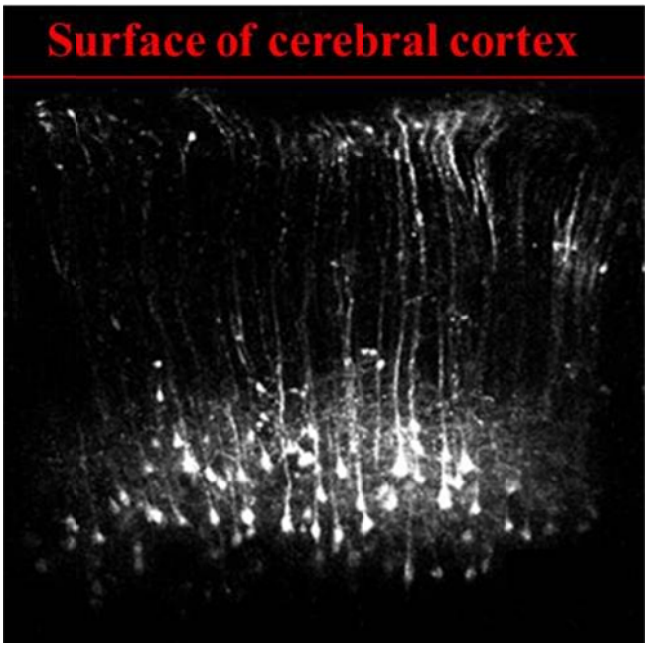

Figure 2.2. Pyramidal neurons’ arrangement along the cortical surface.

2.2. Measuring Method

EEG activity can be measured by placing electrodes on the surface of the scalp with a conductive gel or paste. Figure 2.3 shows an example of an electrode cap used in EEG recording systems. Electrodes are embedded in the cap that is flexible to fit into individuals' head shape.

As for the electrode configuration, the international 10–20 system has been widely used as an international standard, where electrodes are placed at 10 and 20% fractions of the distances between anatomical landmarks of the skull, being nasion, inion, and the pre-auricular points. Figure 2.4(a) and 2.4(b) show the electrode configuration for the international 10–20 system. EEG activity can be measured at 21 electrode positions guided by the international 10–20 system. Additional electrodes can be placed to the standard set-up when some clinical and research applications demand more electrodes. Figure 2.4(c) shows the electrode configuration for the extended 10–20 system (or 10–10 system) in which intermediate 10% electrode positions are used and 75 electrodes can be used for EEG recording.

Figure 2.3. A typical electrode cap used in EEG recording systems (source: www.neuroscan.com).

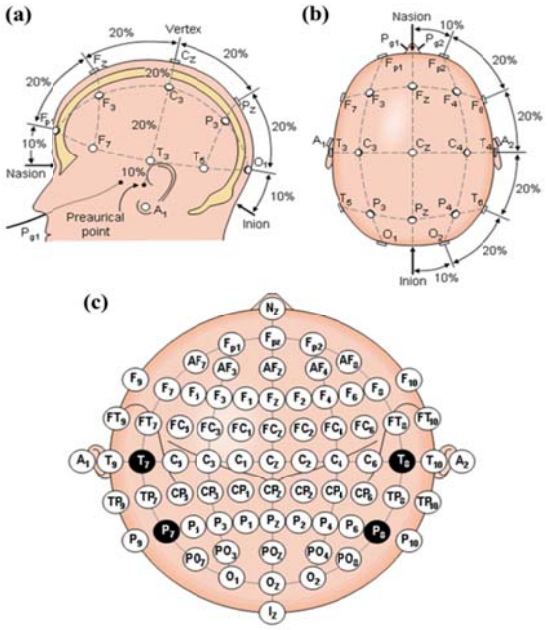

Figure 2.4. The (extended) international 10-20 system for electrode positioning: (a) left view and (b) top view for the international 10-20 system, (c) top view for the extended international 10-20 system. The letters A, F, T, C, P, and O stand for Ear lobe, Frontal, Temporal, Central, Parietal, and Occipital, respectively (source: http://www.bem.fi/book/13/13.htm#03).

2.3. Rhythmic EEG Activity

Neuronal networks can reflect different states of neural synchrony and thereby scalp EEG shows rhythmic oscillations at different frequencies: delta (0–4 Hz), theta (4–8 Hz), alpha (8–13Hz), beta (13–30 Hz), and gamma (30–100 Hz). It has been well established that EEG signals of each frequency band are tightly associated with different states of brain functioning.

A delta rhythm has a frequency of 4 Hz or below. It is the slowest wave and has the highest amplitude as compared to other brain rhythms. The delta rhythm is associated with sleep stages 3 and 4 that are the deepest stages of sleep. It has been also found that the delta wave is also observed during some continuous attention tasks [18].

A theta rhythm has a frequency of 4 to 8Hz and is classified as ‘slow’ brain activity. It is generally seen in young children and in drowsiness or arousal in older children and adults. The theta rhythm is associated with spatial navigation [19] and creative states [20]. It has been also found that the theta rhythm is involved in conducting working memory task [20, 21] and the author confirmed this phenomenon by monitoring theta band connectivity changes during working memory task in this dissertation (see Chapter 5 for details).

An alpha rhythm is a pattern of neural oscillation with a frequency range of 8–13 Hz. Since the alpha rhythm is usually seen in the posterior regions of the head, it is also called the ‘posterior basic rhythm’ or ‘posterior alpha rhythm’. The alpha rhythm significantly appears when closing the eyes, and disappears when opening the eyes [22, 23]. This phenomenon was also observed by the author in the verification experiments of the real-time cortical activity monitoring system (see Chapter 3 for more details). In addition to the posterior basic rhythm, there is another alpha wave that is called the mu rhythm (8-12 Hz) related to motor actions. Since the mu rhythm can be voluntarily modulated by the imagination of the motor actions [24], it has been widely used in realizing brain-computer interface (BCI) systems. In this dissertation, various experiments related to the mu rhythm were conducted and will be introduced in Chapter 3, 4, and 5.

A Beta rhythm occurs with a frequency between 13 and 30 Hz and has relatively low amplitude. It has been revealed that the beta rhythm is associated with normal waking consciousness [25] and motor behavior along with the mu rhythm [24]. In this dissertation, the author demonstrates the characteristics of the beta rhythm with respect to power and functional connectivity changes during real and imaginary motor tasks and the detailed contents will be presented in Chapter 4 and 5.

A gamma rhythm is the fastest brain wave with a frequency between 30 to 100 Hz. It was difficult to record the gamma wave before the development of digital EEG

systems, and the gamma wave was initially regarded as a noise. However, some research results have suggested that the gamma wave is associated with conscious perception [26] and cognitive task execution [27-29]. This fact is also verified by the author in the real-time cortical functional connectivity (see Chapter 5) and mind reading (see Chapter 6) studies.

Chapter 3: An EEG-based Real-time Cortical Rhythmic Activity Monitoring System

This chapter describes the technical details of the developed real-time cortical rhythmic activity imaging method and how the method was successfully applied to a real-time cortical rhythmic activity monitoring system.

3.1. Methods

3.1.1. Concept of a Real-time Cortical Rhythmic Activity Monitoring System

The suggested real-time cortical rhythmic activity monitoring system consists of three parts: (1) data acquisition; (2) pre-processing; (3) processing and visualization. Figure 3.1 shows a schematic diagram to elucidate the concepts of the suggested system.

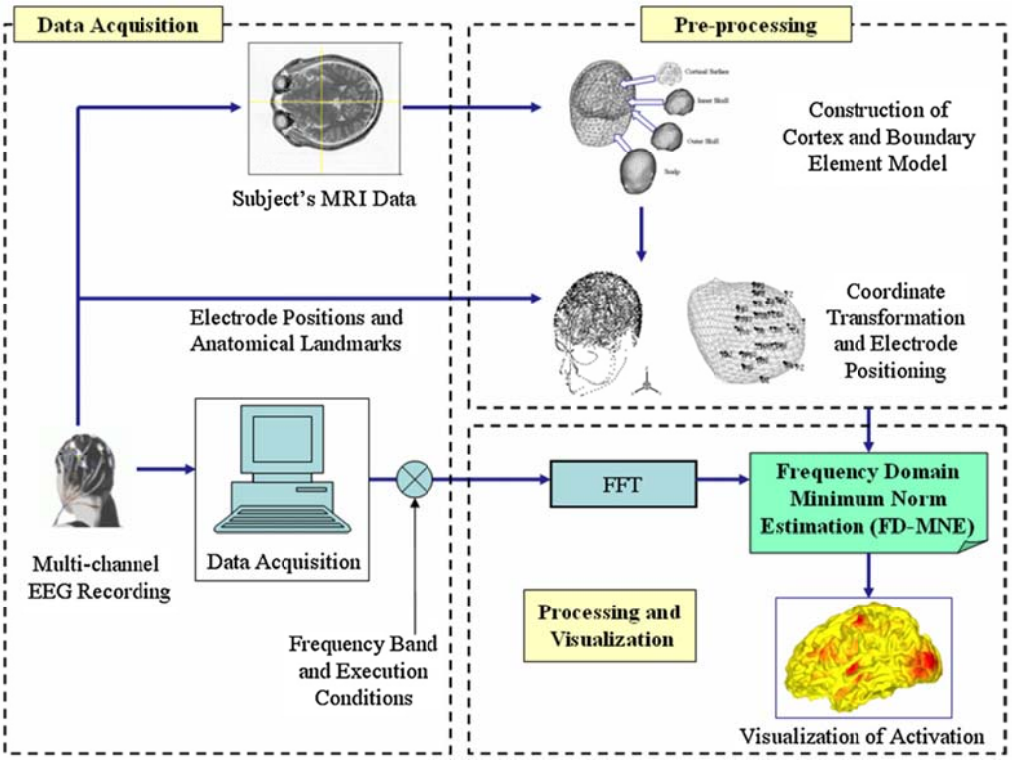

Figure 3.1. Schematic diagram to elucidate the concept of the real-time cortical activation monitoring system.

In the data acquisition part, a subject's structural magnetic resonance imaging (sMRI) data are acquired prior to the EEG data recording. In the present simulation and pilot studies, however, MNI standard brain (http://www.mrc-cbu.cam.ac.uk/Imaging/Common/mnispace.shtml#evans_proc) was utilized instead of the subject's sMRI, since the individual subject's sMRI data were not available. After multi-channel EEG electrodes are attached on the subject's scalp, the relative

locations of electrodes and important anatomical landmarks are measured using a 3D digitizer system. The sMRI data and electrode configurations are then transferred to the pre-processing part.

The pre-processing part plays a role in constructing an inverse operator in which the subject's anatomical information is reflected. Once the linear inverse operator is constructed and saved to a data-storage unit, spatiotemporal changes of cortical rhythmic activities can be monitored in real-time by means of a unified processing and visualization part.

The processing and visualization part is composed of three independent programs– the FFT program, the frequency domain minimum norm estimation (FD-MNE) solver and the visualization program– which are executed one after the other at each time slice.

3.1.2. Forward Calculation and Inverse Estimation

In the present system, a realistic geometry head model was used for accurate EEG forward calculation [30, 31]. A fist-order node-based boundary element method (BEM) was applied to construct a lead field matrix which relates source locations to scalp electrodes. In the present study, three-layer tessellated boundary surfaces, consisting of inner and outer skull boundaries and scalp surface, were generated using

CURRY5 for windows (Compumedics, Inc., El Paso, TX) from structural MRI data. As stated in the previous section, for all studies, MNI standard brain was utilized. The relative conductivity values of the brain, skull and scalp were assumed to be 1, 1/16 and 1, respectively [32, 33]. Coordinate transformation and electrode positioning were performed using in-house software 'BioEST', developed in the Computational Neuroengineering Laboratory of Hanyang University (http://cone.hanyang.ac.kr).

Since synchronously activated pyramidal cortical neurons, which are located perpendicularly on the cortical surface, are widely believed to be the main EEG and MEG generators, many recent studies have adopted this physiological phenomenon as a basic anatomical constraint in EEG or MEG source imaging [34-37]. The source imaging with such an anatomical constraint, which has often been called cortically distributed source model or cortical source imaging, resulted in the elimination of spurious sources [34] as well as the reduction of crosstalk distribution [38], compared to conventional volume based imaging techniques.

To impose the anatomical constraint, many dipolar sources are placed on the cortical surface extracted and tessellated from structural MRI data. Although development of medical image processing and high-resolution structural MRI enabled us to obtain a high resolution cortical surface with sub-millimeter modeling errors [39], it is computationally inefficient to use whole cortical surface vertices for the source reconstruction purpose because of the increased underdetermined relationship

between the limited numbers of sensors and the larger numbers of source locations. Therefore, to reduce the number of possible cortical source locations, we first inflated the cortical surface [40] and generated a down-sampled epi-cortical surface. For the extraction and tessellation of the cortical surface models, we applied *Brain Suite* developed in the University of Southern California, CA, USA [41].

In the present study, about 1000 vertices were down-sampled from more than 400,000 original cortical vertices. Figure 3.2 shows the processes for generating the cortical source space from standard brain MRI data. Figure 3.2(a) and (b) show the original and inflated cortical surfaces, respectively. Figure 3.2(c) shows down-sampled cortical surface on which equivalent dipole sources are placed and Figure 3.2(d) shows the complete boundary element models on which 99 electrodes are attached. Since we used the inflated cortical surface model as the source space, the source orientation constraint was not imposed.

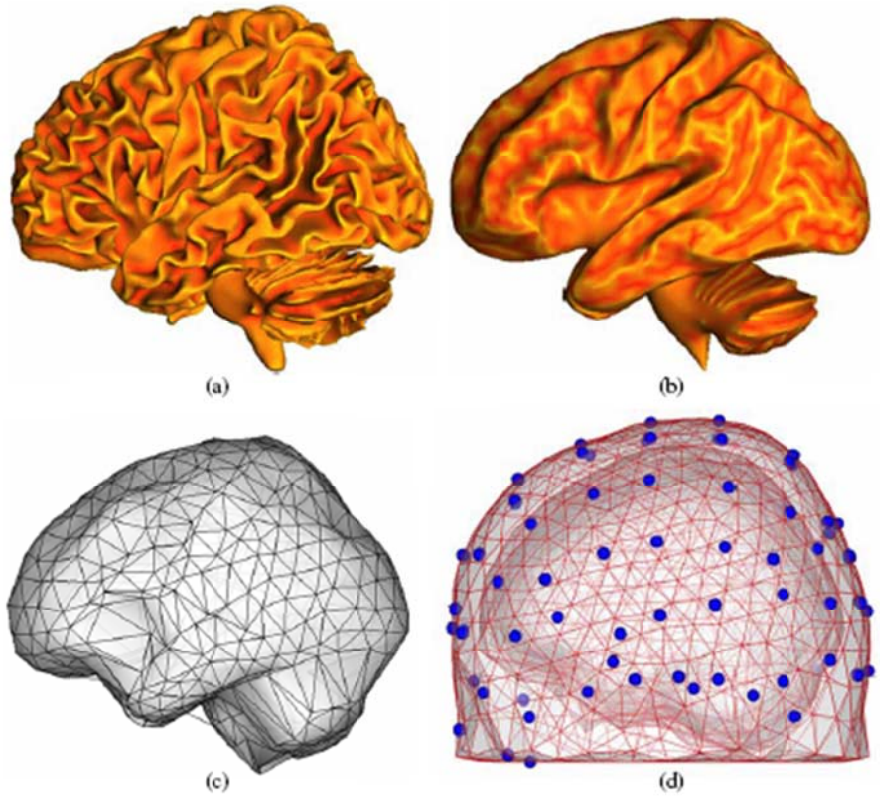

Figure 3.2. Generation of cortical source space and boundary element model: (a) original tessellated cortical surface; (b) inflated cortical surface; (c) down-sampled cortical surface model; (d) boundary element model with 99 electrodes. The colors in (a) and (b) represent the distribution of sulci and gyri.

To reconstruct the cortically distributed brain sources, we used a linear estimation approach [14, 37]. The expression for the inverse operator W is

$$W = RA^T (ARA^T + \lambda^2 C)^{-1}, \tag{3.1}$$

Where A is a lead field matrix which represents the impulse response of each source vector component at every measurement site [42], R is a source covariance matrix representing the inter-source relationship, which is hardly estimated without using intracranial recordings and C is a nose covariance matrix. If we assume that both R and C are scalar multiples of the identity matrix, this approach becomes identical to minimum norm estimation [43]. In this study, the source covariance matrix R was assumed to be a diagonal matrix, which means that we ignored the relationships between neighboring sources. The lead field weightings were imposed on the lead filed matrix to compensate for the sensitivity difference according to the source depth [44]. In this study, the background environmental noise acquired before attaching electrodes on the subject's scalp was used to calculate C [14]. λ^2 is a regularization parameter and determined systematically using the following equation [14]:

$$\lambda^2 = \frac{trace\,(ARA^T)}{trace\,(C)\,SNR^2}, \tag{3.2}$$

where trace($\cdot$) and SNR represent the sum of diagonal terms and the signal-to-noise ratio, respectively. The signal-to-noise ratio could be determined after some preliminary recordings of continuous EEG signals.

3.1.3. Processing and Visualization

The processing and visualization part is composed of three independent programs– the FFT program, the frequency domain minimum norm estimation (FD-MNE) solver and the visualization program– which are executed one after another at each time slice. At a certain time slice, time domain signals in 2^N data samples before the time slice are transformed into frequency domain signals using a self-executable, in-house FFT program coded based on Netlib library routines (http://www.netlib.org). The number N could be modified by users (e.g. N = 7, 8, 9 and 10) according to their purpose of using the monitoring system. In the present study, we used N = 7 for all simulation and pilot studies. Once a specific frequency band is determined, the FFT program stores real and imaginary components at all discrete frequencies within the predetermined frequency band to an ASCII data file. Then, the FD-MNE solver is executed and load the Fourier transformed signals $B(f_i)_{\mathrm{Re}}$ and $B(f_i)_{\mathrm{Im}}$, $i = 1,2,...,n$, where Re and Im represent the real and imaginary parts of the Fourier transformed signals, respectively, as well as the pre-saved inverse operator W. The real part $q_j(f_i)_{\mathrm{Re}}$ and imaginary part $q_j(f_i)_{\mathrm{Im}}$ of the current source vector at the jth cortical vertex with respect to the frequency of interest f_i can then be evaluated by multiplying the corresponding rows ($3j-2$, $3j-1$ and $3j$th rows) in W with the Fourier transformed signals $B(f_i)_{\mathrm{Re}}$ and $B(f_i)_{\mathrm{Im}}$. Finally,

the absolute current source power at the j th cortical vertex with respect to the frequency band of interest is calculated as

$$Q_j = \frac{1}{2n} \sum_{i=1}^{n} (\left\| q_j(f_i)_{\mathrm{Re}} \right\|^2 + \left\| q_j(f_i)_{\mathrm{Im}} \right\|^2), \tag{3.3}$$

This process is equivalent to the conventional frequency domain minimum current estimates (FD-MCEs) proposed by Jenson and Vanni [1]. While the conventional FD-MCEs have used L1 norm-based nonlinear optimization, the FD-MNE approach used in the present study is based on L2 norm-based linear optimization. We adopted the FD-MNE approach since L1 norm based optimization requires time-consuming nonlinear iteration, which is inadequate for the real-time monitoring system.

After the current source power at every cortical vertex is calculated, a 3D visualization program is executed and visualizes the resultant source distribution at a given frequency band. The visualization program named *MeshViewer*, which was coded with visual C++ under an OpenGL environment, can visualize instantaneous and/or averaged source power changes in real-time from any 3D viewpoints.

3.2. Possibility of the Real-time Cortical Rhythmic Activity Monitoring System: a Preliminary Simulation Study

3.2.1. Simulation Setups and Materials

For the verification of the suggested real-time cortical activation monitoring system, offline simulations which perfectly simulated the suggested system were conducted. Four sets of artifact-free, eye-closed, resting EEG data acquired from two male dementia patients and two normal male subjects were used to show the possibility of the suggested system. The experimental data were acquired in the Department of Neuropsychiatry on Inje University Ilsan-Paik Hospital, Korea. Written informed consent was obtained from the subjects or their close relatives. The control subjects had no history of neurological, psychiatric or other severe diseases. The patients had no history of stroke, head trauma or any other neurological diseases except gradual decline of cognitive functions and memory. The number of electrodes used for the recording was 18 (FP1, F3, C3, P3, Fp2, F4, C4, P4, F7, T7, P7, O1, F8, T8, P8, O2, T1, and T2) and the sampling frequency was 250 Hz. Since the individual subject's sMRI data were not available then, a standard cortex-head model extracted from MNI brain atlas was utilized. For more realistic simulations, the 20 s EEG data were stored preliminarily in a computer memory and were transferred to a signal variable array, one after another at every 4 ms. At a specific time slice, time domain signals in 2^N data samples before the time slice are transformed into frequency

domain signals using the FFT program. We used $N = 7$ and updated the cortical activation maps at every 500 ms (2 image frames s^{-1}). As described before, the linear inverse operator W in (3.1) was preliminarily constructed and stored in the computer. Since we had already constructed the standard cortex-head models, the time required for the construction of the inverse operator was less than 3 min. The simulation study was performed in an Intel® Pentium4–3.4 GHz personal computer system with 1 GB memory.

3.2.2. Results of the Simulation Study

Figure 3.3(a) and 3.3(b) show the cortical alpha activity (8 to 13 Hz) changes in the dementia patients. The figures show cortical activation maps averaged over 20 s as well as instantaneous screenshots of the cortical activity maps at 1, 2 and 3 s. The two patients showed similar activation patterns in both instantaneous and averaged cortical activation maps. Figures 3.4(a) and 3.4(b) show the cortical alpha activity changes in the normal subjects, acquired under the same conditions. Both normal subjects showed very typical cortical activations which are located around the occipital lobe [22, 23], whereas the dementia patients showed additional strong cortical activations around the right temporal and frontal lobes and relatively weak additional activations around the left temporal lobe. Such a clear difference in the cortical activation maps of dementia and normal subjects not only shows that the

suggested real-time cortical activation monitoring system is working well but also demonstrates that the monitoring system can be applied to real-time diagnosis of dementia patients.

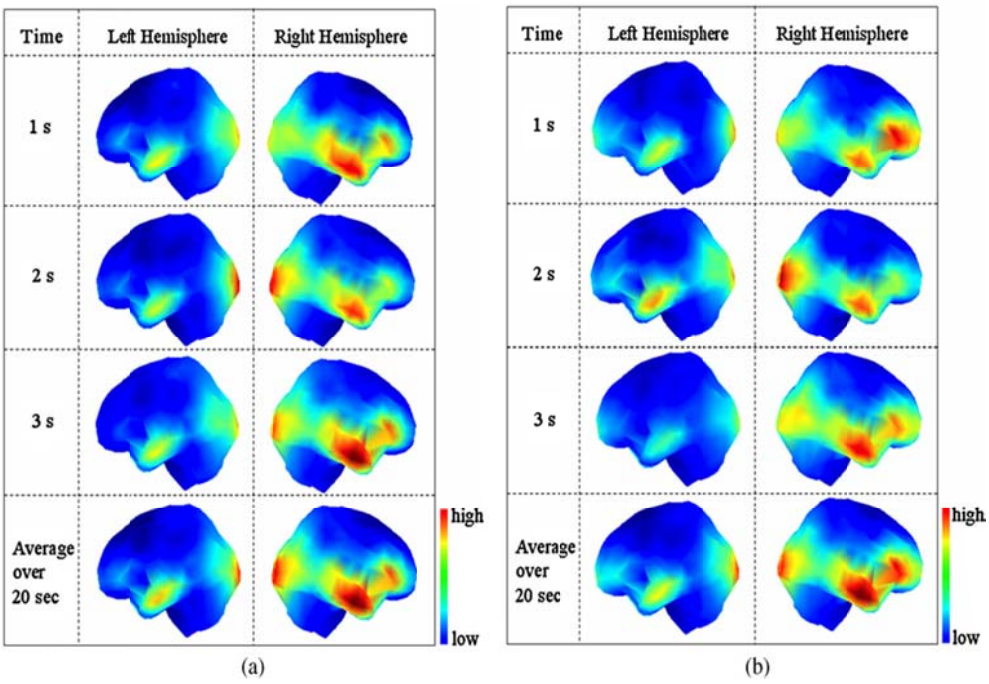

Figure 3.3. Cortical alpha (8-13 Hz) activity changes of dementia patients during a resting EEG recording: (a) dementia patient #1; (b) dementia patient #2.

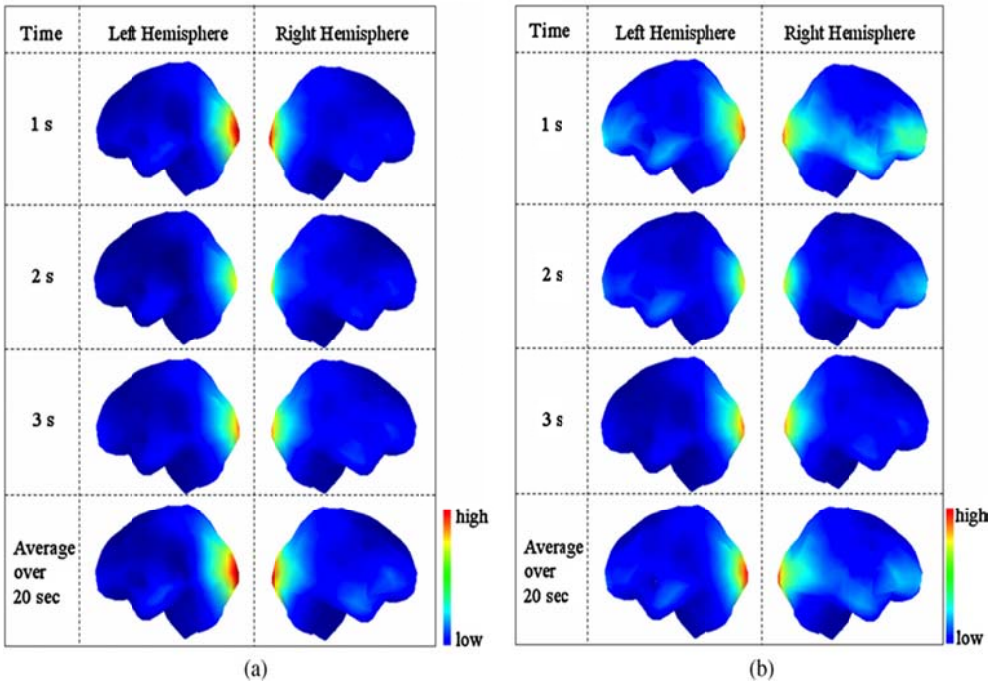

Figure 3.4. Cortical alpha (8-13 Hz) activity changes of normal subjects during a resting EEG recording: (a) control subject #1; (b) control subject #2.

The most important issue in realizing the real-time cortical activation monitoring system is to reduce the delay time. Short delay time implies that one can get more cortical activation images during limited acquisition time. In the present simulation study, therefore, some factors influencing the delay time were investigated.

The simulation study was performed in an Intel® Pentium4–3.4 GHz personal computer system with 1 GB memory. The operating system was Microsoft Window XP® and the main program including FFT and FD-MNE was executed in the

command consol window. The independent visualization software was executed at the first execution and just refreshed at each image frame without closing or opening. During the test, no applications, including virus vaccine, were executed to reduce the system load. For the measurement of the delay time, an intrinsic Fortran function ‘date_and_time()’ was used. The FFT program and the main FD-MNE program were executed repeatedly and each execution time was averaged over 100 times. We could obtain minimal delay time when 128 data samples were used and the source distribution was reconstructed at a single frequency. Then, the execution of the FFT program and the FD-MNE took 43.9 and 94.5 ms, respectively. The maximal computational load was required in the present study when we repeated source imaging with 1024 data samples within the whole frequency band of interest (0–30 Hz). Then, the execution times for FFT and FD-MNE were measured as 59.5 and 128 ms, respectively. When considering about 8-times bigger data size and 123-times more matrix multiplications, the increment of delay time was not significant. The delay time was monotonically increased by the increment of the number of data samples or the number of frequencies of interest. The intrinsic delay time for each program was originated from the CPU time needed for executing programs and time for loading and saving data files. The average time taken to execute the visualization program was 15 ms. Thus, this analysis points out that cortical rhythmic source changes can be monitored at the cortical level with a maximal delay time of about 200 ms when 18 channel EEG data are analyzed.

For comparison, we also repeated the source imaging with 1024 data samples within the whole frequency band of interest (0–30 Hz), for 32-channel EEG data acquired from a different EEG recording system (WEEG-32, Laxtha Inc., Korea). Then, the execution times for FFT and FD-MNE were measured to be 62.7 and 137 ms, respectively, suggesting that the increment of recording channels does not highly affect the overall delay time.

3.3. A First Pilot System: Experimental Results

The first pilot system for the EEG-based real-time cortical rhythmic activity monitoring was implemented at the Bioelectromagnetics and Neuroimaging Laboratory of Yonsei University. The EEG was recorded at 16 electrode locations (Fpz, F3, C3, P3, F4, C4, P4, T7, P7, O1, Cz, T8, P8, O2, T1, and T2) using the WEEG-32 EEG acquisition system (Laxtha Inc., Daejeon, Korea). The electrodes were attached on the subject's scalp according to the extended 10–20 system without using an electrode cap. The EEG was sampled at 256 Hz and the low- and high-pass filters were set at 64 and 0.5 Hz cutoffs, respectively. The recorded EEG signals were transferred to an operating computer in real-time and the values were stored in a two-dimensional array variable. The acquisition program was coded in the laboratory using C++. Since the individual subject's sMRI data were not available then, a standard cortex-head model extracted from MNI standard brain atlas was utilized to construct the inverse operator. At a specific time slice, time domain signals in 128 data samples before the time slice are transformed into frequency domain signals using the FFT program. We updated the cortical activation maps at every 250 ms (4 image frames s^{-1}).

Two male subjects (YJ and JJ, 26 and 24 years old respectively) volunteered to participate in the test experiments in exchange for monetary compensation. Written

informed consent was obtained from the subjects, who had no history of neurological, psychiatric or other severe diseases.

The first subject (YJ) was asked to be relaxed, sitting on a comfortable seat. After the experimental setup is ready, he opened or closed his eyes according to the experimenter's instructions. Figure 3.5 shows a photograph of the first experiment, where the EEG acquisition system is hidden, as well as two screenshots of the cortical alpha activity (8 to 13 Hz) changes by the subject's eye closing. When the subject closed his eyes, a gradual increment of cortical activations around the occipital lobe was clearly observed, coinciding well with the results of previous studies [22, 23].

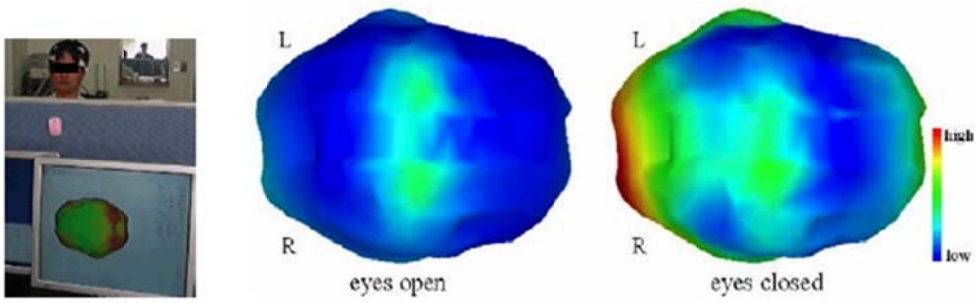

Figure 3.5. Cortical alpha (8-13 Hz) activity changes of subject YJ: The left figure shows a photograph of the experiment; the center and right figures show the alpha activity changes when the subject opened and closed his eyes, respectively. Cortical activity maps are viewed from top. 'L' and 'R' represent 'left' and 'right', respectively. Values in the source images were normalized to a predetermined threshold which was obtained from some preliminary experiments.

The other subject (JJ) was asked to slowly raise his right or left arms according to the experimenter's instructions, while opening his eyes. Figure 3.6 shows a photograph of the second experiment as well as two screenshots of the cortical mu activity (8–12 Hz) changes by the subject's arm movements. An ipsilateral activity around motor cortex was observed, which is consistent with previous reports [45, 56]. The results of both experimental studies coincided well with known physiological phenomena, demonstrating the feasibility of the pilot real-time cortical rhythmic activity monitoring system.

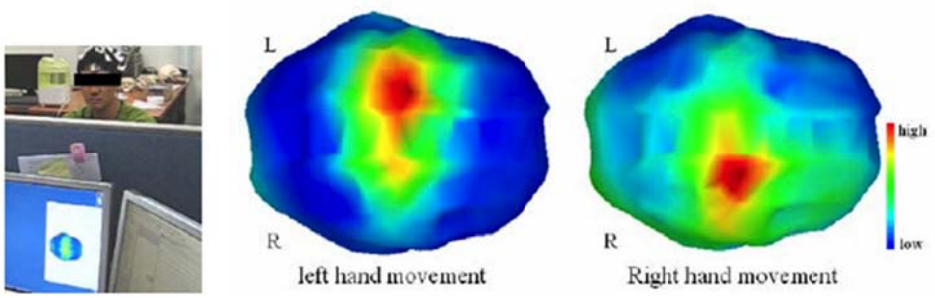

Figure 3.6. Cortical alpha (8-12 Hz) activity changes of subject JJ: The left figure shows a photograph of the experiment; the center and right figures show the mu activity changes when the subject raised his left and right hand, respectively. Cortical activity maps are viewed from top. 'L' and 'R' represent 'left' and 'right', respectively. Values in the source images were normalized to a predetermined threshold which was obtained from some preliminary experiments.

3.4. Discussions and Summary

In the present study, we implemented a real-time cortical rhythmic activity monitoring system which can monitor spatiotemporal changes of cortical rhythmic activity on a subject's cortical surface with high temporal resolution. In the present system, a frequency domain inverse operator was constructed *a priori* and the spectral current power at each cortical vertex was then calculated for the Fourier transforms of successive sections of continuous data. An offline simulation study as well as experimental validation studies demonstrated that cortical rhythmic source changes can be monitored at the cortical level with a maximal delay time of about 200 ms.

For the simulation study, we have used four sets of artifact-free, eye-closed, resting EEG data acquired from two dementia patients and two normal male subjects to show the possibility of the suggested system. The preliminary offline analysis yielded promising results, suggesting that the real-time cortical activation monitoring system can be potentially used for the real-time diagnosis of psychiatric brain diseases such as dementia and schizophrenia. Application of the 'online' cortical activity monitoring system to the real-time diagnosis of psychiatric brain diseases will be performed in our future studies. For the experimental study, cortical alpha rhythm changes by closing eyes and cortical mu rhythm changes by arm movements were observed, which were consistent with previous reports.

Another possible application of the real-time cortical activation monitoring system is the EEG-based brain computer interface (BCI) system. Although such a system has not been realized yet, some offline simulation studies already demonstrated that the use of inverse solutions could enhance the classification capability of the EEG-based BCI system [45-47]. As already introduced in the introduction section, the real-time cortical activation monitoring system can be applied to neurofeedback systems in order to enhance the efficiency of detecting the current mental status of a subject. Moreover, the suggested real-time cortical activation monitoring system can be used for online monitoring of EEG experiments regarding various cognitive and functional brain studies. The experimenter can modify the experimental protocols without stopping the on-going measurement with the aid of the suggested system.

Chapter 4: Neurofeedback-based Motor Imagery Training for Brain-Computer Interface (BCI)

In this chapter, the author introduces an effective motor imagery training system for brain-computer interface (BCI) as one of the applications of the real-time cortical rhythmic activity monitoring system described in Chapter 3.

4.1. Research Background

There are a great numbers of disabled individuals who cannot freely move or control specific parts of their body because of serious neurological diseases such as amyotrophic lateral sclerosis (ALS), brainstem stroke, and so on. Brain-computer interfaces (BCIs) can help them to drive and control external devices using only their brain activity, without the need for physical body movements [48].

Diverse types of electrical brain activities have been used to realize electroencephalography (EEG)-based BCI systems, e.g., mu rhythm [45, 49-52], slow cortical potential [53], event-related p300 [54, 55], and steady-state visual evoked

potential [56, 57]. Among these activities, the one most widely used to monitor brain activities for BCI applications has been the mu (μ) rhythm, which is related to motor actions [49, 58-60]. The mu rhythm can be voluntarily modulated by individuals unlike event related brain activities.

Motor imagery, defined as mental simulation of a kinesthetic movement [16, 17], can also modulate mu rhythm activities in the sensorimotor cortex without any physical movements of the body. It has been well established that the imagination of each left and right hand movement results in event-related desynchronizaion (ERD) of mu-band power in the contralateral sensorimotor areas, which is also the case for physical hand movements [61, 62]. Brain activities modulated by motor imagery of either the left or right hand are regarded as good features for BCIs, because such activities are readily producible and show consistent EEG patterns on the sensorimotor cortical areas [63, 64]. Moreover, thanks to the contralateral localization of the oscillatory activity, the activities evoked from left and right hand motor imagery are, comparatively, readily discriminated [45, 65, 66]. However, many individuals have difficulty in getting used to the feel of motor imagery, since most people do not easily recognize how they can have a concrete feeling of motor imagery and tend to imagine the images of moving their hands or legs instead [67]. Therefore, one of the challenging issues in the EEG-based BCI studies has been how one can efficiently train individuals to perform motor imagery tasks.

Over the last decade, various feedback methods for motor imagery training have been proposed, most of which are based on visual [49, 52, 68] or auditory feedbacks [69, 70]. For example, suppose that a participant is instructed to perform a motor imagery task involving their left or right hand. Then, reference features of brain activities evoked from the left and right hand motor imagery are extracted and the participants' intentions are classified by comparing the reference features with the current features. The participants are then provided with visual or auditory feedback according to the classification results. However, some participants cannot generate more useful features in their sensorimotor cortex after motor imagery training processes, compared to the features extracted before the training [49, 55, 70]. One typical reason to explain the wrong motor imagery is that participants tend to imagine visual images of the movement (visual-motor imagery: VMI), which generates a type of brain activity pattern completely different from that of actual motor imagery [67]. Therefore, even when participants attempt the same motor imagery task, individual differences are often observed, because the results are dependent on their feelings and perception on the motor imagery task, as described by Annett [71].

The goal of the present study was to develop a motor imagery training system that can help individuals easily get the feel of motor imagery. To this end, the author utilized the real-time cortical rhythmic activity monitoring system introduced in Chapter 3, and participants trained themselves to be accustomed to motor imagery while they were monitoring their time-varying cortical activation maps in real-time.

4.2. Materials and Methods

Our experiments consisted of two sessions: motor imagery training session and EEG recording sessions. In the motor imagery training session, the participants were trying to increase their mu rhythm activations around the sensorimotor cortex while they were watching their cortical activation maps through the real-time rhythmic activity monitoring system. Two EEG recordings were performed each before and after the motor imagery training session to demonstrate the effect of our neurofeedback-based motor imagery training system.

4.2.1. Participants and Environment of Experiments

Ten healthy volunteers (all male, all right handed, age 25.1 ± 1.97 years) took part in this study. None of the participants had a previous history of neurological, psychiatric, or other server diseases that may otherwise influence the experimental results. We gave a fully detailed summary of the experimental procedures and protocols to each of the participants before the experiment. All participants gave written consent and received adequate reimbursement for their participation. The study protocol was approved by the Institutional Review Board (IRB) committee of Yonsei University in Korea. None of the participants had previous background knowledge or experience with BCIs, nor had they ever participated in EEG experiment. All experiments were conducted in the Bioelectromagnetics and

Neuroimaging Laboratory of Yonsei University.

Electrodes were attached on the participants' scalp according to the extended international 10-20 system. In the motor imagery training session, the EEG signals were acquired at 16 electrode locations (AF3, FC3, C3, CP3, PO3, FCz, Cz, CPz, AF4, FC4, C4, CP4, PO4, T7, T8, and Oz) using a multi-channel EEG acquisition system (WEEG-32, Laxtha Inc., Daejeon, Korea) in a dimly lit, soundproof room. In the EEG recording sessions, the EEG signals were recorded at 15 electrode locations (Cz, C1, C2, C3, C4, CPz, CP1, CP2, CP3, CP4, FCz, FC1, FC2, FC3, and FC4) covering the sensorimotor area, using the same recording system. The sampling rate was set at 256 Hz in all experiments with a sensitivity of 7 μV. Facial EMG and EOG were also recorded during the EEG recordings and used as references in artifact rejection process.

We used different electrode configurations for the motor imagery training and the EEG recording sessions. In the training session, we used 16 electrodes broadly attached on the participants' scalp because we needed to monitor their brain activity patterns in the whole brain areas including the sensorimotor cortex. On the other hand, in the EEG recording sessions, 15 electrodes were focally attached around their sensorimotor cortex as we were only interested in EEG signals related with motor functions.

4.2.2. Motor Imagery Training

During the motor imagery training sessions five volunteers (EK, GS, DK, KS, and JN) were made to sit on a comfortable armchair facing a 17" monitor and were presented with time-varying maps of their cortical rhythmic activity that were updated every 350ms while they were attempting either left or right hand motor imagery. Figure 4.1 shows screenshots of the experiment, where the subject EK activated his motor cortex without any physical movements of his hands (see Supplementary movie file, http://www.sciencedirect.com/science/article/pii/S0165027009000454). Before the training, we explained to the participants the locations of the sensorimotor cortex and provided them with a movie that explained the expected cortical activation changes. The participants were then instructed to continuously attempt to generate cortical activations around the sensorimotor cortex. In the beginning of the training session, all participants failed to generate brain activities around the sensorimotor cortex; however, through repetitive trials, all participants succeeded in generating brain activity on their sensorimotor cortex without any physical movements. Participants were given 30 min for the motor imagery training.

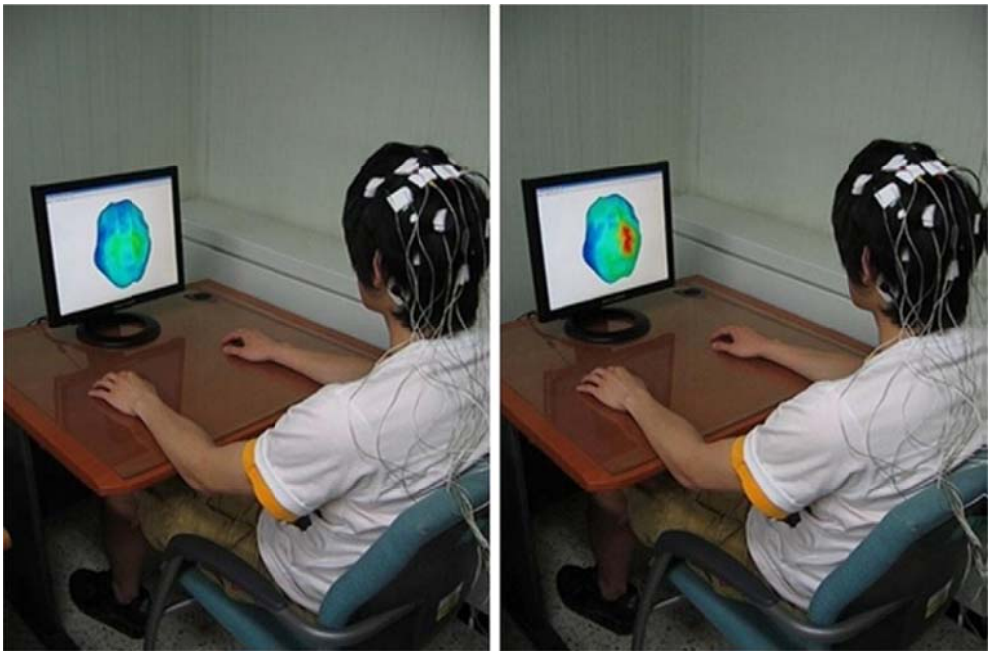

Figure 4.1. Screenshots of real-time mu rhythm activity (8-12 Hz) monitoring. The participant (EK) was instructed to continuously attempt to generate cortical activations around the sensorimotor cortex by imagining his left or right hand movement (see Supplementary movie, http://www.sciencedirect.com/science/article/pii/S0165027009000454). A cortical activation map at rest state (left) and when the participant was performing motor imagery (right).

4.2.3. EEG Data Acquisition

EEG data were acquired before and after the training session to confirm the effect of our motor imagery training system. The whole experiments including the neurofeedback training and the two EEG recordings were conducted on the same day. For the control group participants (JI, BK, HJ, TI and SJ), EEG data were recorded

twice with a 30-min break time. Figure 4.2 shows the experimental paradigm used for the EEG recordings in the present study. First, we used a gray (RGB: 132, 132, 132) background, and after presenting a blank screen for 3 s, a circle with a black-and-white checkerboard pattern appeared randomly on either the left or right side of the screen for next 0.25 s, indicating which hand movement the participant has to imagine. After a 1 s preparation time (blank screen), the letter 'X' appeared at the center of the screen for 0.25 s, at which time, the participant was asked to perform either the left or right hand motor imagery as indicated. This procedure was repeated 180 times: when 90 trials were performed for the right hand motor imagery, the other 90 trials were performed for the left hand motor imagery.

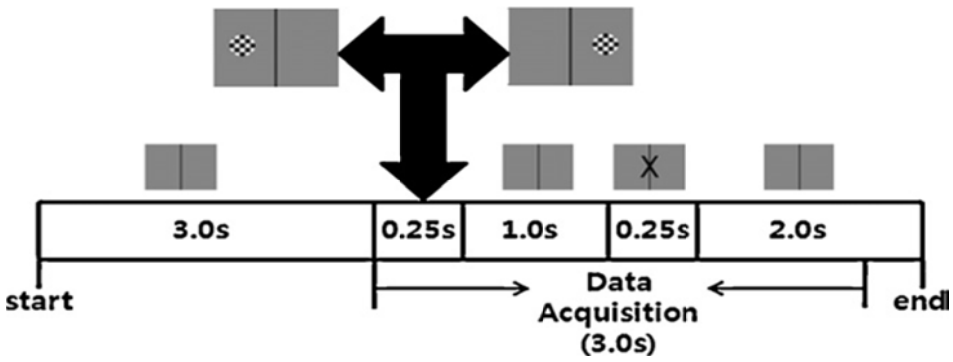

Figure 4.2. The experimental paradigm used for EEG recording: after presenting a blank screen for 3 s, a circle with a black-and-white checkerboard pattern appeared randomly on either the left or right side of the screen for the next 0.25 s, indicating which hand movement the participant was to imagine. After a 1 s preparation time (blank screen), the letter 'X' appeared at the center of the screen and lasted for 0.25 s. At that time, the participant was to

being performing either left or right hand motor imagery. The time period used for the data analysis (3.0 s) is depicted in the figure.

To confirm if the participants physically moved their hands, we also recorded an electromyogram (EMG) from electrodes attached on the participant's both forearms [72] during the EEG recording sessions. Figure 4.3 shows the changes of EMG powers recorded both before and while the participants of the trained group were performing the motor imagery task. No significant difference between the two EMG data sets (less than 10% variations) were found for all five participants, indicating that they did not move their hands when they were attempting to perform the motor imagery task.

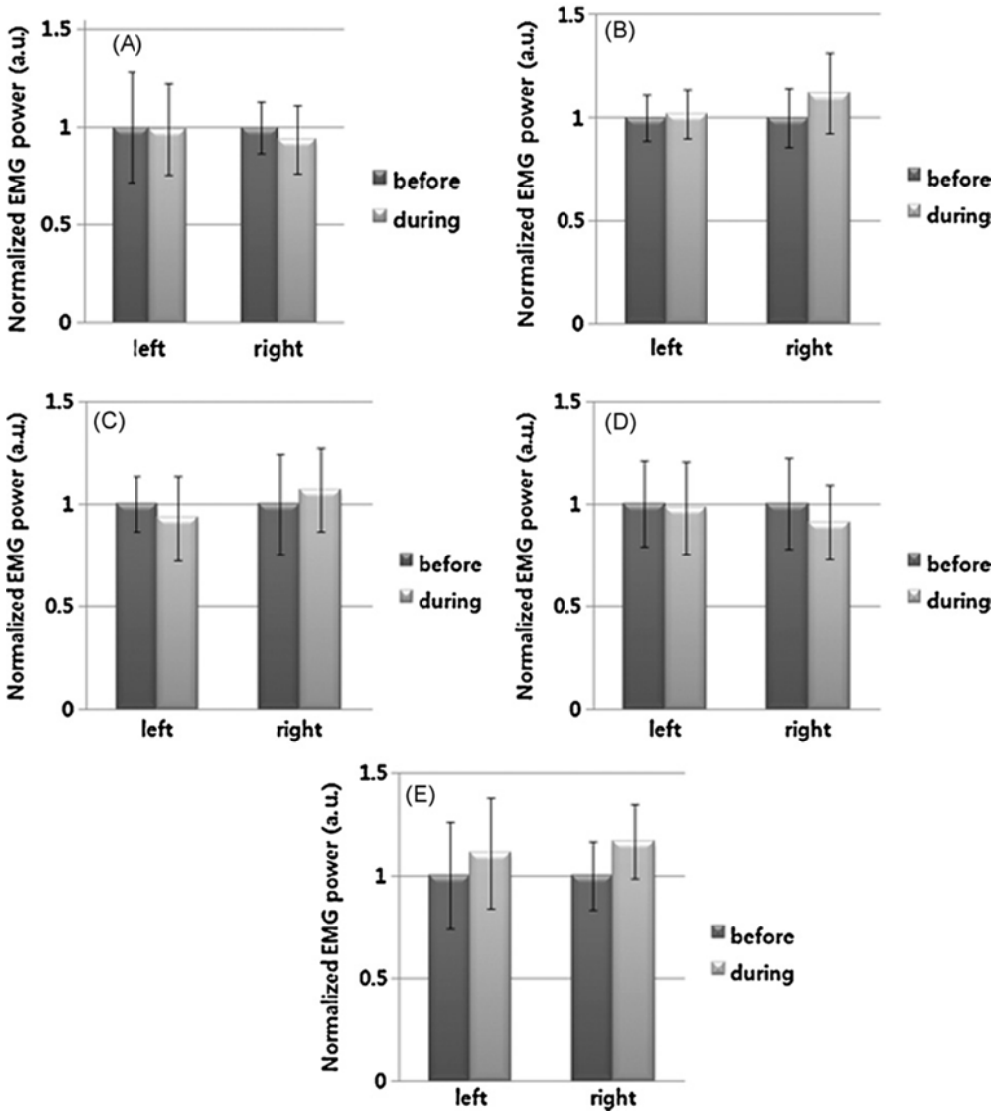

Figure 4.3. Changes in EMG power recorded at both of the participants' forearms before and during performing the motor imagery task. No statistically significant difference between the two EMG data sets (two-tailed paired t-test, $p < 0.05$) was found for all five participants of the trained group, indicating that the participants did not move their hands when they were attempting to perform the motor imagery task. A, B, C, D, and E indicate the EMG power changes of each participant, EK, GS, DK, KS and JN, respectively. In the figure, 'before' and 'during' represent 'before the motor imagery' and 'during the motor imagery', respectively.

4.2.4. EEG Data Analysis

We used the 3.0 s time segment marked in Figure 4.2 for the data analysis because the participant might start the motor imagery before the letter 'X' appeared [45, 65]. After data acquisition, the raw EEG signals were converted to a common average reference (CAR) to compensate for common noise components. The CAR method has been shown to produce good performance in noise reduction along with surface Laplacian filtering [73, 74]. EEG epochs highly contaminated by facial muscle movements were rejected manually by inspecting the simultaneously recorded facial EMG signals. EOG artifacts were not removed since the influence of eye blinks or eye-ball movements upon the EEG channels around the sensorimotor area was not significant.

For the time-frequency analysis we used forth order Butter-worth band-pass filters in which the span of the frequency bands was 2 Hz with a 50% overlapping. The selected frequency bands were 6–30 Hz, including mu and beta bands, which are related to limb movements. After calculating the envelopes of the signals at each frequency bin, a moving average filter was applied to the time domain signals at 400 ms intervals (50% overlapping) to smooth the envelopes. After all, the frequency band and time series were evenly divided into 23 frequency bins and 14 time segments, respectively. We then obtained a time-frequency pattern map by integrating

the enveloped signals at each time segment and frequency bin. Two-tailed *t*-tests were then applied to every possible combination of frequency bins, time segments, and electrodes in order to find combinations that produced significant differences ($p < 0.05$) between left and right hand motor imagery.

To evaluate the classification accuracy, the two time-frequency combinations that had the smallest *p*-value in the time-frequency pattern maps were selected for each participant. Among the 180 trials (90 each for right and left hand motor imagery), 90 trials (45 each for right and left hand motor imagery) were randomly selected and used as a training set, while the remaining motor imagery trails were used as a test set for calculating the classification accuracy. For each trial of the test set, Euclidean distances from the two average feature vectors computed on the reference data sets (45 right and 45 left hand motor imagery trials each) were compared and the trial was assigned to a class based on whichever had the shorter distance.

4.3. Results

4.3.1. Changes in Brain Activity after Motor Imagery Training

Figure 4.4 shows the time-frequency pattern maps for the trained group participants, where the black colored blocks represent time-frequency combinations that showed significant differences ($p < 0.05$) between left and right hand motor imagery. As seen in the figures, where two featured electrodes were selected for each participant, the time-frequency pattern maps did not show any distinguished features before the training session. On the contrary, we observed that the number of the 'black' blocks was increased and the blocks were clustered around the sensorimotor rhythm (around 10 and 20 Hz) after the training session.

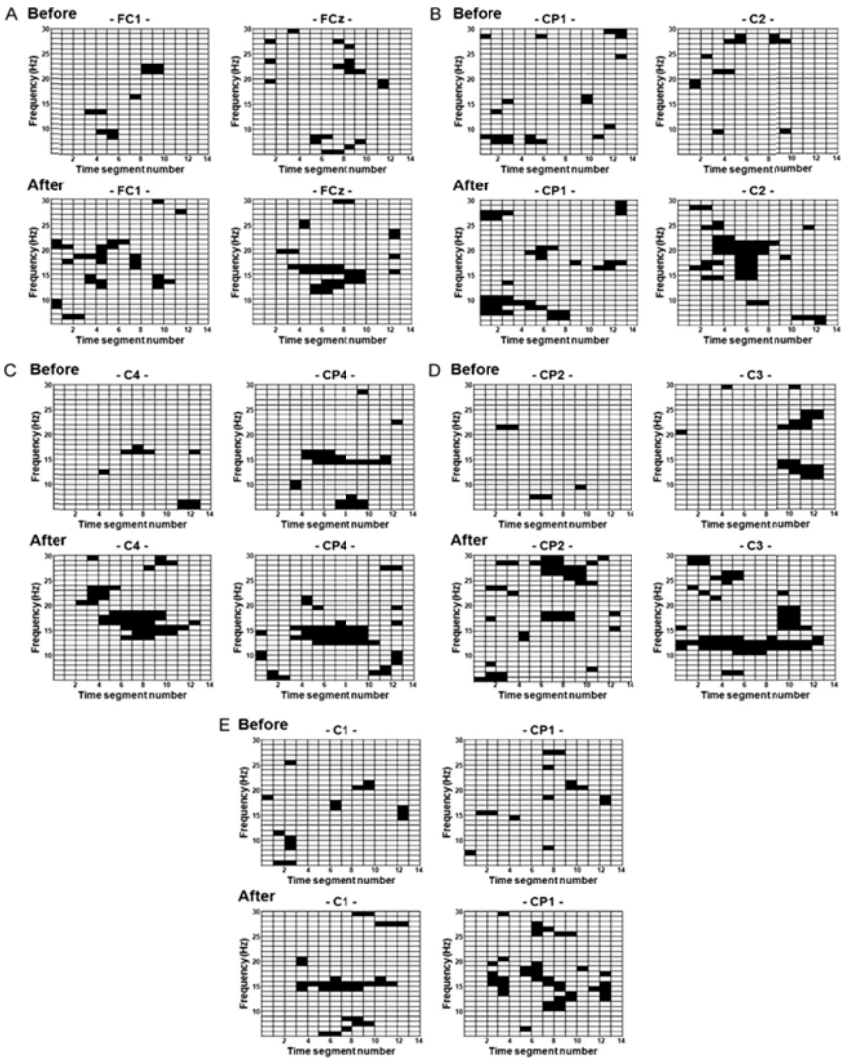

Figure 4.4. Time-frequency pattern maps at the two electrode locations. The black colored blocks represent the time-frequency combinations that showed statistically significant difference ($p < 0.05$) between left and right motor imagery tasks. The time-frequency pattern maps did not show any distinguishable features before the training session, while the number of the 'black' blocks increased and the blocks were clustered around the mu rhythm (around 10 and 20 Hz) after the training session. 'Before' and 'after' represent the time-frequency patterns calculated before the training session and those calculated after the training session, respectively.

Table 1 shows the number of time-frequency combinations that showed significant difference between left and right hand motor imagery, demonstrating that meaningful changes of brain activities occurred in all participants of the trained group after the training session. On the other hand, for the control group, we could not observe any consistent changes in the number of significant time-frequency combinations between the first and second EEG data sets. From these results, we confirmed that it was possible to train participants to generate specific brain activity pattern on the sensorimotor cortex using the proposed system.

Table 4.1. The total number of time-frequency combinations showing a significant difference between left and right hand motor imagery.

Trained Group			Control Group		
Participant	Before	After	Participant	First	Second
EK	220	300	JI	219	207
GS	280	308	BK	269	217
DK	183	275	HJ	379	384
KS	297	446	TI	508	312
JN	275	349	SJ	412	547

'Before' and 'After' represent the number of significant features obtainable before the motor imagery training and after the motor imagery training, respectively. 'First' and 'Second' represent the number of significant features obtainable in the first and second EEG recording sessions, respectively.

4.3.2. Classification Accuracy before and after the Motor Imagery Training

We also investigated the changes in classification accuracy before and after motor imagery training. Table 4.2 shows the accuracy of classifying left and right hand motor imagery of all participants. Since small *p*-values in the time-frequency pattern maps meant that there were significant differences between the left and right hand motor imagery, we selected two time-frequency combinations having smallest *p*-values as the features for classifying left and right hand motor imagery. We found that most of the extracted features corresponded to the mu rhythm which had been used in the neurofeedback training session (frequency bin and electrode in each participant of the trained group– EK: 11–13 Hz in FC1 and 11–13 Hz in C4; GS: 10–12 Hz in FC1 and 9–11 Hz in FC2; DK: 13–15 Hz in FC4 and 13–15 Hz in C2; KS: 12–14 Hz in C3 and 11–13 Hz in C2; JN: 7–9 Hz in C2 and 9–11 Hz in CP3).

A simple Euclidean distance algorithm was then used to estimate classification accuracy. Analysis of the results indicated that the classification accuracy was enhanced considerably for all five individuals in the trained group after the motor imagery training; while the analysis results for the control EEG data set did not show consistent increment in the classification accuracy, demonstrating that the proposed motor imagery training system could be used to enhance the performance of motor-

imagery-based BCI systems. These results have a thread of connection with those of the previous time-frequency analysis, in that the individuals of the trained group were able to generate distinguishable brain activity patterns between the left and right hand motor imagery after a short training session that lasted for 30 min.

To test if the number of features affects the computed classification accuracy, we applied different numbers of features to the same classification algorithm (from 3 to 5). The use of more features enhanced the classification accuracy in most cases, but the difference was not significant and did not affect the findings of our study.

Table 4.2. Changes in classification accuracy before and after motor imagery training (or first and second EEG recordings in control group). We first selected the two time-frequency combinations that had the smallest *p*-values as the features for classifying left and right hand motor imagery. A Euclidean distance algorithm was then used to estimate the classification accuracy.

Trained Group			Control Group		
Participant	Before (%)	After (%)	Participant	First (%)	Second (%)
EK	60	77	JI	57	52
GS	62	67	BK	60	54
DK	59	72	HJ	73	70
KS	58	72	TI	67	75
JN	55	69	SJ	64	66
Mean	58.8	71.4	Mean	64.2	63.4

4.4. Discussions and Summary

For motor imagery training we used a real-time cortical rhythmic activity monitoring system [75] that visualizes source activation maps on the cortical surface, rather than the scalp surface, to show the subjects their time-varying brain activities. The main reason why we chose to use the 'cortical' activity monitoring system was that EEG topographies cannot be directly attributed to the underlying cortical regions. In BCI applications, different types of EEG topographies can be observed even for identical motor imagery tasks [76] because the EEG topography is dependent on neuronal source orientations. Since most participants of motor imagery experiments are not familiar with EEG topographies, the use of inverse solutions could help them easily perform motor imagery training.

Many studies have reported the importance and usefulness of motor imagery in various applications such as learning complex motor skills in sports [77] and re-learning motor skills in clinical applications [78]. Ever since Jastrow's first study of mental simulation [79], motor imagery, a kind of mental process, has been widely used for learning motor skills and enhancing players' performance in sports science. Indeed, mental imagery, including motor imagery, has been demonstrated to be a central factor for motor skill acquisition and execution [77]. Motor imagery has been also been used to diagnose and rehabilitate brain-injured patients [80, 81]. For

example, Tamir et al. [81] applied motor imagery to patients with Parkinson's disease for improving their motor function, and found that the combination of motor imagery and physical practice is more effective than conventional physical training methods, especially for reducing bradykinesia. Although in the present study we applied our proposed motor imagery training system to a noninvasive BCI application, we expect that it can be applied to other applications, including those described above, in order to help the individuals get the feel of the motor imagery tasks and consequently, thereby enhancing efficiency of the relevant studies.

The average classification accuracy in the trained group was 71.4 % after the motor imagery training, which, although relatively low compared to values reported in the literatures concerning similar motor imagery classification [45, 65, 68, 82] was still thought to be an acceptable level for practical BCI applications according to Perelmouter and Birbaumer's report [83]. Nonetheless, the increment of the classification accuracy was thought to be meaningful enough to confirm the effect of our neurofeedback-based motor imagery training, considering that the main purpose of the classification was not to obtain a high classification accuracy, but rather to show how efficiently we were able to train individuals, who were unable to have a concrete feeling of motor imagery, to perform the motor imagery task.

In the present study, we focused on training motor imagery of both hands. According to the literature, imagery of feet and tongue (or mouth) movements can be

also used as effectors in EEG-based BCI systems [51]. Further, it has been reported that the mu rhythm is blocked or desynchronized at sensorimotor cortex during hand movement imagery, whereas it increases during foot or tongue motor imagery [51]. In the same study, it was also reported that EEGs recorded during left hand, right hand, foot, and tongue motor imagery are classifiable. Based on the previous report, it seems that individuals should be able generate distinguishable brain activity patterns of four or more effectors using our motor imagery training system, an exciting prospect that we will focus on in future studies.

In our neurofeedback-based motor imagery training system, we confined mu rhythm to 8–12 Hz frequency band, but the frequency band of mu rhythm nay vary from on individuals to another. Fortunately, in our experimental study, all participants succeeded in generating brain activity around their sensorimotor cortex in the neurofeedback training session with the typical frequency band. However, if the training session fails, the experimenter can adjust the frequency band (e.g. 13–15 Hz) and repeat training session.

In the present study, we confirmed the effect of our neurofeedback-based motor imagery training system by comparing two EEG data sets each recorded with a cue-based (or synchronized) BCI paradigm before and after motor imagery training. Since asynchronous (or self-paced) BCI systems are becoming popular in recent years, we will apply our motor imagery training system to such systems in our future studies. In

addition, we are planning to compare our training method with other conventional training methods in the near future.

In summary, we developed a type of neurofeedback systems that can help individuals to get the feel of motor imagery by presenting them with real-time cortical activation maps on their sensorimotor cortex. Importantly, all of the study participants succeeded in generating brain activation around the sensorimotor cortex during the training session. The EEG data recorded after the motor imagery training showed significant enhancement in both the number of meaningful features and the classification accuracy, demonstrating the efficiency of our motor imagery training system. Lastly, we expect that the proposed motor imagery training system will be useful not only for BCI applications but also for functional brain mapping studies relevant to motor imagery tasks.

Chapter 5: An EEG-based Real-time Cortical Functional Connectivity Imaging System

In this chapter, the author introduces a real-time cortical functional connectivity imaging system that can monitor and trace dynamic changes in cortical functional connectivity between different brain regions. Since the real-time functional connectivity imaging system is based on the real-time cortical rhythmic activity monitoring system introduced in Chapter 3, the concept of the real-time cortical functional connectivity imaging system is nearly identical to the real-time cortical rhythmic activity monitoring system, except for the 3D visualization part.

5.1. Research Background

Traditional neuroimaging studies have focused on either functional mapping of brain areas or investigation of task-dependent changes in brain activities; however, such studies can only provide a limited amount of information with respect to underlying neuronal processes. Recently, an increasing number of neuroscientists have become interested in describing the communications between different brain

areas, since such information might be helpful for better understanding the functional networks of cortical regions [84-90]. Generally, functional interactions among different cortical areas, typically referred to as functional connectivity, can be measured using linear or nonlinear analysis of time series extracted from various brain imaging techniques such as functional magnetic resonance imaging (fMRI) [86], near infrared spectroscopy (NIRS) [87], electroencephalography (EEG), and magnetoencephalography (MEG) [84, 85, 88-90].

EEG and MEG are believed to be more suited for studying interactions among brain areas at the level of cognitive processes due to their superior temporal resolutions as compared to hemodynamics-based imaging modalities such as fMRI and NIRS [84, 91]. Indeed, functional connectivity analyses based on scalp EEG and MEG have been applied extensively to a variety of practical applications including functional characterization of neuropsychiatric diseases[92-94], noninvasive diagnosis of psychiatric diseases by quantifying global synchronization [95-97], and investigation of functional networks associated with various cognitive processes [40, 98]. Further, freely available MATLAB toolboxes for the functional connectivity analysis are widely available [98, 99].

At present, despite recent advances in technology, estimation of functional connectivity from sensor level recordings has been met with severe criticism from many neuroscientists, as these recordings can be corrupted by the effect of volume

conduction (or field spread). Indeed, simulation studies have shown field spread can lead to misinterpretation of connectivity estimates between some pairs of sensors [100] because scalp potentials recorded from scalp EEG are not usually directly attributed to the underlying cortical regions. However, recent developments in source imaging techniques have made possible the ability to estimate temporal changes in underlying cortical sources; functional connectivity can now be estimated at the cortical source level [101, 102]. Therefore, the functional connectivity estimation at the cortical source level has been gradually replacing sensor-level analyses.

To the best of our knowledge, however, real-time imaging of cortical functional connectivity at the cortical source level has not been introduced, despite the rapid developments in computational neuroimaging. Implementation of such a real-time imaging of cortical functional connectivity may be a promising tool for practical applications. For example, such a system could be used as an auxiliary diagnosis tool to provide a prompt measure reflecting a subject's brain responses to certain stimuli, thereby helping patients with neuropsychiatric diseases such as dementia and schizophrenia as well as their relatives to accept diagnostic results [103], since people are apt to put more confidence in high-tech medical diagnostic devices than they are in traditional paper-based diagnosis methods such as the mini-mental state examination (MMSE) and positive and negative symptom scale (PANSS). Moreover, the real-time cortical functional connectivity imaging system can be used for EEG neurofeedback applications, as many researchers have been interested in monitoring

dynamics of functional connectivity during neurofeedback treatment [104-107]. Potential applications of real-time imaging of cortical functional connectivity will be discussed more in Sect. 5.4.

5.2. Methods

5.2.1. Methods for Real-time Connectivity Imaging

The proposed cortical functional connectivity imaging system is based on the EEG-based real-time cortical rhythmic activity monitoring system [75]. The real-time cortical rhythmic activity monitoring system could visualize spatiotemporal changes in cortical rhythmic activity of a specific frequency band on a subject's cortical surface, rather than the subject's scalp surface, with a high temporal resolution. Recently, the real-time imaging system was successfully applied to a neurofeedback-based motor imagery training system that can help individuals to more easily become accustomed to motor imagery tasks [108]. In this section, we will first introduce the brief concepts of the real-time cortical rhythmic activity monitoring system and then describe the technical details of the real-time cortical functional connectivity imaging system.

The EEG-based real-time cortical rhythmic activity monitoring system [75] consisted of pre-processing and real-time processing parts. In the pre-processing part, a linear inverse operator was constructed in which the subject's anatomical information was reflected. Once the linear inverse operator had been constructed and saved to a data-storage unit, spatiotemporal changes in cortical rhythmic activities could be monitored in real-time by means of a unified processing scheme consisting

of three independent programs, namely, a fast Fourier transform (FFT) program, a frequency domain minimum norm estimation (FD-MNE) solver, and a 3D visualization program, which were executed sequentially at each time slice.

The proposed cortical functional connectivity imaging system shares the same platform with the real-time cortical rhythmic activity monitoring system except for the 3D visualization program. Instead of calculating the absolute current source power at cortical vertices with respect to the frequency band of interest, the proposed system calculates instantaneous source power changes for each frequency of interest. The detailed processes are described below.

To construct the cortically distributed brain sources, we used a linear estimation approach. The expression for the inverse operator W was defined as

$$W = RA^T (ARA^T + \lambda^2 C)^{-1}, \tag{5.1}$$

where A is a lead field matrix, which represents impulse response of each source vector component at every measurement site, R is a source covariance matrix representing inter-source relationship, which is hardly estimated without using intracranial recordings, and C is a noise covariance matrix [109]. If we assume that both R and C are scalar multiples of identity matrix, this approach becomes

identical to minimum norm estimation [43]. In this study, the source covariance matrix R was assumed to be an identity matrix, which means that we ignored relationships between neighboring sources. In this study, background environmental noise acquired before attaching electrodes on the subject's scalp was used to calculated C [109]. λ^2 is a regularization parameter and was determined systematically based on the signal-to-noise ratio [109].

Once a specific frequency band was determined, the FFT program calculated real and imaginary components at all discrete frequencies within the predetermined frequency band. Instead of using wavelet transformation [109], we used FFT to obtain constant time-frequency resolution. Then, the FD-MNE solver was executed, which loads the Fourier transformed signals $B(f_i)_{\mathrm{Re}}$ and $B(f_i)_{\mathrm{Im}}$, $i = 1, 2, ..., n$, where Re and Im represent the real and imaginary parts of the Fourier transformed signals, respectively, as well as the pre-saved inverse operator W. The real part $q_j(f_i)_{\mathrm{Re}}$ and imaginary part $q_j(f_i)_{\mathrm{Im}}$ of current source vector at the j th cortical vertex with respect to the frequency of interest f_i can then be evaluated by multiplying the corresponding rows ($3j-2$, $3j-1$, and $3j$ th rows) in W with the Fourier transformed signals $B(f_i)_{\mathrm{Re}}$ and $B(f_i)_{\mathrm{Im}}$. We used the FD-MNE method instead of time-domain MNE method to estimate the current source vectors because under current computing environment maximally 20–30 source images could be

calculated per every second due to the computational time required for the inverse process [75]. Then, the instantaneous source power changes for a frequency (f_i) at the j th cortical vertex can be readily estimated by inverse Fourier transforming each directional component (*x*, *y*, *z*-directional components) of $q_j(f_i)_{\mathrm{Re}}$ and $q_j(f_i)_{\mathrm{Im}}$ into time-domain series $(q_{x,j}(t), q_{y,j}(t), q_{z,j}(t))$ and calculating the power of the source vector $Q_j(t_k)$ as $Q_j(t_k) = q_{x,j}(t_k)^2 + q_{y,j}(t_k)^2 + q_{z,j}(t_k)^2$ at densely discretized time samples (the subscript k represents k th time sample). After evaluating the instantaneous source powers at every cortical vertex, the source powers are averaged over all cortical vertices included in each ROI (see Figure 5.1 in advance), yielding the instantaneous source power changes of each ROI, $RQ_l(t_k)$, where the subscript l represents the l th ROI. For an i th frequency of interest, f_i, the functional connectivity between the m th and n th ROIs was evaluated by simply calculating the correlation coefficient (CC) between the two signal power time series extracted from the two ROIs, $CC_{m,n}(f_i)$. Finally, the CC values evaluated for all possible pairs of ROIs were averaged over the frequency band of interest. ROI pairs in which the connectivity exceeded a predetermined threshold CC value were visualized as a straight line connecting the two ROIs (see Figure 5.2 in advance).

5.2.2. EEG Recording Environments

Scalp EEG readings were recorded at 32 electrode locations (Cz, C3, T7, C4, T8, Fz, F3, F7, F4, F8, AFz, AF7, AF8, FP1, FP2, FC5, FC1, FC2, FC6, Pz, P7, P3, P4, P8, CP5, CP1, CP2, CP6, O1, O2, PO3, and PO4) using a 32-channel EEG acquisition system (WEEG-32, Laxhta Inc., Daejeon, Korea) in a dimly lit, soundproof room. The electrodes were attached to the subject's scalp according to the extended 10–20 system without using an electrode cap. The ground electrode was placed behind the left ear with the reference electrode on the opposite side. The EEG signals was sampled at 512 Hz, and the low- and high-pass filters were set at 64 and 0.5 Hz cutoffs (12dB/octave), respectively, in all experiments. To implement the 'real-time' imaging system, we did not apply any time-consuming signal preprocessing methods for noise/artifact removal to the input EEG signals.

5.2.3. Implementation of a Real-time Cortical Connectivity Imaging System

In the present study, a standard brain atlas [110] provided by the Montreal Neurological Institute (MNI) and a standard configuration of EEG electrodes were utilized, since individual magnetic resonance imaging (MRI) data for the subjects were not available. A first-order node-based boundary element method (BEM) was

applied to construct a lead field matrix. In the preset study, three-layer tessellated boundary surface, consisting of inner and outer skull boundaries and scalp surface, were generated using CURRY6 for windows (Compumedics, Inc., El Paso, TX) from the standard structural MRI data. The conductivity values of brain, skull, and scalp were assumed to be 0.22, 0.014, 1.79 S/m, respectively [33, 111]. Coordinate transformation and electrode positioning were performed using in-house software, 'BioEST' (http://cone.hanyang.ac.kr). For the extraction and tessellation of the cortical surface models, we applied *BrainSuite* developed in the University of Southern California, CA, USA [41]. To reduce the number of cortical surface [40] and generated a down-sampled epi-cortical surface with approximately 1,000 cortical vertices. Figure 5.1(a) shows the processes for the cortical source space, on which the equivalent dipole sources were placed, from standard brain MRI data. Since we used the smoothed cortical surface model as the source space, source orientation constraints were not imposed. Figure 5.1(b) shows the 12 ROIs, of which the locations and sizes were determined according to the following two criteria: (1) whole brain regions have to be taken into account in order to be applicable to a variety of experimental paradigms; and (2) the number of ROIs should not be too many for the real-time processing. Considering the above conditions, we selected six ROIs on each hemisphere: two ROIs in the frontal lobe, two ROIs in the temporal lobe, one ROI in the parietal lobe, and one ROI in the occipital lobe. The main reason why we used approximated and downsampled cortical surface as well as assumed relatively small number of ROIs was that using realistic cortical surface model and many ROIs would

increase the computational cost, thereby making the ‘real-time’ processing difficult. Since the computer system is being developed very rapidly, we believe that more realistic real-time connectivity imaging system would be available in the near future.

Figure 5.2 shows a snapshot of our test experiments. Dual LCD monitors were connected to a high-performance personal computer system (Intel Core2-6300 1.86 GHz environment) and were separated with a partition not to disturb the participants’ attention. Visual stimuli were presented through an LCD monitor placed in front of the participant. Cortical functional connectivity patterns as well as the on-going EEG signals were visualized on the other LCD monitor. During the real-time imaging, EEG signals were transferred to the operating computer in real-time, and the values were stored in a two-dimensional array variable. At a specific time slice, time domain signals in 256 data samples before the time slice were transformed into frequency domain signals using FFT. After execution of the FD-MNE solver and connectivity calculation module, ROI pairs whose connectivity exceeded a predetermined threshold value were visualized as a straight blue line connecting the two ROIs that were depicted as small red dots in the connectivity monitoring software (see Fig. 5.2). The real-time cortical connectivity monitoring was designed to store every instantaneous connectivity pattern as well as the stimulus onset times into the storage unit. We updated the cortical connectivity maps 250 ms intervals (four image frames/second).

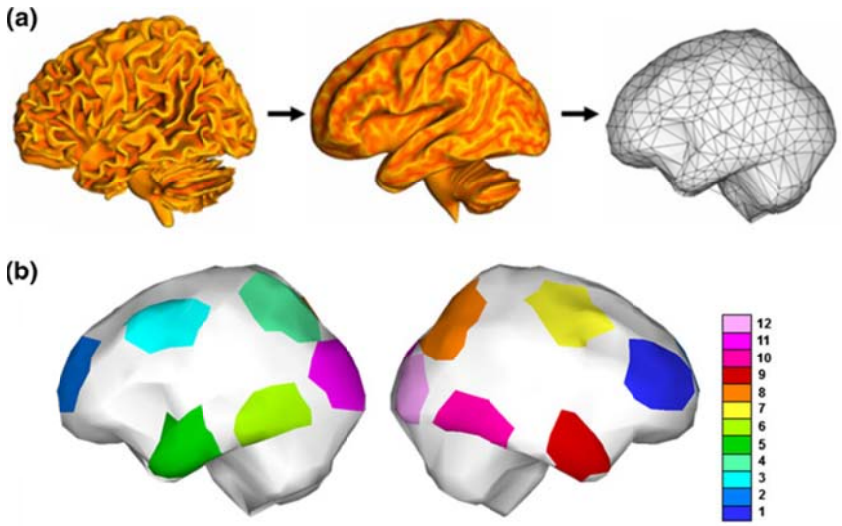

Figure 5.1. (a) Process of generating cortical source space: a high-resolution cortical surface was smoothed and down-sampled for the real-time source imaging. (b) Locations of 12 regions of interest (ROIs): *colors* represent the ROI number (see the *color bar* on the *right side*).

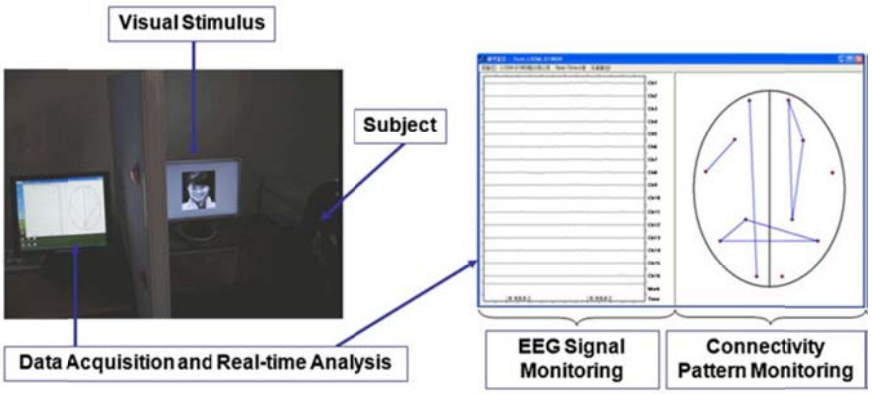

Figure 5.2. A snapshot of a test experiment (*left*), and a screenshot of the real-time cortical functional connectivity monitoring software (*right*): dual LCD monitors were connected to a single computer system and were separated with a partition. The monitoring software can visualize both the on-going EEG signals and the current connectivity patterns.

5.3. Results

To verify the feasibility of the implemented system, we monitored the temporal changes in cortical functional connectivity patterns while participants were performing different tasks. We performed three test experiments: (Exp. 1) monitoring gamma band cortical connectivity changes associated with structural face processing; (Exp. 2) monitoring alpha and beta band connectivity changes during finger movement; and (Exp. 3) monitoring theta band connectivity changes during working memory task.

Six healthy volunteers (six males, all right handed, mean age 25.5 years; range 21–29 years) took part in the first experiment (Exp. 1) and three healthy volunteers (three males, all right handed, mean age 26 years, range 24–28 years) participated in the second and third experiments (Exp. 2 and Exp. 3). None of the participants had a previous history of neurological, psychiatric, or other severe diseases that may otherwise have influenced the experimental results. We gave a fully detailed summary of the experimental procedures and protocols to each of the participants before the experiment. The study protocol was approved by the Institutional Review Board of Yonsei University, Korea.

5.3.1. Gamma-band Cortical Connectivity Monitoring (Exp. 1)

In our first test experiment, we attempted to track temporal changes in cortical functional connectivity patterns during structural face recognition. One hundred full facial images of most famous Koreans (50 males and 50 females) were randomly presented to the participants through a 17" LCD monitor. Original color pictures were converted to gray-scale images with identical sizes and resolutions. The facial images were randomly shuffled and were presented to the participants for 1 s. Every image appeared only once throughout the whole experiment. The reason why we converted the color images into gray-scale images was that the face images used for the present study had various background colors and different chroma characteristics, which might influence some ERP components such as P1, N1, and selection negativity, according to the previous relevant studies [112-114]. Therefore, many EEG experiments associated with face recognition have used gray-scale face images [115-117].

The inter-stimulus interval (ISI) was set at as 5 s, during which only a gray (RGB: 132, 132, 132) background was presented (see the Supplementary movie file, http://www.springerlink.com/content/j077u4422281491q/11517_2011_Article_791_ESM.html). Recordings were conducted in a single session consisting of 50 trials. Thus, the entire experiment lasted for approximately 5 min. During the recordings,

the participants were sat in a comfortable armchair. In order to keep the participants attention, they were asked to count the number of unfamiliar faces, but were not required to provide any physical response. After the experiment, we found that the number of unfamiliar faces was less than five for all of the participants. According to a previous literature [116] that used similar experimental paradigm, the cortical connectivity changes were mainly associated with face structural processing. We also confirmed from some preliminary experiments that counting the number of unfamiliar faces did not influence the main experimental outcomes. We set the frequency band of interest as 30–40 Hz to observe the time-varying gamma-band synchronization. We did not apply any signal processing algorithms [118, 119] for removing artifacts potentially originated form micro-saccades since those algorithms generally required significant computational cost and thus did not seem to be adequate for the real-time signal processing.

Figure 5.3(a) shows some screenshots taken before and after the visual stimulus onset for one participant (subject JK), captured during the online experiment (see the Supplementary movie file). Figure 5.3(b) shows an example of the variation in the number of connections counted at each time slice (every 250 ms), where red arrows represent the visual stimulus onsets. It can be seen from the figures and the Supplementary movie file that the number of connections suddenly increased after the visual stimulus onset.

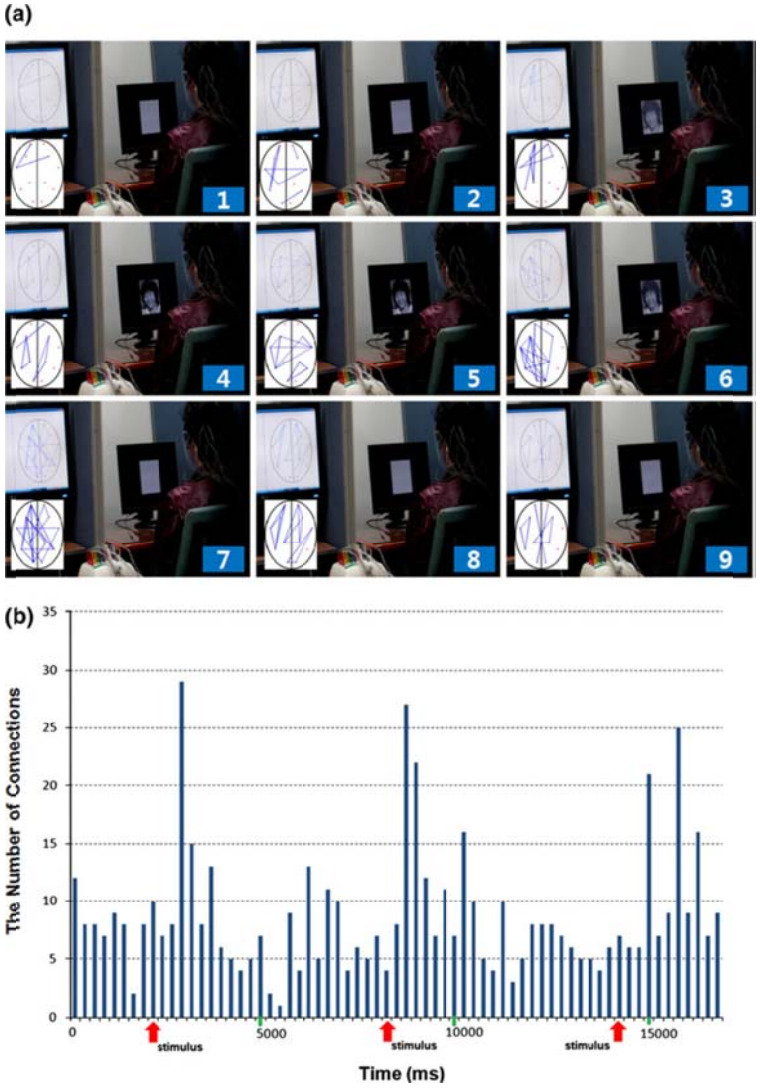

Figure 5.3. Variations in the number of connection in the first experiment (Exp. 1) investigating the dynamics of gamma-band cortical connectivity: (a) Screenshots regularly sampled from the supplementary movie file (4 frames per second). *Numbers* in each picture represent the sequence of the pictures. Visual stimulus appeared in third *picture* and disappeared after *sixth picture*; (b) variation in the number of connections with respect to time: arrows represent stimulus onset. The threshold was set to 0.96. These examples are parts of one participant's data (subject JK).

The average numbers of connectivity connections observed during a 2–s period before and after presenting the facial images were counted and the ratios between the two values are presented in Table 5.1. It can be seen from the table that the number of connectivity connections after presenting the images were greater than that before presenting the images for any tested threshold *CC* values. We also applied a one-tail paired *t* test between the average numbers of connectivity connections counted before and after the stimulus onset, and found statistically significant increment ($p < 0.05$) in the number of connections for all cases considered in Table 5.1. In our experiments, we applied four different threshold *CC* values to all six subjects and found that the slight changes in the threshold value did not affect the main trend of the results– increment in the number of connections after the stimulus onset. Indeed, as presented in the Table 5.1, the use of higher threshold values seemed to result in more distinct connectivity changes. However, when we used higher threshold values exceeding 0.99, we could hardly observe the dynamic changes in connectivity patterns visually since the real-time connectivity imaging system did not show any connections at many time slices as found in the previous offline analysis studies [116, 120]. Therefore, we set the threshold *CC* value to 0.96 when we executed the online monitoring system to generate the results in Figure 5.3. Since one of the main aims of the present system was to visually monitor the dynamic changes in the connectivity patterns, we allowed the potential users of our system to adjust the threshold *CC* values freely. According to our experience, in the online monitoring, the threshold

CC value could be readily adjusted without performing any offline analyses by gradually changing the threshold value and continuously monitoring the changes in the connectivity patterns during a subject's resting state.

The results of our first test experiments are similar to the reports in [31] and [53], which showed the peaked gamma band activity synchronization around 200–400 ms after face images were presented. Moreover, according to the previous studies, the gamma band synchronization between different brain areas during the processing of facial structure is significantly reduced in schizophrenia patients [31, 53]. Based on the previous studies, we are planning to apply the present system to real-time diagnoses of schizophrenia, after conducting clinical examinations.

Table 5.1. The ratio of the average numbers of connectivity connections observed during a 2 s period after presenting the facial images to those observed during a 2 s period before presenting the images.

Threshold	YC	HJ	JK	MK	JL	IL
0.96	1.44 (0.49)	1.43 (0.77)	1.31 (0.61)	1.31 (0.36)	1.19 (0.35)	1.25 (0.46)
0.97	1.41 (0.49)	1.47 (0.87)	1.43 (0.97)	1.29 (0.38)	1.21 (0.37)	1.36 (0.68)
0.98	1.51 (0.63)	1.66 (0.91)	1.51 (1.12)	1.42 (0.43)	1.22 (0.47)	1.29 (0.87)
0.99	1.55 (0.65)	2.09 (1.72)	3.06 (2.86)	1.75 (1.33)	1.35 (0.77)	1.40 (1.19)

YC, HJ, JK, MK, JL, and IL represent initials of the participants. Values in parentheses are standard deviations.

5.3.2. Alpha/Beta-band Cortical Connectivity Monitoring (Exp. 2)

In our second test experiment, we tracked the temporal changes in cortical functional connectivity patterns during finger movements. Since it has been widely known that finger movements can elicit connectivity increase in alpha/beta frequency bands [121], we set the frequency band of interest as 8–30 Hz. The three participants were sat in a comfortable armchair and were asked to touch the tip of the left thumb with the tip of the left index finger. Right after a pure tone beep sound was generated from the computer speaker, they were instructed to detach the two fingers for approximately 0.5 s and then touch the fingers again (see 4th figure of Figure 5.4). The ISI was set as 5 s, during which only a cross fixation (+) was presented at the center of the computer monitor in front of the participants. The participants were also asked to stare the fixation mark during the entire experiments. Recordings were conducted in a single session consisting of 50 trials.

Figure 5.4 shows some screenshots taken before and after the stimulus onset (3rd figure of Figure 5.4) for one participant (subject JI), captured during the online experiment. In the second and third experiments, we fixed the threshold CC value to 0.96, based on the experience attained from the first experiment. Then, the average numbers of connectivity connections observed during a 1.5-s period before and after the stimulus onset were also counted and the ratios between the two values were

evaluated. The ratios for subjects JI, JJ, and JH were 2.14 ± 0.67, 2.87 ± 0.81, and 1.96 ± 0.39, respectively. It could be seen from the figure and the resultant ratio values that the number of connectivity connections was increased after finger movements, demonstrating that the alpha/beta band cortical connectivity changes elicited by finger movement could be monitored using the implemented system.

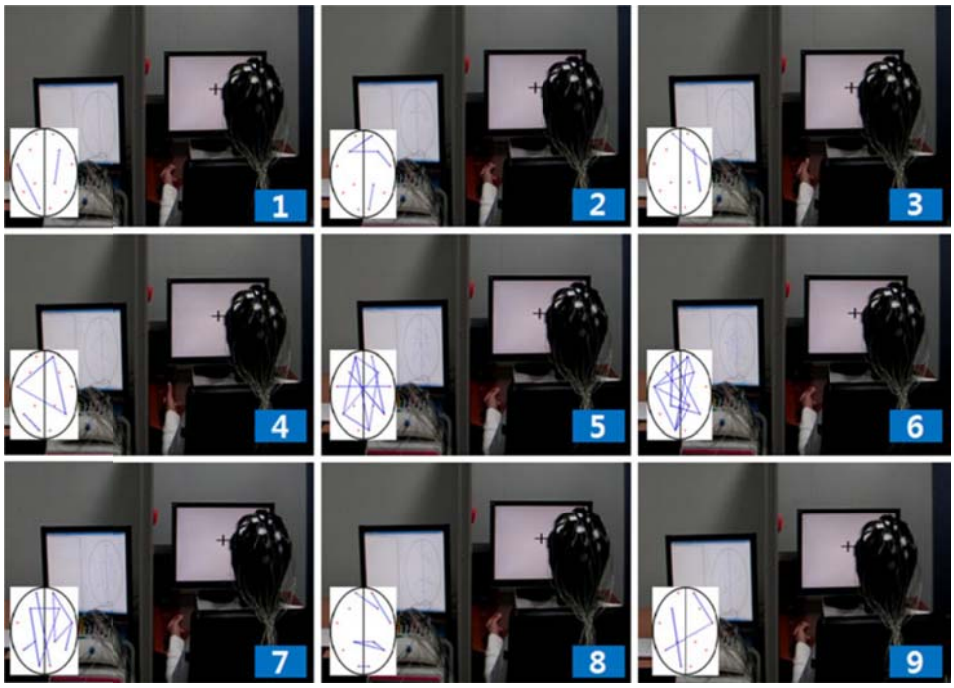

Figure 5.4. Variations in the number of connections in the second experiment (Exp. 2) investigating the dynamics of alpha/beta-band cortical connectivity: Screenshots regularly sampled from a movie file (2 frames per second). *Numbers* in each picture represent the sequence of the pictures. The subject moved his *left fingers* in *fourth picture*.

5.3.3. Theta-band Cortical Connectivity Monitoring (Exp. 3)

In our third test experiment, we tracked the temporal changes in cortical functional connectivity patterns during working memory task. Our paradigm was devised based on the Sarnthein et al.'s [21] work, where the authors reported significant enhancement in the theta band (4–7 Hz) connectivity between prefrontal and posterior areas. During 5-s perception period, the participants were presented with 6-digit randomly generated characters consisting of capital English letters and numbers (e.g., SD9FG4) through a 17" LCD monitor located in front of each participant. During the next 5 s, the participants were instructed to memorize the given characters while staring the cross fixation (+) located at the center of the computer screen. Then, the participants were asked to verbally recall the characters the characters that they memorized. The experimenter checked whether the answer was correct and then manually started the next trial. Before the new combinations of characters were presented, black screen was presented to the participants for 5 s. Recording were conducted in a single session consisting of 50 trials. The correct rations evaluated for subjects JI, JJ, and JH were 88, 90, 90 %, respectively, which were similar to the results reported in the previous study [21].

Figure 5.5 shows some screenshots taken during the online experiment of one participant (subject JJ), captured at every 1.5 s. As mentioned in the previous section,

we fixed the threshold CC value to 0.96. It could be observed from Figure 5.5 that the long-range connectivity between prefrontal area and posterior areas was notably increased during the 5-s retention period, coinciding well with the results of the previous offline study [21]. The average numbers of connectivity connections observed during the 5-s resting period and the 5-s retention period were counted and ratios between the two values were evaluated. The rations for subjects JI, JJ, and JH were 3.01 ± 1.13, 2.57 ± 0.65, and 3.43 ± 0.97, respectively, demonstrating that the theta band cortical connectivity changes associated with working memory could be monitored using the implemented system.

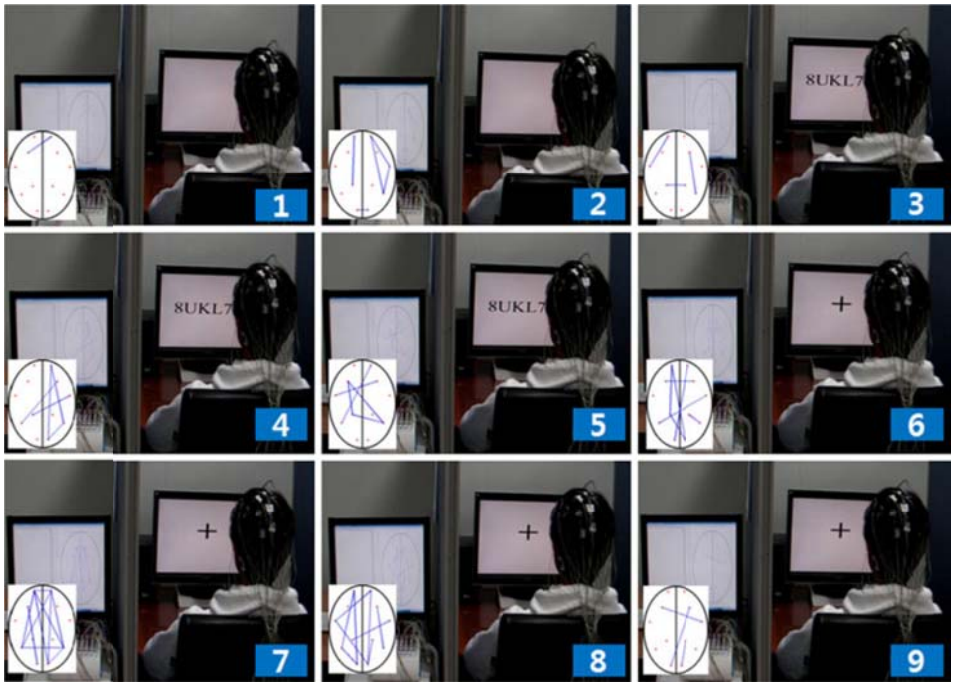

Figure 5.5. Variations in the number of connections in the third experiment (Exp. 3) investigating the dynamics of theta -band cortical connectivity: Screenshots regularly sampled from a movie file (1.5-s interval). *Numbers* in each picture represent the sequence of the pictures. A 6-digit word was presented in *third picture* and the retention interval started in *sixth picture*.

5.4. Discussions and Summary

In the present study, we introduced an EEG-based, real-time, cortical functional connectivity imaging system, which can monitor the dynamic changes in cortical functional connectivity between different ROIs on the cortical surface. To testify the implemented pilot system, we performed three test experiments in which we could monitor the real-time changes in cortical connectivity patterns in gamma, alpha/beta, and theta frequency bands.

Since we adopted a source-level connectivity analysis, our real-time imaging system is not subject to the hypothesis that EEG synchrony computed from scalp EEGs may contain spurious synchronizations resulting from volume conduction [100, 122]. Although in the preset study we simply traced the real-time changes in the overall connectivity patterns, our system can be readily modified for investigating the changes in the connectivity strength between specific cortical ROIs as well as for characterizing the specific spatial patterns in the connectivity maps, e.g., hemispheric lateralization of the connectivity pattern; in either case, the source-level connectivity analysis is more appropriate than the sensor-level connectivity analysis. In our third test experiment (Exp. 3), which monitored dynamic cortical connectivity changes during working memory task, increment of connectivity between prefrontal and posterior cortical areas was observed, demonstrating the possibility of using our

system for investigating dynamic spatial patterns in functional connectivity. In addition, the resultant connectivity patterns obtained from the source-level analysis can be less dependent upon the changes in the electrode than those from the sensor-level analysis because the source-level analysis projects the sensor-level recordings to the cortical source-level signals by solving an inverse problem.

Nevertheless, some issues associated with the source-level connectivity analysis should be investigated further in future studies. In the present study, we selected a simple power-to-power correlation for the calculation of functional connectivity between two ROIs because it was not possible to extract source time series at cortical vertices when minimum norm estimation was applied without source orientation constraints. Please note that without using the orientation constraint only the temporal dynamics of source powers can be obtained because each directional component of a cortical source vector has independent temporal dynamics. To apply the source orientation constraints, we need accurate individual anatomical data including structural MRI data, which unfortunately were not available in our experiments. Therefore, it will be necessary to develop new indices that can better measure the cortico-cortical functional connectivity, when the cortical orientation constraints are not imposed. Since the use of high-quality individual MRI data would make it possible to apply various functional connectivity measures such as phase coherence and phase locking value as well as would enhance the reliability of the source imaging results, we will try to use individual MRI data for real-time cortical

connectivity imaging in our future studies. In addition, proper identification of ROIs on the cortical surface should be studied as a general issue in the source-level connectivity analyses [100]. In the present study, we also determined the locations and sizes of ROIs without applying a well-established criterion, which should be studied further. In the present study, we performed the cortical source imaging with only 32-channel EEG signals because we did not have a higher density EEG recording system. Since the use of more EEG electrodes would enhanced the source imaging accuracy, we will apply the implemented software on other EEG systems with more recording channels.

Functional connectivity patterns associated with various cognitive or sensory tasks have been extensively investigated to characterize various psychiatric diseases such as schizophrenia [120, 123], Alzheimer's disease [124], and alexithymia [125]. Most offline analysis results have shown increased or decreased functional connectivity for specific frequency bands, thereby demonstrating the possibility of using connectivity information for noninvasive diagnoses of psychiatric diseases. We believe that our system also has the potential to be applied to the diagnosis of psychiatric diseases and further clinical investigations will be conducted in our future studies in cooperation with psychiatrists. Moreover, since it is known that functional connectivity is modulated at different sleep stages [126], it may be possible to use our system as a supplementary tool to monitor subjects' sleep stages in sleep studies or to watch if subjects fall asleep while performing a cognitive task. Another potential

application that we are considering is an EEG-based brain-computer interface (BCI). Many recent studies on BCI have reported that the complementary use of conventional power density-based features and functional connectivity-based features could enhance the overall classification accuracies of BCI systems [127-129]. Since cortical source imaging is becoming a promising tool for the enhancement of the performance of EEG-based BCI systems [45, 47], a promising topic will be to combine the real-time cortical rhythmic activity monitoring system with the real-time cortical functional connectivity imaging system for extracting new BCI features.

In the present study, we implemented an EEG-based real-time cortical functional connectivity imaging system, but the same concept can also be applied to MEG without major modifications. In MEG, source-level analysis is relatively more important than in EEG because the MEG sensors are not attached directly on the subject's scalp surface. For example, if a subject's head is tilted in a helmet-type MEG system, so that one hemisphere is close to the sensors than the other is, one could observe stronger activity at sensors closer to the subject's head even when the strengths are equal at the cortical level. Therefore, the real-time cortical functional connectivity imaging system can also be a useful tool in MEG studies. We are currently developing new paradigms to diagnose various psychiatric diseases and also trying to generalize the operating software so as to release it worldwide to potential users.

Chapter 6: Brain Fingerprinting: Classification of Mental States Based on Spatiospectral Patterns of Brain Electrical Activity

This chapter introduces a mental task classification method to utilize cortical source information in order to more accurately classify mental states than using scalp EEG signals, and demonstrates the superiority of using the cortical source imaging in distinguishing different mental states.

6.1. Research Background

Although efforts to comprehend the human mind began in ancient Greece, whether the human mind was associated with the brain or heart remained a controversial issue until a series of modern neuroscience studies demonstrated that human emotions and behaviors are tightly linked with brain activity. Recently, thanks to dramatic advances in technologies for recording human brain activity and methods for statistical pattern recognition, neuroscientists have recognized the possibility of decoding the human mind based on brain activity recorded via multiple neuroimaging

modalities, such as functional magnetic resonance imaging (fMRI), near infrared spectroscopy (NIRS), electroencephalography (EEG), and magnetoencephalography (MEG) [130-142]. These “mind reading” or “brain reading” technologies have been explored not only to advance our understanding of neural information processing but also to develop new applications such as brain-computer interfaces (BCI) [131, 132, 135, 140, 141], lie detection [130, 134, 136, 137, 142], and communication with severely locked-in patients [133, 138, 139].

Among the neuroimaging modalities, EEG has been widely used in mind reading studies because of its excellent temporal resolution, usability, and safety. At present, many EEG-based mind reading studies have succeeded in discriminating different mental tasks or cognitive states with fairly high classification accuracy [143-152]. The successful results have significantly contributed to realizing several practical BCI systems and progressing in our knowledge about neural information processing.

Recently, some studies have shown that source imaging analysis methods could increase the classification accuracy of distinguishing motor imagery tasks rather than using scalp EEG signals [43, 153, 154]. These results are physiologically plausible because cortical sources reconstructed from the scalp EEG signals might compensate the distortion caused by the effect of volume conduction. However, to my best knowledge, the cortical source imaging method has not yet been tested for a variety of mental tasks such as mental calculation, internal speech, spatial navigation imagery,

and so on. It is needed to apply the source imaging method to a diversity of mental tasks so as to expand our understanding of neural information processing and realize a high performance BCI system. Thus, the author explored whether the enhanced accuracy could also be obtained by using the cortical source imaging method instead of using raw scalp EEG signals.

6.2. Methods

6.2.1. Participants and Experimental Conditions

Eight healthy volunteers (all male, all right-handed, aged 20-27 years) participated in the present study. None of them had a previous history of neurological, psychiatric, or other severe diseases that may have influenced the experimental results, nor had they ever participated in EEG-based experiments. All participants were asked to abstain from alcohol for 24 hours prior to the experiment in order to maximize concentration on the experiment. The author provided a fully detailed summary of the experimental procedures and protocols to all participants prior to the experiment. All participants gave written consent and received monetary reimbursement for their participation.

In the EEG data acquisition session, the participant sat on a comfortable armchair facing a 17" LCD monitor. Electrodes were mounted on their scalp according to the extended international 10–20 system. A total of 30 electrodes were evenly and broadly attached to the participants' scalps covering whole brain areas (AF3, AF4, Fz, F3, F4, F7, F8, FC1, FC2, FC5, FC6, Cz, C3, C4, CP1, CP2, CP5, CP6, Pz, P3, P4, P7, P8, POz, PO7, PO8, O1, O2, T7 and T8) and a multi-channel EEG acquisition system (WEEG-32, Laxtha Inc., Daejeon, Korea) was used for data

acquisition. The EEG signals were acquired in a dimly lit, soundproof room. The sampling rate was set at 512 Hz in all experiments. The study protocol was approved by the Institutional Review Board (IRB) at Yonsei University, South Korea.

6.2.2. Mental Tasks

Four different mental tasks were chosen on the basis of previous studies associated with EEG-based mind reading [51, 148, 151]. The participants were asked to use a consistent strategy for each mental task to minimize inter-trial variability [137]. The following paragraphs provide descriptions of these tasks.

(Task A) Counting the Number of Strokes of Given Chinese Characters

Participants were asked to count the number of strokes of given Chinese characters. All words used for this task consisted of four Chinese characters with particular meanings. Prior to the main recording sessions, the participants were asked not to think about the meanings of the words to avoid the acquisition of unwanted EEG signals.

(Task B) Mental Mathematical Calculation

Participants were given nontrivial multiplication problems in which they were asked to multiply a two digit number by a second two digit number, mentally, as fast

as they could. Participants were also asked not to vocalize the numbers and to make no movements while solving the problems. The pairs of two digit numbers used in a session were not repeated to prevent the participants from becoming accustomed to the problems.

(Task C) Mental Singing of the National Anthem

Participants were required to sing a song internally, without performing movements to keep the beat. The Korean national anthem was selected as the song to reduce inter-participant variability of the EEG signals.

(Task D) Motor Imagery of the Tongue

The participants were asked to perform kinesthetic imagination of tongue movement. Since even small tongue movements may contaminate the EEG signals, the participants were instructed not to swallow their saliva during the task period.

In addition to these mental tasks, eye-closed, resting state EEG signals were recorded for three minutes prior to the main recordings; these were used as a baseline EEG dataset. During the resting EEG recordings, participants were asked to relax and not to think of anything.

6.2.3. EEG Data Acquisition

The EEG data were acquired while the participants were performing the four different mental tasks described in the previous section. Figure 6.1 depicts the experimental design used in the present study. A gray (RGB: 132, 132, 132) color was selected as the background to prevent eyestrain [155]. At the beginning of each trail, a blank screen was presented for a variable duration (three to eight seconds) and then instructions for the next task appeared in the center of the screen for two seconds for task A, C, and D (also see Figure 6.1). The preparation period for the mental mathematical calculation (task B) lasted longer (four seconds) than that for the other tasks (two seconds) as the participants generally needed a longer time to memorize the pair of two digit numbers. Immediately after a beeping sound was presented to the participants for 125 ms, a black cross fixation was presented at the center of the screen for 10 s for tasks B, C, and D. During this time, participants were to perform the instructed mental task for 10 s. In the case of task A (counting the number of strokes of given Chinese character), a Chines word consisting of four Chines characters appeared for 10 s, as it was not trivial for native Koreans to memorize the Chinese words. A single experimental session was composed of 20 independent trials, each of which appeared five times in random order. Seven out of eight participants performed four sessions; while the other participant (JJ) underwent only three sessions due to mental fatigue. Consequently, seven participants performed each

mental task 20 times and one participant (JJ) performed each 15 times.

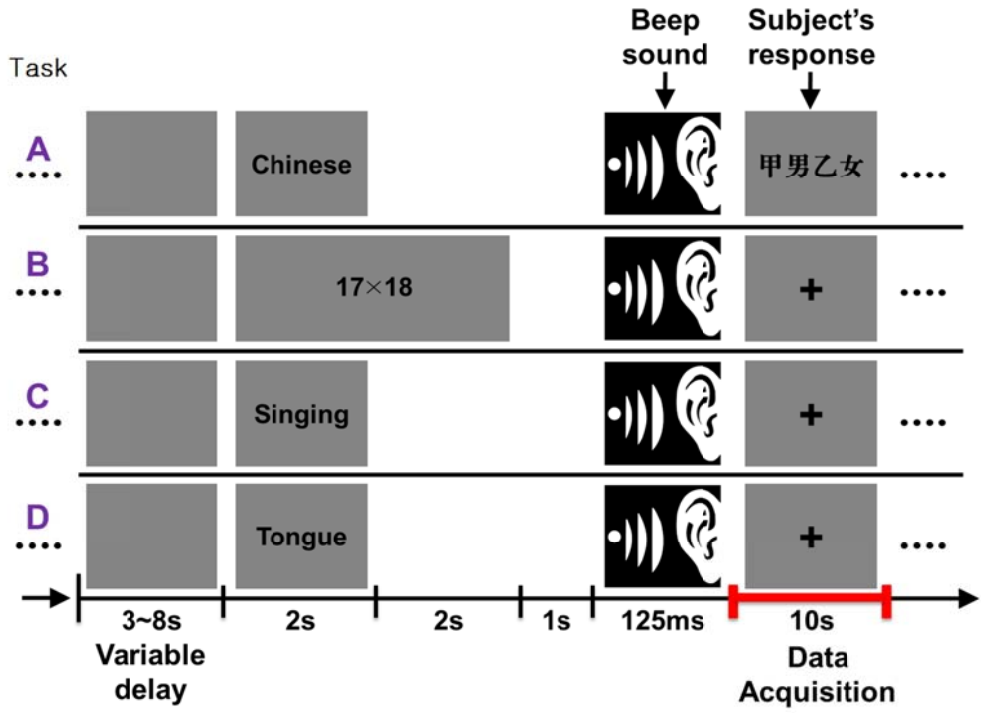

Figure 6.1. Experimental paradigm used in this study. There was a variable delay from 3 s to 8 s before instructing a subject to perform one of the mental tasks. The preparation periods were set to be 2 s for Task A, Task C, and Task D and 4 s for Task B. The preparation period for Task B was longer than the others because the subjects had to memorize a pair of two-digit numbers presented on a screen in order to perform the task. After a warning signal was presented for 125 ms (a beeping pure tone sound), the subject was asked to perform the instructed mental task for 10 s. During the data acquisition period, a cross fixation was presented at the center of the screen, except the Task A for which four Chinese characters were presented instead of the cross fixation.

6.2.4. EEG Data Analysis

6.2.4.1. Regions of Interest (ROIs)

The processes for generating the cortical source space were identical to those described in Chapter 3. Please refer to 'Section 3.1.2. Forward Calculation and Inverse Estimation', for more detailed technical explanations. The whole cortical source space was divided into 18 ROIs, which were made to cover the whole brain areas and to have similar sizes as much as possible. Figure 6.2 shows the 18 ROIs, in which each color represents each ROI. The author selected six ROIs on the frontal lobe (ROI1–6), six ROIs on the parietal lobe (ROI7–12), four ROIs on the temporal lobe (ROI13–16), and two ROIs on the occipital lobe (ROI17–18).

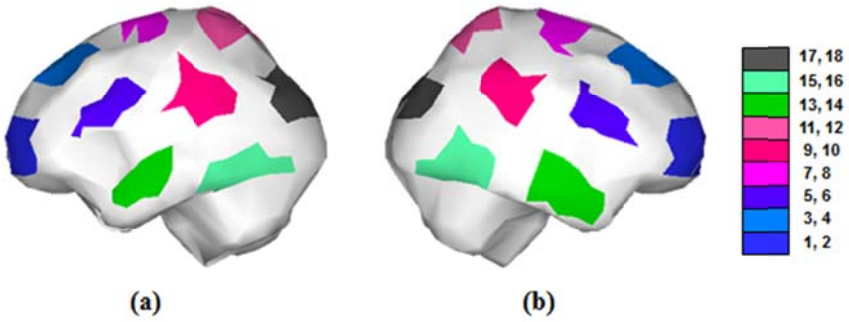

Figure 6.2. Locations of 18 regions of interest (ROIs): (a) the left hemisphere; (b) the right hemisphere. The color bar on the right side represents the ROI number in which odd numbers are for the left hemisphere and even numbers are for the right hemisphere.

6.2.4.2. Feature Extraction

To classify different mental tasks, the author developed a new feature extraction method that utilizes the whole spatial and wide spectral information contained in the reconstructed cortical sources. The cortical source information were converted into 2D spatiospectral pattern maps, of which each element was filled with -1, 0, and 1 reflecting the degrees of ERD and ERS at each ROI and frequency bin. The following paragraph provides the detailed explanation on how the author constructed the spatiospectral pattern maps.

Five second epochs (2.5–7.5 s from task onset) were extracted from the ten-second EEG signals for each trial and were used for analysis. Each epoch was then divided into one-second segments with 50% overlap, yielding a total of nine time segments in every epoch. Each segment was transformed into the frequency domain using the fast Fourier transform (FFT), and then an absolute current source power was evaluated by solving inverse problem at each cortical vertex (see also ‘Section 3.1.2 Forward Calculation and Inverse Estimation’ for more detailed explanation of inverse estimation). After an average source power for each cortical vertex and each frequency was estimated by averaging the source powers of the nine time segments, ROI powers at the 18 locations were calculated by averaging all cortical vertices included in each ROI. Consequently, a two-dimensional spectral source power map consisting of the spectral source power values at each ROI and frequency was

obtained for each trial (see Fig. 6.3; denoted as the task map). The frequency resolution was set at 1 Hz and the frequency band ranged from 4 Hz to 45 Hz, including theta (4–7 Hz), alpha (8–13 Hz), beta (14–30 Hz), and low gamma (30–45 Hz) frequency bands [28, 29, 156, 157]. The 2-D spectral source power maps for the baseline were also constructed by applying inverse estimation with the same analysis window size (1 s) and overlapping ratio (50%; see Fig. 6.3a, denoted as the baseline map). The mean value and standard deviation of the spectral source powers during the baseline period were then evaluated for each ROI-frequency combination. Then, three signed integer values, +1, 0, and -1, were assigned to each element of the 2-D spectral source power maps based on the following rules: an event-related synchronization (ERS) value (+1) was assigned to an element for which the source power value was larger than ‘mean of baseline source powers + one standard deviation of baseline source powers’; an event-related desynchronization (ERD) value (-1) was assigned to an element for which the source power value was smaller than ‘mean of baseline source powers – one standard deviation of baseline source powers’; and the other elements, the source powers of which were not significantly different from the baseline source powers, were filled with zeroes (0). By applying this transformation to all of the 2-D ROI-frequency power maps, we constructed new 2-D spatiospectral pattern maps filled with +1, 0, and -1 values for each mental task (see Fig. 6.3a; denoted as the template ERS/ERD map).

6.2.4.3. Classification of Mental States

In order to investigate how well the different mental tasks could be classified, the leave-one-out cross-validation (LOOCV) method was applied, considering the relatively small number of task trials. The author used a single spatiospectral pattern map as validation data, and the remaining pattern maps as training (or template) data. This process was repeated such that every spatiospectral pattern map was used once as the validation data. For the classification of mental tasks, the author implemented a simple fitness evaluation technique that measured the similarity between a validation pattern map and each class of template pattern maps corresponding to each mental task, and the validation pattern map was assigned to a class that demonstrated the highest fitness value.

For a given spatiospectral pattern map *X*, the fitness of *X* with respect to a set of template pattern maps corresponding to a specific mental task was evaluated. Similarity between a validation pattern map *X* and the *n*-th template pattern map in a set corresponding to a specific mental task, $Y^{(n)}$, was defined as:

$$h(X, Y^{(n)}) = \sum_{r=1}^{R} \sum_{f=1}^{F} X_{r,f} \, Y_{r,f}^{(n)} , \tag{6.1}$$

where R and F are the number of ROIs and frequencies, respectively, the subscripts r and f represent the r-th low and f-th column of the ROI-frequency grid, respectively. As readily seen from (6.1), '1' was assigned to an element at which two pattern maps had identical ERS/ERD values; '-1' was assigned to an element at which two pattern maps had opposite ERS/ERD values; and '0' was assigned to an element at which one or both pattern maps had no significant ERS/ERD values.

The similarity values estimated for all template patterns in a class were then averaged into a single value measuring fitness between a validation pattern map X and a set of template pattern maps Y, $F(X, Y)$, as given below:

$$F(X,Y)=\frac{1}{N}\sum_{n=1}^{N}h(X,Y^{(n)}) \tag{6.2}$$

The fitness values between the validation pattern map X and the other sets of template pattern maps were also calculated by applying the same procedure. Finally, a certain validation pattern map corresponding to a specific mental task was assigned to the class that demonstrated the greatest fitness value. Figure 6.3 is a schematic illustration of the proposed mental task classification method. Figure 6.3a depicts the process of constructing spatiospectral pattern maps for different mental tasks. Figure 6.3b describes the process for classifying an input pattern map. For comparison, both feature extraction and classification methods were applied to the scalp EEG data.

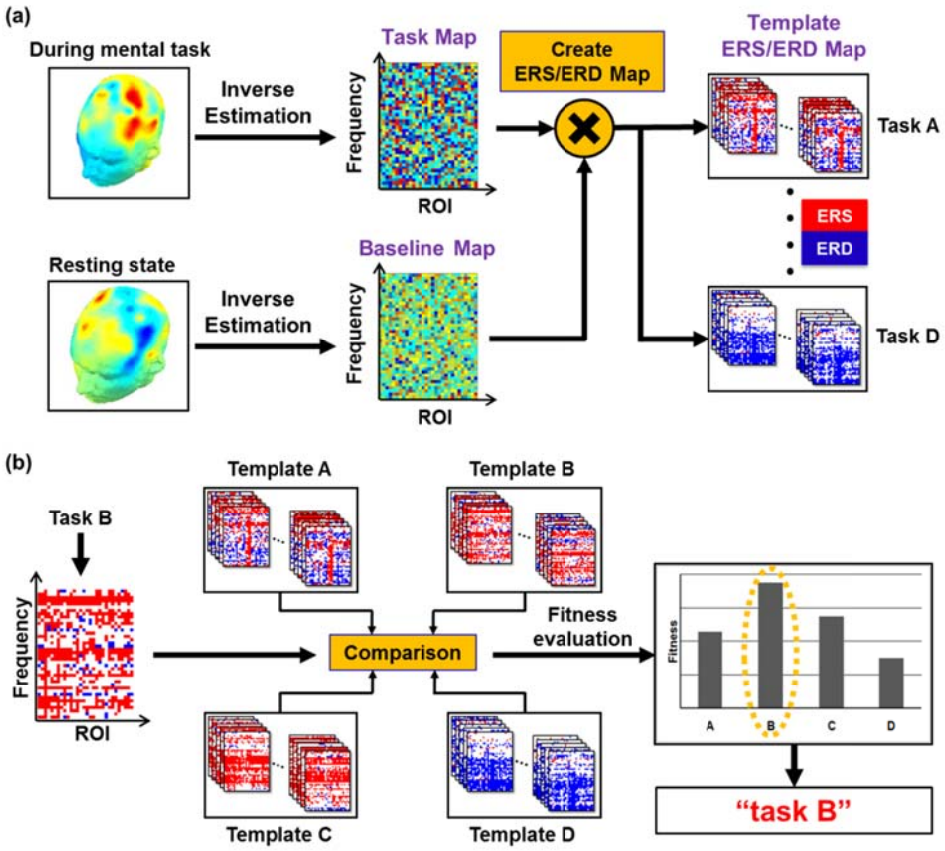

Figure 6.3. Schematic illustration of the proposed mental task classification method: (a) A two-dimensional source power pattern map for a specific mental task was constructed by calculating spectral source power at each ROI and frequency. The 2D source power pattern map (denoted as "Task Map") was converted into a 2D spatiospectral pattern map consisting of event-related (de)synchronization (ERD/S) values (ERS: red color; ERD: blue color), based on the 2D source power pattern map constructed for the resting state (denoted as "Baseline Map"). This procedure was applied to all trials of four mental tasks, Tasks A-D, and template ERD/S maps for each mental task were obtained. (b) When a new 2D spatiospectral pattern map was fed into the proposed classification algorithm, this pattern map was compared with the template pattern maps constructed from the process described in (a). The input pattern map was then assigned to the class with the highest fitness value.

6.3. Results

Figures 6.4 and 6.5 show two examples of the 2D spatiospectral maps obtained from two subjects, IU and DK, respectively, who demonstrated the highest classification accuracy (see Appendix A for the other six participants' spatiospectral maps), where the tasks A, B, C, and D indicate the four mental tasks described in the previous section. It is evident from visual inspection of Figure 6.4 and 6.5 that the pattern maps obtained while a subject was performing the same mental task exhibited similar and consistent trends, and those corresponding to different mental tasks showed discriminable patterns, demonstrating the possibility of using these spatiospectral pattern maps for classifying different mental tasks. Unfortunately, however, the author did not observe clear inter-subject similarities for specific mental tasks, thought to be secondary to different levels of baseline activities for each participant. Among the eight participants, subject IU had the most consistent intra-class similarity, also reflected in the overall classification accuracy provided in the next paragraph. Compared to subjects IU and DK, subject JI demonstrated the least consistent spatiospectral patterns, which also resulted in the lowest classification accuracy (see Fig. 6.6, in advance).

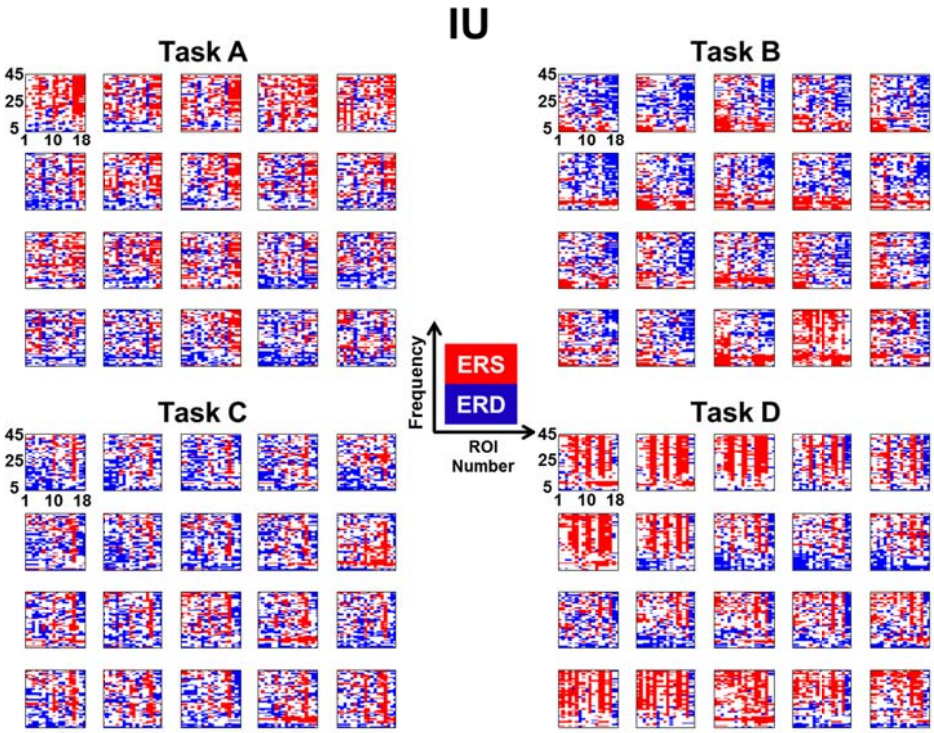

Figure 6.4. Two-dimensional spatiospectral pattern maps for all mental tasks performed by subject IU. Event-related synchronization (ERS) is plotted in red while event-related desynchronization (ERD) is plotted in blue. Consistent intra-class similarity was commonly observed for each task.

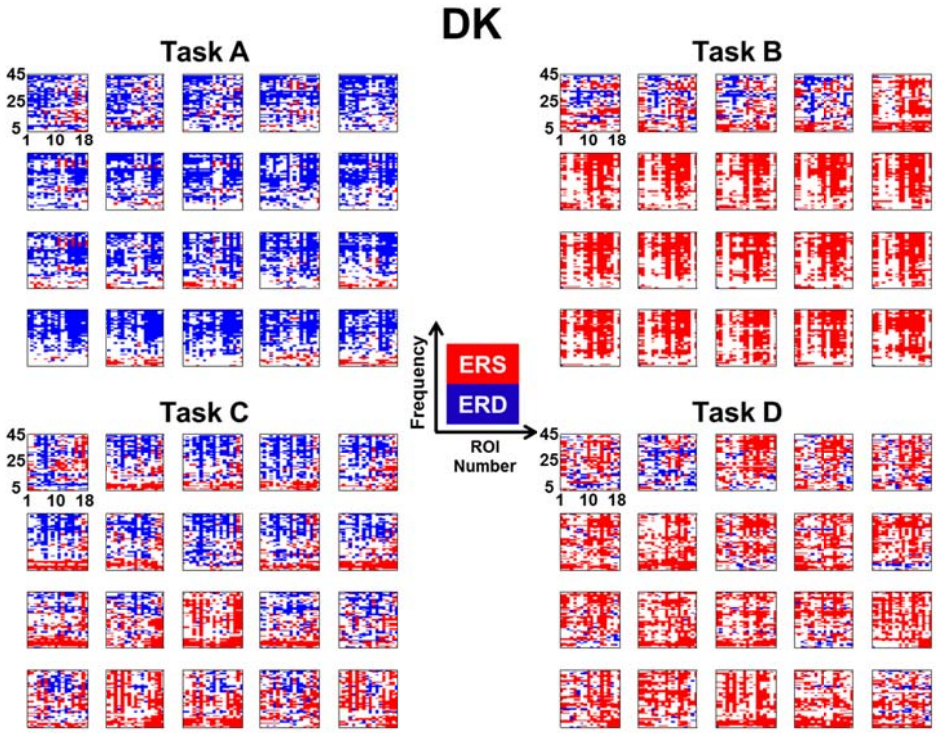

Figure 6.5. Two-dimensional spatiospectral pattern maps for all mental tasks performed by subject DK. Event-related synchronization (ERS) is plotted in red while event-related desynchronization (ERD) is plotted in blue. Consistent intra-class similarity was commonly observed for each task.

The proposed classification method was applied to both the raw EEG data and the reconstructed cortical source data in order to compare performance in classifying different mental tasks; results are summarized in Figure 6.6. The analysis demonstrated that the classification accuracy was considerably enhanced in all participants except the subject WH using the cortical source information. All classification accuracy values exceeded the chance level (25%) for correct classification. The average classification accuracies were 76.31% (±12.84) for the cortical level analysis and 68.13% (±9.64) for the sensor level analysis.

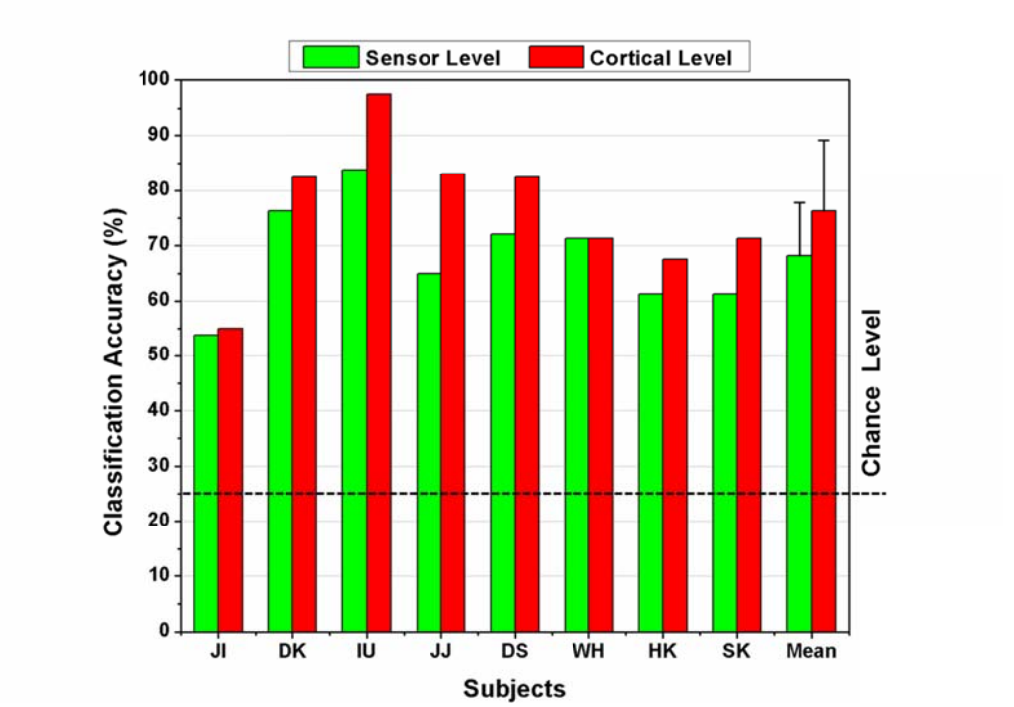

Figure 6.6. Comparison of classification accuracies between cortical level and sensor level analyses.

6.4. Discussions and Summary

In order to more accurately interpret individuals' intentions, the author utilized spatiospectral pattern maps of cortical source information reconstructed from scalp EEG signals. The author referred to the proposed approach as 'brain fingerprinting' since the author was able to obtain distinct two-dimensional spatiospectral patterns corresponding to different mental tasks, similar to fingerprint patterns. The experimental results suggest that the cortical source imaging method can be used to enhance the accuracy of detecting individuals' various intentions, which is in line with the previous motor imagery classification studies [45, 153, 154]. Based on these results, a real-time mind reading system will be developed by using the real-time cortical source imaging technology in the future studies.

Besides classification accuracy, the proposed classification approach has also advantage over the conventional methods in that the feature extraction and classification methods do not require complex procedures for selecting specific feature sets and training a classifier. Instead of selecting an optimal combination of feature vectors, the author converted full spatial and spectral information into spatiospectral pattern matrices and classified the patterns by calculating inner-product of two pattern matrices.

Although clear inter-subject similarity did not be found in the spatiospectral patterns, well-known physiological findings were frequently observed in most of the participants' pattern maps. The increment of gamma band brain activity is widely believed to be tightly linked with cognitive task execution [28], and this phenomenon was also replicated in the current study; a widespread increment of gamma band activities was observed in most of the participants' spatiospectral pattern maps for most cognitive tasks. Moreover, the augmentation of theta band power along with gamma ERS was also observed in a large number of frontal and central sites for all subjects, excluding subject DS, while performing the numerical multiplication task (task B). This observation agreed with previous studies [28, 158] that reported increased frontal and central theta powers while one was performing specific mental tasks requiring high levels of attention, such as mental arithmetic and reasoning. Additionally, most participants' spatiospectral maps, excepting subject JI, demonstrated significant increases in alpha power (alpha ERS) around the sensorimotor cortex during the tongue motor imagery task (task D), agreeing with a previous study that reported dominant alpha ERS in the sensorimotor (central) cortex during tongue motor imagery [51]. Since characterizing patterns of brain activity associated with specific mental states is still thought to be an important issue that may expand our understanding of how a specific mental task is encoded in the brain [159-162], we will further investigate this issue in future studies.

Some parameters used in the present study were selected empirically. First the spectral source powers were evaluated with a one second time window with a 50% overlap and were averaged across all time windows in each epoch. The author varied the analysis window sizes and picked the optimal window size (1,000 ms) from trials of 500, 750, 100, 1,500, and 2,000 ms. Second, the threshold values of ERD and ERS were set to represent the 'mean of baseline source powers $\pm$ one standard deviation of baseline source powers' for all participants. This threshold value was also determined empirically, but these values need to be optimized in future studies.

One of the promising applications of this study would be in developing brain-computer interface (BCI) technology. BCI is cutting edge technology that may help the disabled control external devices and communicate with the outside world. The most widely studied mental task has been motor imagery defined as the mental simulation of a kinesthetic movement [16, 17]. The motor imagery task is believed to be particularly effective for controlling external devices, since it does not require any external stimuli, as in the steady-state visual evoked potential (SSVEP) and P300-based BCI paradigms. However, motor imagery tasks may not always be the best effectors, as some people do not develop a concrete feel for performing motor imagery even after extensive training [49, 55, 163]. It has also been reported that people who have been paralyzed or undergone amputations are generally less capable of performing motor imagery tasks; sometimes called the chaotic motor imagery phenomenon [164, 165]. There the non-motor imagery tasks used in this study may

represent alternative effectors that could be potentially applied to BCI applications. Prior studies have already demonstrated that it is possible to classify non-motor imagery tasks with an acceptable classification accuracy [143, 144, 150-152, 166].

Chapter 7: Conclusion

In this dissertation, a real-time cortical rhythmic activity imaging technology was developed and its usefulness was demonstrated by various practical applications, i.e. the real-time cortical rhythmic activity and functional connectivity monitoring, neurofeedback-based motor imagery training, and classification of mental states.

The real-time cortical rhythmic activity imaging technology was first applied to monitoring individuals' brain activation states. Both offline simulations and online human experiments demonstrated that the developed monitoring system could correctly visualize instantaneous cortical activation images reflecting current brain states in real-time.

The developed real-time cortical rhythmic activity monitoring system was utilized to efficiently train individuals to perform motor imagery tasks for brain-computer interface (BCI). After the motor imagery training for approximately 30 min, all participants in the trained group succeeded in performing motor imagery to activate their motor cortex without any physical movements. The analysis results of EEG data recorded before and after training showed significant differences in the sensorimotor rhythms, and classification accuracy was also enhanced considerably in all participants after the motor imagery training. On the other hand, the analysis

results of the control group did not show any meaningful changes in both mu rhythm and classification accuracy, demonstrating that the suggested system can be used as a tool for training motor imagery task in BCI applications.

The real-time cortical functional connectivity monitoring system was also implemented as one of the applications of the real-time cortical activity imaging technology. For the verification of the developed system, the author performed three test experiments: 1) structural face processing in gamma band, 2) finger movements in alpha/beta bands, and 3) working memory task in theta band. The online experiment results were consistent with the results of previous offline studies. These results demonstrated the possibility of imaging cortical functional connectivity in real-time.

To more accurately interpret human intentions, the cortical rhythmic activity imaging technology was applied to classifying different mental tasks. Two-dimensional spatiospectral pattern maps were first constructed from cortical source information and classified through the similarity evaluation. The above procedure was repeated for raw scalp EEG signals for comparison. The average classification accuracies were 76.31% ($\pm$12.84) for the cortical level analysis and 68.13% ($\pm$9.64) for the sensor level analysis. The analysis result demonstrated that the classification accuracy can be considerably enhanced by using the cortical source information. Based on this preliminary offline experiment, the author will implement a real-time

mind reading system that utilizes the developed real-time cortical activity imaging technology.

Besides the applications mentioned in this dissertation, the proposed real-time cortical activity imaging technology can be applied to other potentially practical applications such as real-time lie detection, diagnosis of psychiatric brain diseases, neurofeedback-based autism and attention deficit hyperactivity disorder (ADHD) treatment, sleep stages monitoring and so on. In the future, these applications will be investigated in cooperation with medical doctors. Also, the author has a plan to increase the temporal resolution of the real-time cortical activity imaging technology by not only developing a high speed inverse solution, but introducing parallel computing methods, in order to more accurately detect fast-changing brain activities. Lastly, the author will generalize the application software, which would enable worldwide researchers to easily utilize the proposed real-time cortical rhythmic activity imaging technology for their studies.

References

[1] Jensen, O. and Vanni, S., "A new method to identify multiple sources of oscillatory activity from magnetoencephalographic data," *Neuroimage,* vol. 15, pp. 568-74, 2002.

[2] Gruber, T., Muller, M. M., Keil, A. and Elbert, T., "Selective visual-spatial attention alters induced gamma band responses in the human EEG," *Clin Neurophysiol,* vol. 110, pp. 2074-2085, 1999.

[3] Kaiser, J., Ripper, B., Birbaumer, N. and Lutzenberger, W., "Dynamics of gamma-band activity in human magnetoencephalogram during auditory pattern working memory," *Neuroimage,* vol. 20, pp. 816-27, 2003.

[4] Kwon, J. S., *et al.*, "Gamma frequency-range abnormalities to auditory stimulation in schizophrenia," *Arch Gen Psychiat,* vol. 56, pp. 1001-1005, 1999.

[5] Miltner, W. H. R., Braun, C., Arnold, M., Witte, H. and Taub, E., "Coherence of gamma-band EEG activity as a basis for associative learning," *Nature,* vol. 397, pp. 434-436, 1999.

[6] Salenius, S., Kajola, M., Thompson, W. L., Kosslyn, S. and Hari, R., "Reactivity of magnetic parieto-occipital alpha rhythm during visual imagery," *Electroencephalogr Clin Neurophysiol,* vol. 95, pp. 453-62, 1995.

[7] Salmelin, R. and Hari, R., "Spatiotemporal characteristics of sensorimotor neuromagnetic rhythms related to thumb movement," *Neuroscience,* vol. 60, pp. 537-50, 1994.

[8] Osipova, D., Ahveninen, J., Jensen, O., Ylikoski, A. and Pekkonen, E., "Altered generation of spontaneous oscillations in Alzheimer's disease," *Neuroimage,* vol. 27, pp. 835-841, 2005.

[9] Kubler, A., Kotchoubey, B., Kaiser, J., Wolpaw, J. R. and Birbaumer, N., "Brain-computer communication: Unlocking the locked in," *Psychol Bull,* vol. 127, pp. 358-375, 2001.

[10] Congedo, M., Lubar, J. F. and Joffe, D., "Low-resolution electromagnetic tomography neurofeedback," *IEEE T Neur Sys Reh*, vol. 12, pp. 387-397, 2004.

[11] Salmelin, R., Schnitzler, A., Schmitz, F. and Freund, H. J., "Single word reading in developmental stutterers and fluent speakers," *Brain*, vol. 123, pp. 1184-1202, 2000.

[12] Gross, J., *et al.*, "Dynamic imaging of coherent sources: Studying neural interactions in the human brain," *Proc Natl Acad Sci USA*, vol. 98, pp. 694-699, 2001.

[13] Singh, K. D., Barnes, G. R., Hillebrand, A., Forde, E. M. E. and Williams, A. L., "Task-related changes in cortical synchronization are spatially coincident with the hemodynamic response," *Neuroimage*, vol. 16, pp. 103-114, 2002.

[14] Lin, F. H., *et al.*, "Spectral spatiotemporal imaging of cortical oscillations and interactions in the human brain," *Neuroimage*, vol. 23, pp. 582-595, 2004.

[15] Congedo, M., "Subspace projection filters for real-time brain electromagnetic imaging," *IEEE Trans Biomed Eng*, vol. 53, pp. 1624-1634, 2006.

[16] Decety, J. and Ingvar, D. H., "Brain structures participating in mental simulation of motor behavior: a neuropsychological interpretation," *Acta Psychol*, vol. 73, pp. 13-34, 1990.

[17] Jeannerod, M. and Frak, V., "Mental imaging of motor activity in humans," *Curr Opin Neurobiol*, vol. 9, pp. 735-739, 1999.

[18] Kirmizi-Alsan, E., *et al.*, "Comparative analysis of event-related potentials during Go/NoGo and CPT: Decomposition of electrophysiological markers of response inhibition and sustained attention," *Brain Res*, vol. 1104, pp. 114-128, 2006.

[19] Kahana, M. J., Sekuler, R., Caplan, J. B., Kirschen, M. and Madsen, J. R., "Human theta oscillations exhibit task dependence during virtual maze navigation," *Nature*, vol. 399, pp. 781-784, 1999.

[20] Klimesch, W., "EEG alpha and theta oscillations reflect cognitive and memory performance: a review and analysis," *Brain Res Rev*, vol. 29, pp. 169-195, 1999.

[21] Sarnthein, J., Petsche, H., Rappelsberger, P., Shaw, G. L. and von Stein, A., "Synchronization between prefrontal and posterior association cortex during human working memory," *Proc Natl Acad Sci USA*, vol. 95, pp. 7092-7096, 1998.

[22] Salmelin, R. and Hari, R., "Characterization of spontaneous MEG rhythms in healthy adults," *Electroencephalogr Clin Neurophysiol*, vol. 91, pp. 237-48, 1994.

[23] Vanni, S., Revonsuo, A. and Hari, R., "Modulation of the parieto-occipital alpha rhythm during object detection," *J Neurosci*, vol. 17, pp. 7141-7147, 1997.

[24] McFarland, D. J., Miner, L. A., Vaughan, T. M. and Wolpaw, J. R., "Mu and beta rhythm topographies during motor imagery and actual movements," *Brain Topogr*, vol. 12, pp. 177-186, 2000.

[25] Pichitpornchai, C., "Normal electroencephalogram," *Siriraj Med J*, vol. 60, pp. 81-84, 2008.

[26] Singer, W. and Gray, C. M., "Visual Feature Integration and the Temporal Correlation Hypothesis," *Annu Rev Neurosci*, vol. 18, pp. 555-586, 1995.

[27] Desmedt, J. E. and Tomberg, C., "Transient Phase-Locking of 40 Hz Electrical Oscillations in Prefrontal and Parietal Human Cortex Reflects the Process of Conscious Somatic Perception," *Neurosci Lett*, vol. 168, pp. 126-129, 1994.

[28] Fitzgibbon, S. P., Pope, K. J., Mackenzie, L., Clark, C. R. and Willoughby, J. O., "Cognitive tasks augment gamma EEG power," *Clin Neurophysiol*, vol. 115, pp. 1802-9, 2004.

[29] Gross, D. W. and Gotman, J., "Correlation of high-frequency oscillations with the sleep-wake cycle and cognitive activity in humans," *Neuroscience,* vol. 94, pp. 1005-18, 1999.

[30] Hamalainen, M. S. and Sarvas, J., "Realistic conductivity geometry model of the human head for interpretation of neuromagnetic data," *IEEE Trans Biomed Eng,* vol. 36, pp. 165-71, 1989.

[31] He, B., *et al.,* "Electric dipole tracing in the brain by means of the boundary element method and its accuracy," *IEEE Trans Biomed Eng,* vol. 34, pp. 406-14, Jun 1987.

[32] Haueisen, J., Ramon, C., Eiselt, M., Brauer, H. and Nowak, H., "Influence of tissue resistivities on neuromagnetic fields and electric potentials studied with a finite element model of the head," *IEEE Trans Biomed Eng,* vol. 44, pp. 727-35, 1997.

[33] Oostendorp, T. F., Delbeke, J. and Stegeman, D. F., "The conductivity of the human skull: Results of in vivo and in vitro measurements," *IEEE Trans Biomed Eng,* vol. 47, pp. 1487-1492, 2000.

[34] Babiloni, F., *et al.,* "Linear inverse source estimate of combined EEG and MEG data related to voluntary movements," *Hum Brain Mapp,* vol. 14, pp. 197-209, 2001.

[35] Kincses, W. E., Kaiser, S., Elbert, T. and Braun, C., "Modeling extended sources of event-related potentials using anatomical and physiological constraints," *Hum Brain Mapp,* vol. 8, pp. 182-193, 1999.

[36] Dale, A. M., *et al.,* "Dynamic statistical parametric mapping: Combining fMRI and MEG for high-resolution imaging of cortical activity," *Neuron,* vol. 26, pp. 55-67, 2000.

[37] Dale, A. M. and Sereno, M. I., "Improved Localization of Cortical Activity by Combining Eeg and Meg with Mri Cortical Surface Reconstruction - a Linear-Approach," *J Cogn Neurosci,* vol. 5, pp. 162-176, Spr 1993.

[38] Liu, A. K., Belliveau, J. W. and Dale, A. M., "Spatiotemporal imaging of human brain activity using functional MRI constrained magnetoencephalography data: Monte Carlo simulations," *Proc Natl Acad Sci USA*, vol. 95, pp. 8945-8950, 1998.

[39] Dale, A. M., Fischl, B. and Sereno, M. I., "Cortical surface-based analysis - I. Segmentation and surface reconstruction," *Neuroimage*, vol. 9, pp. 179-194, 1999.

[40] Fischl, B., Sereno, M. I. and Dale, A. M., "Cortical surface-based analysis - II: Inflation, flattening, and a surface-based coordinate system," *Neuroimage*, vol. 9, pp. 195-207, 1999.

[41] Shattuck, D. W. and Leahy, R. M., "BrainSuite: An automated cortical surface identification tool," *Med Image Anal*, vol. 6, pp. 129-142, 2002.

[42] Baillet, S., *et al.*, "Evaluation of inverse methods and head models for EEG source localization using a human skull phantom," *Phys Med Biol*, vol. 46, pp. 77-96, 2001.

[43] Liu, A. K., Dale, A. M. and Belliveau, J. W., "Monte Carlo simulation studies of EEG and MEG localization accuracy," *Hum Brain Mapp*, vol. 16, pp. 47-62, 2002.

[44] Lin, F. H., *et al.*, "Assessing and improving the spatial accuracy in MEG source localization by depth-weighted minimum-norm estimates," *Neuroimage*, vol. 31, pp. 160-171, 2006.

[45] Kamousi, B., Amini, A. N. and He, B., "Classification of motor imagery by means of cortical current density estimation and Von Neumann entropy," *J Neural Eng*, vol. 4, pp. 17-25, 2007.

[46] Qin, L., Ding, L. and He, B., "Motor imagery classification by means of source analysis for brain-computer interface applications," *J Neural Eng*, vol. 1, pp. 135-41, 2004.

[47] Kamousi, B., Liu, Z. M. and He, B., "Classification of motor imagery tasks for brain-computer interface applications by means of two equivalent dipoles analysis," *IEEE T Neur Syst Reh Eng,* vol. 13, pp. 166-171, 2005.

[48] Wolpaw, J. R., Birbaumer, N., McFarland, D. J., Pfurtscheller, G. and Vaughan, T. M., "Brain-computer interfaces for communication and control," *Clin Neurophysiol,* vol. 113, pp. 767-91, 2002.

[49] Blankertz, B., Dornhege, G., Krauledat, M., Muller, K. R. and Curio, G., "The non-invasive Berlin Brain-Computer Interface: Fast acquisition of effective performance in untrained subjects," *Neuroimage,* vol. 37, pp. 539-550, 2007.

[50] Chatterjee, A., Aggarwal, V., Ramos, A., Acharya, S. and Thakor, N. V., "A brain-computer interface with vibrotactile biofeedback for haptic information," *J NeuroEng Rehabil,* vol. 4, 2007.

[51] Pfurtscheller, G., Brunner, C., Schlogl, A. and da Silva, F. H. L., "Mu rhythm (de)synchronization and EEG single-trial classification of different motor imagery tasks," *Neuroimage,* vol. 31, pp. 153-159, 15 2006.

[52] Pineda, J. A., Silverman, D. S., Vankov, A. and Hestenes, J., "Learning to control brain rhythms: Making a brain-computer interface possible," *IEEE T Neur Sys Reh Eng,* vol. 11, pp. 181-184, Jun 2003.

[53] Birbaumer, N., *et al.*, "A spelling device for the paralysed," *Nature,* vol. 398, pp. 297-298, 1999.

[54] Bayliss, J. D., "Use of the evoked potential P3 component for control in a virtual apartment," *IEEE T Neur Sys Reh Eng,* vol. 11, pp. 113-116, Jun 2003.

[55] Hoffmann, U., Vesin, J. M., Ebrahimi, T. and Diserens, K., "An efficient P300-based brain-computer interface for disabled subjects," *J Neurosci Methods,* vol. 167, pp. 115-125, 2008.

[56] Lalor, E. C., *et al.*, "Steady-state VEP-based brain-computer interface control in an immersive 3D gaming environment," *EURASIP J Appl Signal Process,* vol. 2005, pp. 3156-3164, 2005.

[57] Middendorf, M., McMillan, G., Calhoun, G. and Jones, K. S., "Brain-computer interfaces based on the steady-state visual-evoked response," *IEEE Trans Rehabil Eng,* vol. 8, pp. 211-4, 2000.

[58] Galan, F., *et al.*, "A brain-actuated wheelchair: Asynchronous and non-invasive Brain-computer interfaces for continuous control of robots," *Clin Neurophysiol,* vol. 119, pp. 2159-2169, 2008.

[59] Neuper, C., Muller, G. R., Kubler, A., Birbaumer, N. and Pfurtscheller, G., "Clinical application of an EEG-based brain-computer interface: a case study in a patient with severe motor impairment," *Clin Neurophysiol,* vol. 114, pp. 399-409, 2003.

[60] Pfurtscheller, G., *et al.*, "Graz-BCI: State of the art and clinical applications," *IEEE T Neur Sys Reh Eng,* vol. 11, pp. 177-180, 2003.

[61] Lotze, M., *et al.*, "Activation of cortical and cerebellar motor areas during executed and imagined hand movements: An fMRI study," *J Cogn Neurosci,* vol. 11, pp. 491-501, 1999.

[62] Pfurtscheller, G. and Neuper, C., "Motor imagery and direct brain-computer communication," *Proc IEEE,* vol. 89, pp. 1123-1134, 2001.

[63] Höllinger, P., Beisteiner, R., Lang, W., Lindinger, G. and Berthoz, A., "Mental representations of movements. Brain potentials associated with imagination of eye movements," *Clin Neurophysiol,* vol. 110, pp. 799-805, 1999.

[64] Pfurtscheller, G. and Neuper, C., "Motor imagery activates primary sensorimotor area in humans," *Neurosci Lett,* vol. 239, pp. 65-68, 19 1997.

[65] Ince, N. F., Tewfik, A. H. and Arica, S., "Extraction subject-specific motor imagery time-frequency patterns for single trial EEG classification," *Comput Biol Med,* vol. 37, pp. 499-508, 2007.

[66] Model, D. and Zibulevsky, M., "Learning subject-specific spatial and temporal filters for single-trial EEG classification," *Neuroimage,* vol. 32, pp. 1631-1641, 2006.

[67] Neuper, C., Scherer, R., Reiner, M. and Pfurtscheller, G., "Imagery of motor actions: Differential effects of kinesthetic and visual-motor mode of imagery in single-trial EEG," *Cogn Brain Res,* vol. 25, pp. 668-677, 2005.

[68] Leeb, R., *et al.*, "Walking by Thinking: The Brainwaves Are Crucial, Not the Muscles!," *Presence- Teleoper Virtual Environ,* vol. 15, pp. 500-514, 2006.

[69] Hinterberger, T., *et al.*, "A multimodal brain-based feedback and communication system," *Exp Brain Res,* vol. 154, pp. 521-526, 2004.

[70] Nijboer, F., *et al.*, "An auditory brain-computer interface (BCI)," *J Neurosci Methods,* vol. 167, pp. 43-50, 2008.

[71] Annett, J., "Motor imagery: perception or action?," *Neuropsychologia,* vol. 33, pp. 1395-417, 1995.

[72] Wolpaw, J. R. and McFarland, D. J., "Control of a two-dimensional movement signal by a noninvasive brain-computer interface in humans," *Proc Natl Acad Sci U S A,* vol. 101, pp. 17849-54, 2004.

[73] Hjorth, B., "An on-line transformation of EEG scalp potentials into orthogonal source derivations," *Electroencephalogr Clin Neurophysiol,* vol. 39, pp. 526-530, 1975.

[74] McFarland, D. J., McCane, L. M., David, S. V. and Wolpaw, J. R., "Spatial filter selection for EEG-based communication," *Electroencephalography Clinical Neurophysiology,* vol. 103, pp. 386-394, 1997.

[75] Im, C. H., Hwang, H. J., Che, H. and Lee, S., "An EEG-based real-time cortical rhythmic activity monitoring system," *Physiol Meas,* vol. 28, pp. 1101-1113, 2007.

[76] McFarland, D. J., Miner, L. A., Vaughan, T. M. and Wolpaw, J. R., "Mu and beta rhythm topographies during motor imagery and actual movements," *Brain Topogr,* vol. 12, pp. 177-86, 2000.

[77] Murphy, S. M., "Imagery Interventions in Sport," *Med Sci Sport Exer,* vol. 26, pp. 486-494, 1994.

[78] Dijkerman, H. C., Ietswaart, M., Johnston, M. and MacWalter, R. S., "Does motor imagery training improve hand function in chronic stroke patients? A pilot study," *Clin Rehabil,* vol. 18, pp. 538-549, 2004.

[79] Jastrow, J., "Study of involunatry movements," *J Psychol,* vol. 4, pp. 398-407, 1892.

[80] Owen, A. M., *et al.*, "Detecting awareness in the vegetative state," *Science,* vol. 313, pp. 1402-1402, 2006.

[81] Tamir, R., Dickstein, R. and Huberman, M., "Integration of motor imagery and physical practice in group treatment applied to subjects with Parkinson's disease," *Neurorehabil Neural Repair,* vol. 21, pp. 68-75, 2007.

[82] Wang, T., Deng, J. and He, B., "Classifying EEG-based motor imagery tasks by means of time-frequency synthesized spatial patterns," *Clin Neurophysiol,* vol. 115, pp. 2744-53, 2004.

[83] Perelmouter, J. and Birbaumer, N., "A binary spelling interface with random errors," *IEEE T Rehabil Eng,* vol. 8, pp. 227-232, 2000.

[84] David, O., Cosmelli, D. and Friston, K. J., "Evaluation of different measures of functional connectivity using a neural mass model," *Neuroimage,* vol. 21, pp. 659-673, 2004.

[85] Gow, D. W., Segawa, J. A., Ahlfors, S. P. and Lin, F. H., "Lexical influences on speech perception: A Granger causality analysis of MEG and EEG source estimates," *Neuroimage,* vol. 43, pp. 614-623, 2008.

[86] Hampson, M., Peterson, B. S., Skudlarski, P., Gatenby, J. C. and Gore, J. C., "Detection of functional connectivity using temporal correlations in MR images," *Hum Brain Mapp,* vol. 15, pp. 247-262, 2002.

[87] Im, C. H., *et al.*, "Estimation of directional coupling between cortical areas using Near-Infrared Spectroscopy (NIRS)," *Opt Express,* vol. 18, pp. 5730-5739, 2010.

[88] Korzeniewska, A., Crainiceanu, C. M., Kus, R., Franaszczuk, P. J. and Crone, N. E., "Dynamics of event-related causality in brain electrical activity," *Hum Brain Mapp,* vol. 29, pp. 1170-92, 2008.

[89] Mormann, F., Lehnertz, K., David, P. and Elger, C. E., "Mean phase coherence as a measure for phase synchronization and its application to the EEG of epilepsy patients," *Physica D,* vol. 144, pp. 358-369, 1 2000.

[90] Pfurtscheller, G. and Andrew, C., "Event-related changes of band power and coherence: Methodology and interpretation," *J Clin Neurophysiol,* vol. 16, pp. 512-519, 1999.

[91] Le Van Quyen, M. and Bragin, A., "Analysis of dynamic brain oscillations: methodological advances," *Trends Neurosci,* vol. 30, pp. 365-73, Jul 2007.

[92] Leuchter, A. F., *et al.*, "Changes in brain functional connectivity in Alzheimer-type and multi-infarct dementia," *Brain,* vol. 115, pp. 1543-61, 1992.

[93] Murias, M., Webb, S. J., Greenson, J. and Dawson, G., "Resting state cortical connectivity reflected in EEG coherence in individuals with autism," *Biol Psychiat,* vol. 62, pp. 270-273, 2007.

[94] Peled, A., *et al.*, "Functional connectivity and working memory in schizophrenia: An EEG study," *Int J Neurosci,* vol. 106, pp. 47-61, 2001.

[95] Koenig, T., *et al.*, "Decreased functional connectivity of EEG theta-frequency activity in first-episode, neuroleptic-naive patients with schizophrenia: preliminary results," *Schizophr Res,* vol. 50, pp. 55-60, 2001.

[96] Park, Y. M., *et al.*, "Decreased EEG synchronization and its correlation with symptom severity in Alzheimer's disease," *Neurosci Res,* vol. 62, pp. 112-117, 2008.

[97] Reijneveld, J. C., Ponten, S. C., Berendse, H. W. and Stam, C. J., "The application of graph theoretical analysis to complex networks in the brain," *Clin Neurophysiol,* vol. 118, pp. 2317-2331, 2007.

[98] Kim, K. H., Choi, J. W. and Yoon, J., "Difference in gamma-band phase synchronization during semantic processing of visually presented words from primary and secondary languages," *Brain Res,* vol. 1291, pp. 82-91, 2009.

[99] Delorme, A. and Makeig, S., "EEGLAB: an open source toolbox for analysis of single-trial EEG dynamics including independent component analysis," *J Neurosci Methods,* vol. 134, pp. 9-21, 2004.

[100] Schoffelen, J. M. and Gross, J., "Source Connectivity Analysis With MEG and EEG," *Hum Brain Mapp,* vol. 30, pp. 1857-1865, 2009.

[101] Astolfi, L., *et al.*, "Tracking the time-varying cortical connectivity patterns by adaptive multivariate estimators," *IEEE Trans Biomed Eng,* vol. 55, pp. 902-913, 2008.

[102] Hoechstetter, K., *et al.*, "BESA source coherence: a new method to study cortical oscillatory coupling," *Brain Topogr,* vol. 16, pp. 233-8, 2004.

[103] Verdoux, H., Cougnard, A., Grolleau, S., Besson, R. and Delcroix, F., "How do general practitioners manage subjects with early schizophrenia and collaborate with mental health professionals? A postal survey in South-Western France," *Soc Psychiatry Psychiatr Epidemiol,* vol. 40, pp. 892-898, 2005.

[104] Coben, R., "Assessment guided neurofeedback for ASD: EEG analyses," *Appl Psychophys Biof,* vol. 33, pp. 176-176, 2008.

[105] Coben, R., "Efficacy of Connectivity Guided Neurofeedback on Language Functions and IQ in Autistic Children," *Appl Psychophys Biof,* vol. 35, pp. 179-179, 2010.

[106] Coben, R. and Myers, T. E., "The Relative Efficacy of Connectivity Guided and Symptom Based EEG Biofeedback for Autistic Disorders," *Appl Psychophys Biof,* vol. 35, pp. 13-23, 2010.

[107] Ibric, V. L., Dragomirescu, L. G. and Hudspeth, W. J., "Real-Time Changes in Connectivities During Neurofeedback," *J Neurotherapy,* vol. 13, pp. 156-165, 2009.

[108] Hwang, H. J., Kwon, K. and Im, C. H., "Neurofeedback-based motor imagery training for brain-computer interface (BCI)," *J Neurosci Methods,* vol. 179, pp. 150-6, 2009.

[109] Lin, F. H., *et al.*, "Spectral spatiotemporal imaging of cortical oscillations and interactions in the human brain," *Neuroimage,* vol. 23, pp. 582-95, 2004.

[110] Evans, A., Collins, D. and Milner, B., "An MRI-based stereotactic atlas from 250 young normal subjects," *Soc Neurosci Abstr,* vol. 18, p. 408, 1992.

[111] Haueisen, J., Ramon, C., Eiselt, M., Brauer, H. and Nowak, H., "Influence of tissue resistivities on neuromagnetic fields and electric potentials studied with a finite element model of the head," *IEEE Trans Biomed Eng,* vol. 44, pp. 727-735, 1997.

[112] Fonteneau, E. and Davidoff, J., "Neural correlates of colour categories," *Neuroreport,* vol. 18, pp. 1323-1327, 2007.

[113] Hillyard, S. A. and Anllo-Vento, L., "Event-related brain potentials in the study of visual selective attention," *Proc Natl Acad Sci U S A,* vol. 95, pp. 781-787, 1998.

[114] Holmes, A., Franklin, A., Clifford, A. and Davies, I., "Neurophysiological evidence for categorical perception of color," *Brain Cogn,* vol. 69, pp. 426-34, 2009.

[115] Bentin, S., Allison, T., Puce, A., Perez, E. and McCarthy, G., "Electrophysiological studies of face perception in humans," *J Cogn Neurosci,* vol. 8, pp. 551-565, 1996.

[116] Lee, S. H., Kim, D. W., Kim, E. Y., Kim, S. and Im, C. H., "Dysfunctional gamma-band activity during face structural processing in schizophrenia patients," *Schizophr Res,* vol. 119, pp. 191-7, 2010.

[117] Vuilleumier, P. and Pourtois, G., "Distributed and interactive brain mechanisms during emotion face perception: Evidence from functional neuroimaging," *Neuropsychologia,* vol. 45, pp. 174-194, 2007.

[118] Keren, A. S., Yuval-Greenberg, S. and Deouell, L. Y., "Saccadic spike potentials in gamma-band EEG: Characterization, detection and suppression," *Neuroimage,* vol. 49, pp. 2248-2263, 2010.

[119] McMenamin, B. W., *et al.*, "Validation of ICA-based myogenic artifact correction for scalp and source-localized EEG," *Neuroimage,* vol. 49, pp. 2416-2432, 2010.

[120] Uhlhaas, P. J., *et al.*, "Dysfunctional long-range coordination of neural activity during Gestalt perception in schizophrenia," *J Neurosci,* vol. 26, pp. 8168-8175, 2006.

[121] Manganotti, P., *et al.*, "Task-related coherence and task-related spectral power changes during sequential finger movements," *Electromyogr Motor C,* vol. 109, pp. 50-62, 1998.

[122] Menon, V., *et al.*, "Spatio-temporal correlations in human gamma band electrocorticograms," *Electroencephalogr ClinNeurophysiol,* vol. 98, pp. 228-228, 1996.

[123] Spencer, K. M., *et al.*, "Abnormal neural synchrony in schizophrenia," *J Neurosci,* vol. 23, pp. 7407-7411, 2003.

[124] Stam, C. J., Jones, B. F., Nolte, G., Breakspear, M. and Scheltens, P., "Small-world networks and functional connectivity in Alzheimer's disease," *Cereb Cortex,* vol. 17, pp. 92-99, 2007.

[125] Matsumoto, A., Ichikawa, Y., Kanayama, N., Ohira, H. and Iidaka, T., "Gamma band activity and its synchronization reflect the dysfunctional emotional processing in alexithymic persons," *Psychophysiology,* vol. 43, pp. 533-540, 2006.

[126] Massimini, M., *et al.*, "Breakdown of cortical effective connectivity during sleep," *Science,* vol. 309, pp. 2228-32, 2005.

[127] Brunner, C., Scherer, R., Graimann, B., Supp, G. and Pfurtscheller, G., "Online control of a brain-computer interface using phase synchronization," *IEEE Trans Biomed Eng,* vol. 53, pp. 2501-2506, 2006.

[128] Gysels, E. and Celka, P., "Phase synchronization for the recognition of mental tasks in a brain-computer interface," *IEEE Trans Neur Syst Rehabil Eng*, vol. 12, pp. 406-415, 2004.

[129] Wei, Q. G., Wang, Y. J., Gao, X. R. and Gao, S. K., "Amplitude and phase coupling measures for feature extraction in an EEG-based brain-computer interface," *J Neural Eng*, vol. 4, pp. 120-129, 2007.

[130] Abootalebi, V., Moradi, M. H. and Khalilzadeh, M. A., "A new approach for EEG feature extraction in P300-based lie detection," *Comput Meth Prog Bio*, vol. 94, pp. 48-57, 2009.

[131] Allison, B. Z., *et al.*, "Toward a hybrid brain-computer interface based on imagined movement and visual attention," *J Neural Eng*, vol. 7, 2010.

[132] Bakardjian, H., Tanaka, T. and Cichocki, A., "Optimization of SSVEP brain responses with application to eight-command Brain-Computer Interface," *Neurosci Lett*, vol. 469, pp. 34-38, 2010.

[133] Coleman, M. R., *et al.*, "Do vegetative patients retain aspects of language comprehension? Evidence from fMRI," *Brain*, vol. 130, pp. 2494-2507, 2007.

[134] Davatzikos, C., *et al.*, "Classifying spatial patterns of brain activity with machine learning methods: Application to lie detection," *Neuroimage*, vol. 28, pp. 663-668, 2005.

[135] Fruitet, J., McFarland, D. J. and Wolpaw, J. R., "A comparison of regression techniques for a two-dimensional sensorimotor rhythm-based brain-computer interface," *J Neural Eng*, vol. 7, p. 16003, 2010.

[136] Hanchak, E., *et al.*, "Polygraph and EEG correlates of lie detection," *Psychophysiology*, vol. 45, pp. S109-S109, 2008.

[137] Lee, T. M. C., *et al.*, "Lie detection by functional magnetic resonance imaging," *Hum Brain Mapp*, vol. 15, pp. 157-164, 2002.

[138] Owen, A. M., *et al.*, "Detecting awareness in the vegetative state," *Science*, vol. 313, p. 1402, 2006.

[139] Owen, A. M., *et al.*, "Using functional magnetic resonance imaging to detect covert awareness in the vegetative state," *Arch Neurol,* vol. 64, pp. 1098-1102, 2007.

[140] Royer, A. S. and He, B., "Goal selection versus process control in a brain-computer interface based on sensorimotor rhythms," *J Neural Eng,* vol. 6, 2009.

[141] Schreuder, M., Blankertz, B. and Tangermann, M., "A New Auditory Multi-Class Brain-Computer Interface Paradigm: Spatial Hearing as an Informative Cue," *Plos One,* vol. 5, 2010.

[142] Stark, R., Ambach, W., Lange, J., Bauer, E. and Vaitl, D., "Lie-detection in a mock crime scenario: Insights by functional magnetic resonance imaging," *J Psychophysiol,* vol. 20, pp. 115-115, 2006.

[143] Cabrera, A. F. and Dremstrup, K., "Auditory and spatial navigation imagery in Brain-Computer Interface using optimized wavelets," *J Neurosci Methods,* vol. 174, pp. 135-146, 2008.

[144] Cabrera, A. F., Farina, D. and Dremstrup, K., "Comparison of feature selection and classification methods for a brain-computer interface driven by non-motor imagery," *Med Biol Eng Comput,* vol. 48, pp. 123-132, 2010.

[145] Gevins, A. S., Zeitlin, G. M., Doyle, J. C., Schaffer, R. E. and Callaway, E., "EEG patterns during 'cognitive' tasks. II. Analysis of controlled tasks," *Electroencephalogr Clin Neurophysiol,* vol. 47, pp. 704-10, 1979.

[146] Gevins, A. S., *et al.*, "EEG patterns during 'cognitive' tasks. I. Methodology and analysis of complex behaviors," *Electroencephalogr Clin Neurophysiol,* vol. 47, pp. 693-703, 1979.

[147] Keirn, Z. A. and Aunon, J. I., "Man-Machine Communications through Brain-Wave Processing," *IEEE Eng Med Biol Mag,* vol. 9, pp. 55-57, 1990.

[148] Keirn, Z. A. and Aunon, J. I., "A New Mode of Communication between Man and His Surroundings," *IEEE Trans Biomed Eng,* vol. 37, pp. 1209-1214, 1990.

[149] Mensh, B. D., Werfel, J. and Seung, H. S., "BCI Competition 2003--Data set Ia: combining gamma-band power with slow cortical potentials to improve single-trial classification of electroencephalographic signals," *IEEE Trans Biomed Eng*, vol. 51, pp. 1052-6, 2004.

[150] Palaniappan, R., "Utilizing gamma band to improve mental task based brain-computer Interface design," *IEEE Trans Neural Syst Rehabil Eng*, vol. 14, pp. 299-303, 2006.

[151] Penny, W. D., Roberts, S. J., Curran, E. A. and Stokes, M. J., "EEG-Based communication: A pattern recognition approach," *IEEE Trans Rehabil Eng*, vol. 8, pp. 214-215, 2000.

[152] Zhang, L., He, W., He, C. H. and Wang, P., "Improving Mental Task Classification by Adding High Frequency Band Information," *J Med Syst*, vol. 34, pp. 51-60, 2010.

[153] Lotte, F., Lecuyer, A. and Arnaldi, B., "FuRIA: An Inverse Solution Based Feature Extraction Algorithm Using Fuzzy Set Theory for Brain-Computer Interfaces," *IEEE Trans Signal Proces*, vol. 57, pp. 3253-3263, 2009.

[154] Noirhomme, Q., Kitney, R. I. and Macq, B., "Single-trial EEG source reconstruction for brain-computer interface," *IEEE Trans Biomed Eng*, vol. 55, pp. 1592-1601, 2008.

[155] Hwang, H. J., Kwon, K. and Im, C. H., "Neurofeedback-based motor imagery training for brain-computer interface (BCI)," *J Neurosci Methods*, vol. 179, pp. 150-156, 2009.

[156] Desmedt, J. E. and Tomberg, C., "Transient phase-locking of 40 Hz electrical oscillations in prefrontal and parietal human cortex reflects the process of conscious somatic perception," *Neurosci Lett*, vol. 168, pp. 126-9, 1994.

[157] Sauve, K., "Gamma-band synchronous oscillations: recent evidence regarding their functional significance," *Conscious Cogn*, vol. 8, pp. 213-24, 1999.

[158] Ishii, R., *et al.*, "Medial prefrontal cortex generates frontal midline theta rhythm," *Neuroreport*, vol. 10, pp. 675-679, 1999.

[159] Davidson, R. J. and Ehrlichman, H., "Lateralized cognitive processes and the electroencephalogram," *Science*, vol. 207, pp. 1005-7, 1980.

[160] Doyle, J. C., Ornstein, R. and Galin, D., "Lateral specialization of cognitive mode: II. EEG frequency analysis," *Psychophysiology*, vol. 11, pp. 567-78, 1974.

[161] Galin, D. and Ornstein, R., "Lateral specialization of cognitive mode: an EEG study," *Psychophysiology*, vol. 9, pp. 412-8, 1972.

[162] Gevins, A. S., *et al.*, "Shadows of thought: shifting lateralization of human brain electrical patterns during brief visuomotor task," *Science*, vol. 220, pp. 97-9, 1983.

[163] Nijboer, F., *et al.*, "An auditory brain-computer interface (BCI)," *J Neurosci Methods*, vol. 167, pp. 43-50, 2008.

[164] Birch, G. E., Bozorgzadeh, Z. and Mason, S. G., "Initial oh-line evaluations of the LF-ASD brain-computer interface with able-bodied and spinal-cord subjects using imagined voluntary motor potentials," *IEEE Trans Neural Syst Rehabil Eng*, vol. 10, pp. 219-224, 2002.

[165] Sharma, N., Pomeroy, V. M. and Baron, J. C., "Motor imagery - A backdoor to the motor system after stroke?," *Stroke*, vol. 37, pp. 1941-1952, 2006.

[166] Curran, E., *et al.*, "Cognitive tasks for driving a brain-computer interfacing system: A pilot study," *Ieee T Neur Sys Reh*, vol. 12, pp. 48-54, 2004.

Appendix

Appendix A: Two-dimensional Spatiospectral Pattern Maps

This chapter will show the two-dimensional spatiospectral pattern maps of the other six participants, which are not suggested in Chapter 6.

A.1. Two-dimensional Spatiospectral Pattern Maps for Subject DS

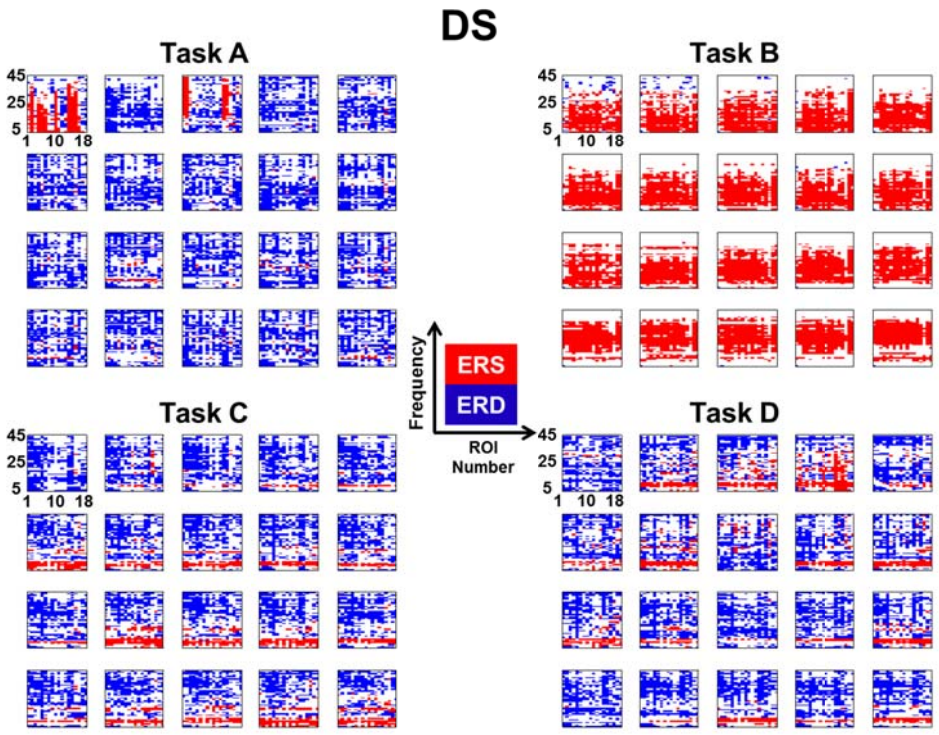

A.2. Two-dimensional Spatiospectral Pattern Maps for Subject HK

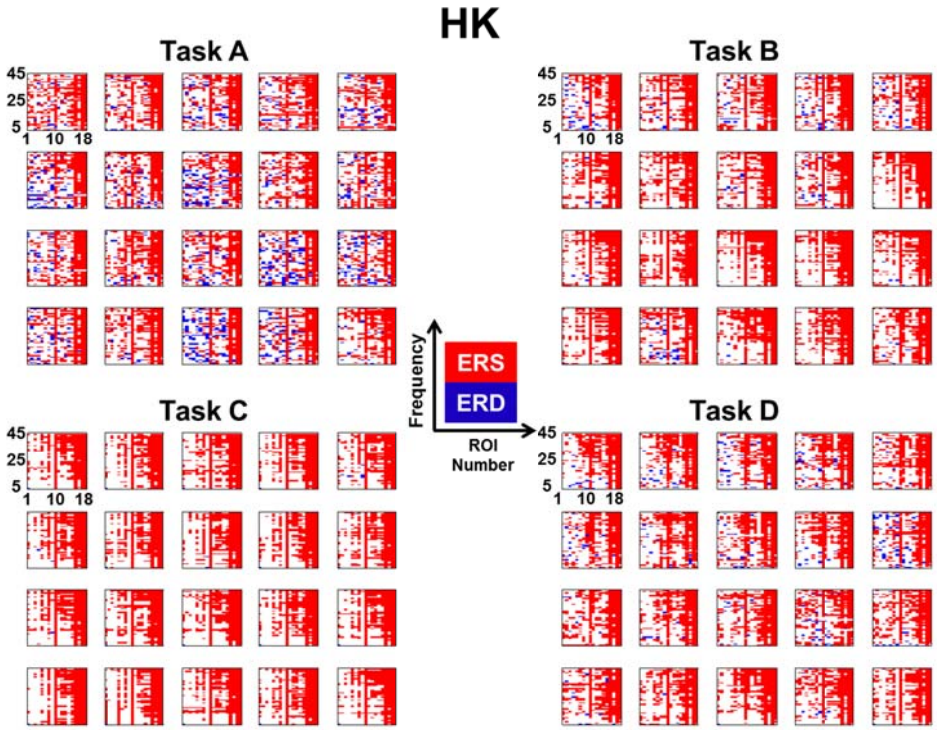

A.3. Two-dimensional Spatiospectral Pattern Maps for Subject JI

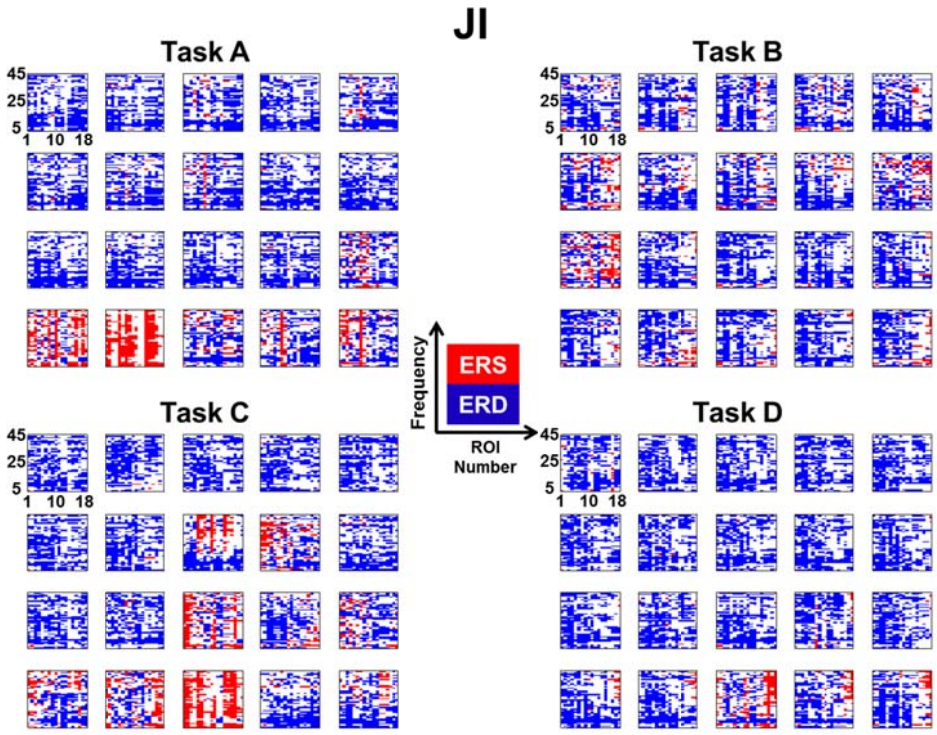

A.4. Two-dimensional Spatiospectral Pattern Maps for Subject SK

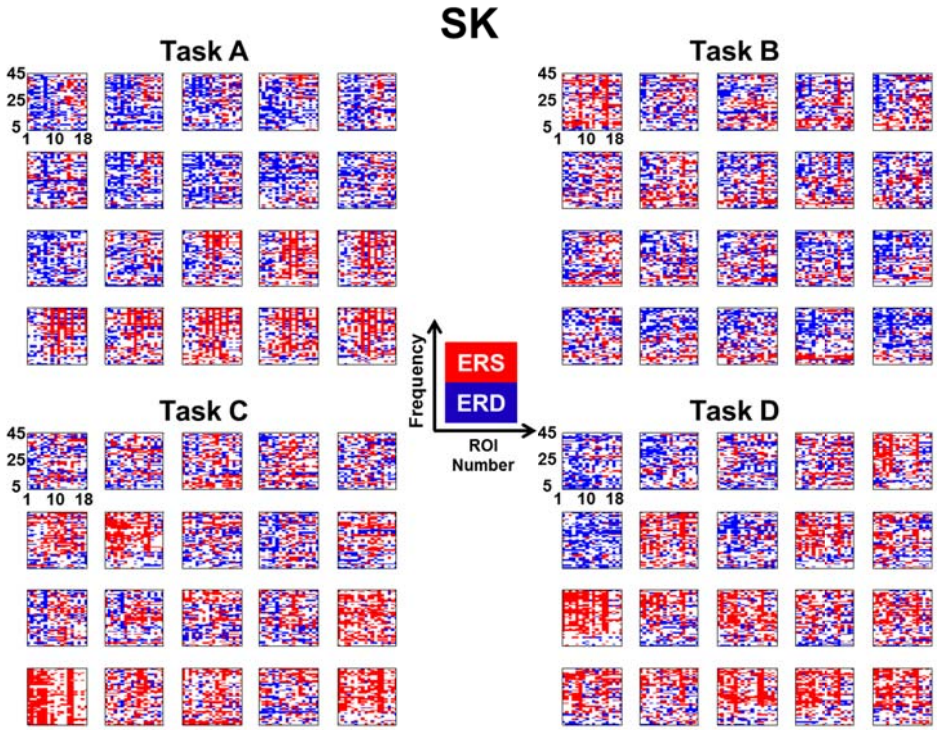

A.5. Two-dimensional Spatiospectral Pattern Maps for Subject WH

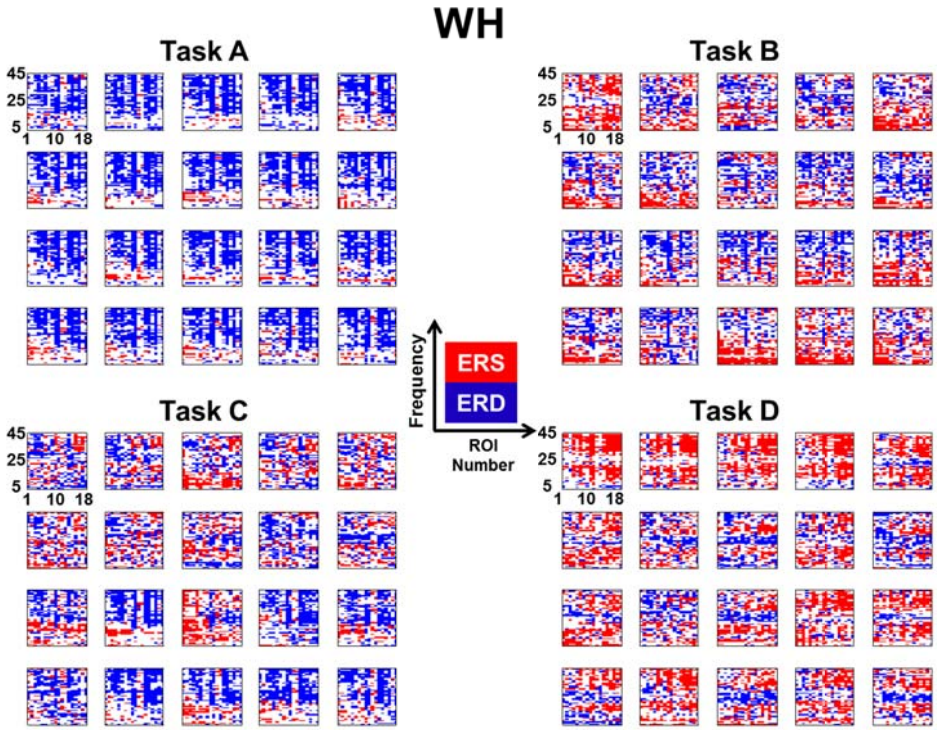

A.6. Two-dimensional Spatiospectral Pattern Maps for Subject JJ

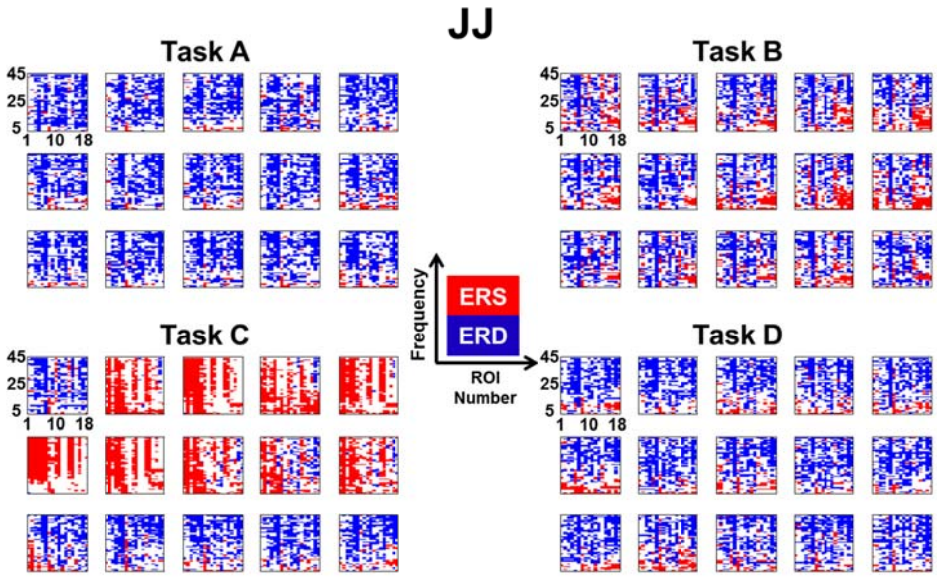

Abstract in Korean

실시간 피질 리듬 활동 영상화 기술의 개발 및 활용

연세대학교 대학원

의공학과

황 한 정

본 학위 논문의 목적은 실시간 피질 리듬 활동 영상화 기술의 개발과 이를 실시간 뇌 활동 관찰, 뇌 질환 진단, 뉴로피드백, 뇌-컴퓨터 접속, 인간 의도의 분류와 같이 다양하고 실용적인 분야에 적용하는 것이다.

실시간 피질 리듬 활동 영상화 기술의 구현 가능성 여부를 조사하기 위해, 먼저 뇌파 기반 실시간 뇌활동 모니터링 시스템을 개발하였다. 개발된 실시간 뇌활동 모니터링 시스템에서는 피험자 뇌의 해부학적인

정보와 실험에 사용하는 전극 구성 정보를 이용하여 주파수 영역의 역산 연산자를 사전에 계산하여 저장하였다. 피질의 각 위치에서의 특정 주파수 신호원의 변화는 실시간으로 획득되는 뇌파 신호를 퓨리에 변환을 이용하여 주파수 영역의 신호로 변환 한 후, 이를 기구축한 역산 연산자와의 실시간 곱을 통해서 추정하였다. 예비 연구로 수행한 오프라인 시뮬레이션에서는 두 명의 치매 환자와 두명의 정상인 피험자가 눈을 감고 편안한 상태에서 측정한 노이즈가 없는 뇌파 신호를 이용하였다. 예비 실험을 통해 18 채널 뇌파 데이터를 이용할 경우, 뇌활동의 시공간적 변화를 약 200 ms 의 지연 시간으로 관찰 할 수 있음을 증명하였다. 예비 실험을 바탕으로 한 온라인 실험에서는 2 명의 피험자를 대상으로 눈을 감고 뜰 때의 알파 리듬의 변화와 팔 움직임과 관련된 뮤(mu) 리듬의 변화를 각각 관찰 하였으며, 개발된 시스템의 유용성을 증명할 수 있었다.

검증이 완료된 실시간 뇌활동 모니터링 시스템은 뇌파 기반 뇌-컴퓨터 접속 연구에서 중요한 연구 주제 중 하나인 운동 상상 (motor imagery) 훈련에 활용하였다. 10 명의 피험자가 본 실험에 참가하였으며, 그 중 5 명은 실시간 뇌활동 모니터링 시스템을 이용하여 운동 상상 훈련을 수행하였으며, 나머지 5 명은 어떠한 훈련도 수행하지 않았다. 운동 상상 훈련을 수행한 5 명의 피험자는 신체적인 움직임 없이 상상만으로

그들의 운동 피질 영역을 활성화 시키는데 성공하였다. 제안한 운동 상상 훈련 시스템의 효과를 검증하기 위해, 운동 상상 훈련 전, 후의 뇌파 신호를 피험자가 왼손과 오른손 운동 상상을 수행할 때 운동 피질 영역에서 획득하였다. 운동 상상 훈련을 받지 않은 나머지 피험자들의 뇌파 신호는 약간의 휴식 시간과 함께 2 번에 나눠서 동일한 방법으로 측정하였다. 측정된 모든 뇌파 신호는 시간-주파수 분석 기법을 이용하여 분석을 하였다. 운동 상상 훈련을 받은 피험자들의 운동 상상 전, 후에 측정한 뇌파 신호를 분석한 결과, 운동 상상 훈련 후에 왼손과 오른손 운동 상상을 수행 할 때 운동 피질 영역의 뇌파가 두드러지게 차이가 났으며, 이는 분류 정확도가 향상되는 결과로 나타났다. 이와 반대로, 운동 상상 훈련을 수행하지 않은 피험자들의 뇌파 데이터를 분석한 결과, 운동 피질 영역의 뇌파 신호와 분류 정확도의 두드러진 변화를 확인 할 수 없었다. 이상의 연구 결과를 통해, 제안한 운동 상상 훈련 시스템이 운동 상상을 훈련하는 좋은 도구가 될 수 있음을 증명할 수 있었다.

실시간 뇌활동 모니터링 시스템의 일부를 수정하여, 서로 다른 뇌 영역 사이의 기능적 연결성 변화를 실시간으로 영상화할 수 있는 시스템을 개발 하였다. 개발한 시스템을 검증하기 위해, 구조적 얼굴 처리, 손가락 움직임, 작업 기억 (working memory) 태스크를 이용하여 다양한

주파수에서 검증 실험을 수행하였다. 만약, 특정 2 개 뇌 영역 신호의 상관도 (correlation)가 기설정된 역치값을 넘을 경우 이 2 개 뇌 영역은 연결성이 있는 것으로 간주하였으며, 실험을 수행하는 동안 실시간으로 변화하는 뇌 영역 사이의 연결성 개수를 기록하였다. 정량적 분석 결과는 과거 동일한 실험을 수행한 오프라인 연구 결과와 일치하는 경향을 보였으며, 피질상에서 실시간으로 기능적 연결성을 도시화할 수 있음을 증명하였다.

피질 리듬 영상화 기술은 인간의 다양한 의도를 두피 표면에서 측정한 뇌파 신호를 이용할 때 보다 높은 정확도로 분류하는데에도 활용되었다. 실험에 참가한 8 명의 피험자가 서로 다른 4 가지 인지 과제를 수행하는 동안 그들의 뇌파를 측정하였다. 기설정된 각 뇌 영역에서 뇌 신호원을 추정하였으며, 2 차원 시공간 패턴 맵을 각 태스크 별로 구축하였다. 2 차원 시공간 패턴 맵은 −1, 0, 1 의 3 개의 값을 가지며 이는 사건−관련 (비)동기화 (event−related (de)synchronization: ERS/ERD) 정도를 반영하여 결정하였다. 같은 인지 과제를 수행할 때 그렇지 않은 경우보다 일정한 ERS/ERD 패턴을 보였으며, 이는 구축한 시공간 패턴 맵이 서로 다른 인간의 의도를 구분할 수 있음을 암시하였다. 피험자의 의도는 특정 인지 과제를 수행할 때 측정한 뇌파 신호로 부터 구축한 2 차원 시공간

패턴 맵과 데이터베이스에 저장된 시공간 패턴 맵들 사이의 내적 계산을 수행하는 유사성 평가를 통해 분류되었다. 분류 정확도는 leave-one-out cross-validation (LOOCV) 기법을 이용하여 계산하였다. 비교 평가를 위해, 두피 표면에서 측정된 뇌파 신호를 이용하여 앞서 언급한 분석 방법과 동일한 절차를 거쳐 분류 정확도를 계산하였다. 피질 리듬 영상화 기술을 이용하여 분석한 분류 정확도는 평균 76.31% (±12.84%) 였으며, 두피 표면에서 측정한 뇌파를 이용하여 분석한 평균 분류 정확도는 68.13% (±9.67%) 였다. 본 결과를 통해 피질 리듬 영상화 기술이 인간의 다양한 의도를 보다 높은 분류 정확도로 분류할 수 있음을 확인 할 수 있었다.

본 학위 논문에서 저자는 실시간 피질 리듬 활동 이미징 기술의 개발에 대해 소개하였으며, 실용적이고 다양한 응용 분야에 개발한 기술을 성공적으로 적용함으로써 개발한 기술의 유용성과 우수함을 입증할 수 있었다.

핵심 되는 말: 피질 리듬 영상화, 실시간 뉴로이미징, 피질 리듬 활동, 뇌전도, 역문제, 뇌-컴퓨터 접속, 운동 상상, 뉴로피드백, 기능적 연결성, 뇌 질환 진단, 인지 과제 분류, 독심술